

2015

Investigation Of Ultrasound Targeted Microbubbles As A Therapeutic Gene Delivery System For Prostate Cancer

Rounak Paramjeet Nande
nande@marshall.edu

Follow this and additional works at: <http://mds.marshall.edu/etd>

 Part of the [Genetic Processes Commons](#), [Genetic Structures Commons](#), [Medical Cell Biology Commons](#), and the [Oncology Commons](#)

Recommended Citation

Nande, Rounak Paramjeet, "Investigation Of Ultrasound Targeted Microbubbles As A Therapeutic Gene Delivery System For Prostate Cancer" (2015). *Theses, Dissertations and Capstones*. Paper 915.

**INVESTIGATION OF ULTRASOUND TARGETED MICROBBUBLES AS A
THERAPEUTIC GENE DELIVERY SYSTEM FOR PROSTATE CANCER**

A dissertation submitted to
the Graduate College of
Marshall University
In partial fulfillment of
the requirements for the degree of
Doctor of Philosophy
in
Biomedical Sciences
by
Rounak Paramjeet Nande
Approved by
Dr. Pier Paolo Claudio, Committee Chairperson
Dr. Travis Salisbury
Dr. W. Elaine Hardman
Dr. Jagan Valluri
Dr. Piyali Dasgupta

Marshall University
May, 2015.

DEDICATION

I would like to dedicate my dissertation work to the circle of family and friends. A special gratitude towards my loving and hard-working parents, Paramjeet Singh and Shagufta Nande, whose constant encouragement and support enabled me to stay on the straight, narrow and ungilded path of research and writing. Special thanks to my brother, Roshan Nande, without whose emotional support, I may never have completed my dissertation. I would also like to give my thanks to my uncle, Javid Sonde, and my aunt, Shaista Chaudhry, for all the proofreading they have done for me during my studies. The love and faith of all my uncles, aunts, cousins and friends has instilled in me a desire to persevere in my goals and directed me to work hard in my endeavors.

ACKNOWLEDGEMENTS

I was guided and supported in my research by my mentor, Dr. Pier Paolo Claudio. His enthusiasm, motivation, knowledge, patience and adaptability have truly allowed me to grow as an individual both professionally and personally. He has instilled in me the methodical approach and thoroughness of analysis necessary to become an independent and successful researcher. I will always be grateful for his guidance and support during each step of my studies and I value everything he has taught me over the years. His guidance, support and encouragement have made this journey such a rewarding experience. Thank you, Dr. Claudio for believing in me and giving me the opportunity to work with you.

I would particularly like to recognize my friends and labmates: Altomare Di Benedetto, Adelaide Greco, Flavia De Carlo, Ilaria Naldi, Sarah Daron, Miranda Carper, Allison Wolf, Colleen Colon and Logan Lawrence for their guidance, input, and support throughout my time at Marshall. I would like to also thank my mentee students, Olivia Boskovic, Kenny Nyugen, Danielle McCallister, Stefano Morganti, Razin Ahmed and others. Each of these individuals has contributed to my success in some way, and I am fortunate to have been given the opportunity to work alongside them.

I am also thankful to the other members of McKown Translational Genomic Research Institute: Johannes Fahrman, Sarah Miles, Ted Witte, and Margaret McFarland. I would also like to thank Dr. Jeffrey Lopez and Dr. Michael Gossman and his team at the Tri-State Regional Cancer center, Ashland, Kentucky for allowing me to perform my animal irradiation studies at their facility. It has been a pleasure to work with such great individuals. I would also like to personally thank Dr. Michael Gossman for taking me golfing all over the Tri-State area; it has been a welcomed distraction from the rigors of research.

I would also like to thank other members of my thesis committee, Dr. W. Elaine Hardman, Dr. Jagan Valluri, Dr. Piyali Dasgupta, and Dr. Travis Salisbury for their continued encouragement and insightful comments towards my research. Their guidance and expertise have been instrumental to the success of my project. It has been a pleasure and honor to have them guide me through my research career at Marshall.

Specials thanks to the Biomedical Science Program at Marshall University; I am so fortunate to have had the opportunity to be a part of this program. I am grateful towards NIH and WV-NASA Space Grant Consortium for funding my research.

I am also thankful for my parents, brother and other family members who have continuously encouraged and supported me in all my endeavors. I would have given up a long time ago if it had not been for their support. They were my cheerleaders and constantly reminded me that I could accomplish anything I put my mind to.

TABLE OF CONTENTS

| | |
|--|-------|
| Dedication | ii |
| Acknowledgements | iii |
| List of Tables | viii |
| List of Figures | ix |
| List of Abbreviations | xiii |
| Abstract | xviii |
| Chapter I: Prostate Cancer and Treatment Strategies | 1 |
| Prostate Cancer | 1 |
| Treatment Strategies | 3 |
| Radiation Therapy | 3 |
| High Intensity Focused Ultrasound | 6 |
| Gene Therapy | 7 |
| Adenoviruses | 9 |
| Conditionally Replication-competent Adenoviruses | 11 |
| Barriers to Virotherapy | 13 |
| Chapter II: Ultrasound Contrast Agents in Cancer Therapy | 17 |
| Abstract | 18 |
| Introduction | 19 |
| Historical Overview | 19 |
| Ultrasound Contrast Agents or Microbubbles | 22 |
| Types of Microbubbles | 25 |
| Interaction of Ultrasound and Microbubbles | 32 |
| Bio-Effects | 39 |
| Uses of Microbubbles | 49 |
| Chapter III: Ultrasound Targeted Microbubble Delivery In Prostate Cancer Cells | 51 |
| Abstract | 51 |
| Background | 51 |
| Hypothesis | 51 |
| Methods | 51 |
| Results | 52 |
| Conclusion | 52 |
| Introduction | 53 |
| Materials and Methods | 55 |
| Cell Lines and Cell Culture | 55 |
| Cytological Observations | 55 |
| Adenovirus Production and Purification | 56 |
| Viral Burst Assay | 56 |
| Antibodies | 57 |
| Western Blot Analysis | 57 |
| Flow Cytometry Assay | 58 |
| Annexin V Assay | 58 |
| UTMD for Prostate Cancer Cells | 59 |
| Statistical Analysis | 59 |
| Results | 60 |
| Cytological Observations after Adenoviral Gene Transfer | 60 |

| | |
|--|-----|
| Quantification of the Ad.GFP Viral Uptake | 61 |
| Quantification of Ad Receptors Present on the Surface of the Cells | 61 |
| Verification of protein expression by western blots | 62 |
| Viral Burst Assay to Assess the Capacity of Replicative HAd5 to Produce Viral Particles..... | 63 |
| Annexin-V Staining for Cell Death | 63 |
| UTMD for Prostate Cancer Cells..... | 66 |
| Discussion | 70 |
| Chapter IV: Eradication of Therapy-resistant Human Prostate Tumors Using an Ultrasound- guided Site-specific Cancer Terminator Virus Delivery Approach..... | 72 |
| Abstract | 74 |
| Introduction..... | 75 |
| Materials and Methods..... | 78 |
| Cell Lines, Cell Culture and Adenovirus Production | 78 |
| Preparation of Microbubbles and Ultrasound Platform | 78 |
| Antibodies and Western Blot Analysis | 79 |
| Animal Study and Ultrasonic Bubble Destruction..... | 80 |
| Statistical Analysis..... | 81 |
| Results..... | 82 |
| Targeson Microbubbles and a SonoSite Portable Micro-Maxx Ultrasound (US) Platform Efficiently Targets Ad-GFP Viruses to Tumors | 82 |
| Microbubble Assisted Ad.mda-7 Gene Delivery Inhibits DU145 Human Prostate Cancer Growth <i>In Vivo</i> | 85 |
| Microbubble Assisted CTV Gene Delivery Eradicates Prostate Cancer Growth <i>In Vivo</i> | 91 |
| Discussion | 98 |
| Acknowledgements..... | 103 |
| Chapter V: Microbubble-Assisted p53, RB, and p130 Gene Transfer in Combination with Radiation Therapy in Prostate Cancer. | 104 |
| Abstract | 105 |
| Introduction..... | 106 |
| Materials and Methods..... | 109 |
| Cell Lines, Cell Culture, and Adenoviral Production | 109 |
| Radiation..... | 110 |
| Flow Cytometry Analysis | 111 |
| Antibodies and Western Blot Analysis | 111 |
| Preparation of MBs and US Platform | 112 |
| Animal Study | 113 |
| <i>In Vivo</i> Bioluminescence Imaging | 114 |
| Statistical Analyses | 115 |
| Results..... | 116 |
| Phase Contrast Microscopic Analysis: Irradiated DU145 Cells that were then Transduced with p53, RB, and p130 Genes..... | 116 |
| Transgene Expression of p53, pRb, and p130 in Irradiated DU145 Cells..... | 119 |
| Cell Cycle Analysis of DU145 Cells Following X-ray Irradiation and Gene Transduction | 120 |

| | |
|--|-----|
| External Beam Radiation Followed by Adenoviral p53, pRb, p130 Transduction Increased the Apoptotic Rate of DU145 Cells <i>In Vitro</i> | 124 |
| Microbubble Assisted Adenoviral p53, pRb, and p130 Gene Transfer in Combination with External Beam Radiation Enhanced Therapy of Radio- Resistant DU145 Tumor Xenografts | 129 |
| Microbubble-Assisted p53, pRB, and p130 Gene Transfer Results in Enhanced Protein Expression of Targeted Genes..... | 140 |
| Discussion | 142 |
| Acknowledgements..... | 149 |
| Chapter VI: Conclusion and Future Directions | 150 |
| References..... | 153 |
| Appendix: | 168 |
| Letters from Office of Research Integrity IRB Approval..... | 168 |
| Curriculum Vitae | 170 |

LIST OF TABLES

| | |
|---|-----|
| Table 1: Comparison of Commercially Available Contrast Agents | 29 |
| Table 2. Determination of the expression of surface Adenoviral receptors by flow cytometry. . | 62 |
| Table 3. ANOVA (Analysis of Variance) significance table with a Post Hoc Tukey’s multiple comparison test for Annexin-V assay between TRAMP-C2 and DU145 cells transduced with Ad.mda-7/IL-24. | 65 |
| Table 4. The percentage of DU145 cells in G1, S and G2 cell cycle phase with its standard deviation that received treatments of adenovirus, radiation and combined (radiation + adenovirus) treatment as analyzed by flow cytometry at 24-96 hours. | 121 |
| Table 5. Multiple comparison ANOVA (Analysis of Variance) significance table with a Dunnett’s T3 test for Annexin-V assay experiment of DU145 cells following radiation and adenoviral gene transfer for 96hrs time point. | 127 |
| Table 6. Mean percentage inhibition rate and standard deviation of final tumor volume at week 19 compared against the control non-treated group. | 133 |
| Table 7. Multiple comparisons ANOVA (Analysis of Variance) significance table with a post hoc Dunnett’s T3 test for the <i>in vivo</i> experiment following radiation and adenoviral gene transfer on the treated right tumors at week 19. | 136 |

LIST OF FIGURES

| | |
|---|----|
| Figure 1. Life cycle of adenoviruses. | 9 |
| Figure 2. Schematic diagram of the cancer-selective killing efficacy of oncolytic Ads. | 12 |
| Figure 3. Barriers to systemic delivery of oncolytic viruses. | 13 |
| Figure 4. Schematic representation of a coated microbubble. | 22 |
| Figure 5. Schematic representation of different coated microbubbles. | 31 |
| Figure 6. Optical frame images and streak image of ultrasound contrast agents. | 33 |
| Figure 7. Schematic representation of lipid (left column) and polymer (right column) microbubble interaction with ultrasound of increasing intensity (top to bottom). | 34 |
| Figure 8. Schematic representation of ultrasound causing microbubbles to behave in different ways that leads to endothelial pore formation and increase vascular permeability. | 36 |
| Figure 9. Ultrasound interacts with the microbubble, causing oscillation and eventual destruction, leading to the release of genetic material. | 39 |
| Figure 10. Enhanced drug and gene delivery achieved with the combination of particles and ultrasound. | 40 |
| Figure 11. Ultrasound mediated drug delivery through different means of transport. | 41 |
| Figure 12. Proposed model of the oscillating microbubble enforced pore formation in the cell membrane. | 43 |

| | |
|--|----|
| Figure 13. Possible mechanisms for blood–brain barrier disruption via ultrasound + microbubbles. | 45 |
| Figure 14. Manipulation of the microbubble shell for gene and/or drug delivery. | 49 |
| Figure 15. Fluorescence microscopy images of Ad.GFP (10, 25, 50 MOI) transduced TRAMP-C2 and DU145 cells. | 60 |
| Figure 16. <i>In vitro</i> assessment of Ad.GFP uptake in murine and human carcinoma cell lines. .. | 61 |
| Figure 17. Western blot analysis of TRAMP-C2 and DU145 cells infected with different MOIs of Ad.GFP or Ad.mda-7/IL-24. | 62 |
| Figure 18. Subconfluent murine and human cell lines were infected with replicative competent HAdV at 100 pfu/mL and 1,000 pfu/mL and harvested 24- and 48-hours later. | 63 |
| Figure 19. Annexin-V/PI staining of TRAMP-C2 and DU145 cells infected with Ad.mda-7/IL-24. | 64 |
| Figure 20. DU145 cells infected with Ad.GFP at 10MOI and Ultrasound application. | 67 |
| Figure 21. DU145 Cells infected with Ad.GFP/MBs at 10MOI and Ultrasound application. | 68 |
| Figure 22. TRAMP-C2 cells infected with Ad.GFP at 10MOI and Ultrasound application. | 68 |
| Figure 23. TRAMP-C2 cells infected with Ad.GFP/MBs at 10MOI and Ultrasound application. | 69 |
| Figure 24. Schematic representation of the microbubble delivery of Ad-GFP complexes and ultrasound (US) release in a tumor target site of the mouse. | 84 |

| | |
|---|-----|
| Figure 25. Growth curves and western blot analysis of large DU145 and DU-Bcl-xL tumor xenografts treated with microbubble encapsulated Ad-GFP, Ad.mda-7, or cancer terminator virus (CTV) (Ad.PEG-E1A-mda-7) and treated with ultrasound (US) in the right tumor. | 89 |
| Figure 26. B-mode ultrasound (US) imaging of DU145 tumor xenografts treated with microbubble/US-guided Ad.mda-7 and therapy resistant DU-Bcl-xL tumor xenografts treated with microbubble/US-guided cancer terminator virus (CTV). | 92 |
| Figure 27. Growth curves of control DU145 tumor xenografts injected i.v. using unprotected Ad-GFP, Ad.mda-7 or CTV (Ad.PEG-E1A-mda-7) and treated or not with US. | 94 |
| Figure 28. Growth curves of control DU-Bcl-xL tumor xenografts injected i.v. using unprotected Ad-GFP, Ad.mda-7 or CTV (Ad.PEG-E1A-mda-7) and treated or not with US. | 96 |
| Figure 29a. Microscopy images analysis of DU145 cells transduced with Ads carrying tumor suppressor genes (<i>p53</i> , <i>RB</i> and <i>p130</i>) \pm radiation from 72hrs. | 117 |
| Figure 29b. Microscopy images of adenovirally transduced tumor suppressor genes (<i>p53</i> , <i>RB</i> and <i>p130</i>) \pm radiation from 24-72hrs. | 118 |
| Figure 30. Western Blot analysis of the cell lysates collected at 24, 48, 72 & 96 hours post-adenoviral transduction. | 120 |
| Figure 31. The accumulation/reduction of cells in G1- and G2-phase of cell cycle from a population of DU145 cells that received adenoviral <i>p53</i> (panels a and b), <i>RB</i> (panels c and d) or <i>p130</i> (panels e and f) with or without radiation treatments. | 123 |
| Figure 32. Bar graph representation of apoptosis assay with Annexin-V and Propidium Iodide | |

staining of adenoviral infected tumor suppressor genes (p53, RB and p130) ± external beam radiation at 96hrs analyzed on Accuri C6 flow cytometer.125

Figure 33. Graph representation of apoptosis assay by Annexin-V and Propidium Iodide staining of adenovirally transduced tumor suppressor genes (p53, pRB and p130) ± radiation from 24-72hrs analyzed on Accuri C6 flow cytometer.126

Figure 34. Detection of MB-assisted Firefly Luciferase gene transfer through whole animal imaging.130

Figure 35. *In vivo* study timeline.134

Figure 36. Bar graph of DU145 tumor xenografts volumes (± SD) at week 19 after direct intratumoral injection (IT) of Ad-GFP, Ad.p53, Ad.pRB, or Ad.p130 with and without radiation.134

Figure 37. Bar graph representation of mean tumor volume for all groups (left and right flank mean tumor volume) with standard deviation error bars.135

Figure 38. B-mode ultrasound (US) images of DU145 tumor xenografts treated with MBs/US-guided Ad.p53, Ad.RB or Ad.p130 gene delivery and combination with radiation at different times during treatment schedule.139

Figure 39. Western Blot analysis of the tumors collected at week 19 from *in vivo* study.....140

LIST OF ABBREVIATIONS

| | |
|--------|---|
| 3D-CRT | Three dimensional conformal radiotherapy |
| 4D-RT | Four dimensional radiotherapy |
| ACS | American Cancer Society |
| Ad5 | Adenovirus serotype 5 |
| Ads | Adenoviruses |
| ADT | Androgen deprivation therapy |
| ANOVA | Analysis of Variances |
| ASTRO | American Society for Therapeutic Radiology and Oncology |
| ATCC | American Type Culture Collection |
| BBB | Blood Brain Barrier |
| bRFS | Biochemical relapse free survival rate |
| BD | Becton, Dickinson and Company |
| BLI | Bioluminescence imaging |
| bp | Base pairs |
| CA | Contrast agents |
| CAR | Coxsackie adenovirus receptor |
| CD46 | Membrane cofactor protein |
| CD95 | Cluster of Differentiation 95 or FAS receptor |
| CMV | Cytomegalovirus |
| CTV | Cancer Terminator Virus |
| CRCA | Conditionally replication-competent adenovirus |
| DMEM | Dulbecco's Modified Eagle Medium |

| | |
|-------------------------------|--|
| DR4 | Death Receptor 4 |
| DSB | Double stranded breaks |
| DSG2 | Desmoglein-2 |
| EBRT | External Beam Radiation Therapy |
| ECL | Enhanced Chemiluminescence |
| ECM | Extracellular matrix |
| EPR | Enhanced permeability and retention |
| ESCC | Esophageal squamous cell carcinoma |
| FACS | Fluorescence-activated cell sorting |
| FBS | Fetal Bovine Serum |
| FCS | Fetal Calf Serum |
| FDA | Food and Drug Administration |
| FITC | Fluorescein Isothiocyanate |
| FIX/FX | Coagulation Factor IX/X |
| G ₂ | Gap-2 |
| GAPDH | Glyceraldehyde 3-phosphate dehydrogenase |
| GFP | Green Fluorescent Protein |
| GM-CSF | Granulocyte-Macrophage Colony-Stimulating Factor |
| GST | Glutathione S-transferase |
| GTPase | Guanosine Triphosphate Hydrolase enzyme |
| Gy | Gray, unit of radiation |
| H ₂ O ₂ | Hydrogen Peroxide |
| HAdV | Human adenoviruses |

| | |
|---------------|--|
| H&E | Haematoxylin and eosin stain |
| HEK | Human Embryonic Kidney |
| HIFU | High Intensity Focused Ultrasound |
| HRPC | Hormone-refractory prostate cancer |
| HSPG | Heparan sulfate proteoglycan |
| HT | Hormone Therapy |
| hu-Ads | Human Adenoviruses |
| IFN- γ | Interferon gamma |
| IFNs | Interferons |
| IFP | Interstitial fluid pressure |
| IL | Interleukin |
| IL2 | Interleukin 2 |
| Ig | Immunoglobulin |
| IgG | Immunoglobulin G |
| IMRT | Intensity-modulated external beam radiotherapy |
| IR | Irradiation |
| IT | Intratumoral |
| IV | Intravenous |
| Kb | Kilobase |
| LINAC | Linear particle accelerator |
| LUC | Firefly luciferase gene |
| M | Mitosis |
| MAP | Mitogen-activated protein kinases |

| | |
|----------------|--|
| MB | Microbubble |
| Mda-7 | Melanoma differentiation associated gene-7 |
| MI | Mechanical Index |
| MOI | Multiplicity of infection |
| MS | Mechanosensitive |
| MU | Monitor Units |
| NF- κ B | Nuclear factor kappa-light-chain-enhancer of activated B cells |
| NIH | National Institute of Health |
| NP | Nanoparticle |
| OCT | Optimum cutting temperature compound |
| PAGE | Polyacrylamide Gel Electrophoresis |
| PBS | Phosphate Buffered Saline |
| PC | Prostate Cancer |
| PCR | Polymerase Chain Reaction |
| PEG-3 | Progression Elevated gene 3 |
| PEG | Polyethylene glycol |
| PET | Positron emission tomography |
| PI | Propidium Iodide |
| pTEN | Phosphatase and Tensin homolog gene |
| Prom | Promoter |
| PSA | Prostate-specific antigen |
| Ras-DN | Ras family dominant negative gene |
| Rb | Retinoblastoma |

| | |
|---------|---|
| RB | Retinoblastoma gene |
| RBL2 | Retinoblastoma Like 2 |
| RNAse A | Ribonuclease A |
| ROS | Reactive oxygen species |
| RP | Radical Prostatectomy |
| RPMI | Roswell Park Memorial Institute |
| RT | Radiation Therapy |
| SAHFs | Senescence-associated heterochromatic foci |
| SAS | Statistical Analysis System |
| SDS | Sodium dodecyl sulfate |
| SWOG | Southwest Oncology Group |
| TBST | Tris-Buffered Saline and Tween 20 |
| TLR | Toll-like receptor |
| TRAMP | Transgenic Adenocarcinoma of the Mouse Prostate |
| UCA | Ultrasound Contrast Agent |
| US | Ultrasound |
| UTMD | Ultrasound Targeted Microbubble Destruction |
| UV | Ultraviolet |
| wt | Wild type |

ABSTRACT

A major challenge for effective gene therapy is systemic delivery of viruses carrying therapeutic genes into affected tissue. The immunogenic nature of human adenoviruses (Ads) limits their use for intratumoral (IT) injection in gene therapy. Ads transfection is further hampered by the fluctuating presence of Coxsackie and Adenovirus Receptor (CAR) and integrins on the cells' surface. To circumvent these limitations we developed a novel approach wherein Ads are encapsulated inside the shell of lyophilized, lipid-encapsulated, perfluorocarbon microbubbles (MBs)/ultrasound (US) contrast agents, which act as delivery vehicles for a site-specific gene transfer system.

We performed infection studies with Ad.GFP (Green Fluorescent Protein), Ad.mda-7 (melanoma differentiation associated gene 7) and CTV.mda-7 on human DU145 and mouse prostate cancer cells as well as observed enhanced GFP expression when Ad.GFP was delivered by MBs and US. Our results show that US breaks open the MB/Ads complexes by undergoing cavitation at the sonoporated site, which allows Ads to transfer their transgene only to the sonoporated region. Cavitation collapse of the MBs creates small shockwaves that increase cell permeability by forming temporary micropores on the cell surface bypassing the receptor-mediated dependence of Ads for transfection. Fetal bovine serum (FBS) containing complement did not allow the unprotected Ads to infect the cells; however, MBs complexed with Ad.GFP did infect DU145 and TRAMP-C2 cells in a FBS rich media.

We studied MB assisted gene delivery of reporter (GFP) and therapeutic genes (p53, Rb, Rb2 (p130) and Mda-7/IL-24) into prostate cancer (PC) xenografted in immune-compromised athymic mice. The results demonstrated that MBs protect the host from unspecific viral immune response thus protecting the viral payload and allowing for intravenous (IV) injection rather than

IT injection. Additionally, Ad gene transfer was enhanced at the targeted/sonoporated mice tumor xenografts. This research demonstrated mda-7's efficacy in reducing primary (treated) and untreated tumors that simulated the presence of metastasis in athymic mice xenograft models bearing human PC cells. Bystander anti-tumor activity of mda-7, a secreted cytokine was noted for non-targeted tumors.

Earlier *in vitro* studies on the combination of radiation and gene therapy (Ad.p53, Ad.Rb, and Ad.p130) demonstrated an increase in the percentage of cell death for DU145 cells. We also studied UTMD (ultrasound targeted microbubble destruction) gene therapy in combination with external beam radiation for radiation resistant PC. The results demonstrated an enhanced therapeutic benefit of tumor suppressor genes in radiation resistant PC. We also demonstrated an increase in the expression of tumor suppressor genes at the tumor site due to MBs and US.

These findings highlight the potential therapeutic benefit of this novel image guided gene transfer technology alone or in combination with external beam radiation for prostate cancer patients with therapy resistant disease.

CHAPTER I: PROSTATE CANCER AND TREATMENT STRATEGIES

Prostate cancer

Prostate cancer (PC) is the most common malignancy in men and the second leading cause of cancer related deaths in the United States [1]. According to the American Cancer Society (ACS), PC represents 25% of newly diagnosed cancers every year [2]. There are more than 1,100,000 new cases of PC and 300,000 related deaths worldwide each year. In the United States about 240,000 new cases of PC are reported annually with a mortality rate >15% due to widespread implementation of prostate-specific antigen (PSA) testing and effective treatment of early stage PC disease [3-5].

The disease is primarily diagnosed in men above the age of 40, with a median age above 60 years [3]. The risk of incidence increases as one grows older. PC biology is heterogeneous as it ranges from indolent type where tumors progress slowly or not at all for several years to others that may progress more rapidly and be fatal after a few years. PC arises from different stresses such as chronic inflammation, oxidative stress, immune surveillance loss, and somatic alterations, which lead to genetic changes that transform the normal epithelium into pre-neoplastic lesions to invasive carcinoma. Therapeutic options vary depending on the severity of the condition, age of the patient, staging, Gleason score and serum PSA level [6].

Organ confined disease staged T1/T2 with Gleason score ≤ 7 that lacks aggressive features [7] is suitable for radical prostatectomy (RP) and radiation therapy (RT) with external beam irradiation therapy (EBRT) or brachytherapy [8, 9]. This treatment option has shown 5 to 10 year survival rate with significant morbidity, erectile dysfunction in 30-70% of cases and stress incontinence in up to 10% of the patients [6, 10]. In recent years, minimally invasive therapies have been developed for patients with localized prostate cancer such as three-

dimensional conformal radiotherapy (3D-CRT), brachytherapy, intensity-modulated external beam radiotherapy (IMRT), cryosurgical ablation of the prostate and laparoscopic radical prostatectomy. These treatment strategies are for patients who are either not eligible for surgery or who do not want to risk the potential side-effects of surgery [6, 11-14].

Cancer with a Gleason score ≥ 8 which exhibits aggressive features and found outside the prostate [7] and spread to other organs such as bladder, rectum and lymph nodes results in poor survival rate compared to localized PC. Approximately 30-35% is initially diagnosed as metastatic while 25% of patients develop metastases during follow up. Metastases are commonly found on the bone with an X-ray showing osteoblastic lesions or a bone scan as hot spots with areas of increased activity [15]. In such cases, RP followed by RT with hormone therapy (HT) can prolong survival but with negative quality of life [3]. HT with anti-androgens is the standard therapy for stage T4 PC that reduces serum levels of testosterone to castration levels, which eventually becomes non-responsive to androgen ablation. When these therapies fail and the cancer reoccurs there is a median survival of 2.5 years [15, 16]. Current therapy options for patients with hormone-refractory prostate cancer (HRPC) include RT and cytotoxic chemotherapeutic agents, such as mitoxantrone, estramustine and taxanes [15, 17]. These approaches only have a palliative benefit and show no consistent impact on survival [15]. No effective therapy exists for patients with metastases thus mandating the development of novel, more efficacious and innovative treatment approaches [18].

Different approaches have been tested with varying results. For example, gene therapy has been used to combat and cure a wide range of pathologies including locally advanced cancer but the major limiting factor has been the development of an effective delivery system. Metabolism of genetic materials by serum esterases prohibits intravenous administration.

Additionally, genes are macromolecules and their size greatly hinders passage across the capillary fenestrations of blood vessels without assistance. We and others have demonstrated viral vectors to be efficient delivery systems resulting in high levels of transgene expression. However, the antigenic nature of viruses leads to their rapid inactivation by the immune system. Additionally, the viruses are non-specific. This requires direct target organ injection with or without image guidance or operative bed injection. Current gene therapy technology is still in its infancy but the promise of molecular medicine is so immense that further research is needed.

Treatment Strategies:

Radiation Therapy

Ionizing radiation is primarily used to treat cancers by targeting critical cell components resulting in DNA damage directly by high radiation or indirectly by the action of free radicals formed as a result of ionization of water molecules by low radiation [19, 20]. The resulting DNA damage can result in double stranded breaks (DSB) that are difficult to repair and most toxic to the cancer cells [19]. Normal cells have intact mechanisms that repair the majority of DNA damage thus protecting the normal cells from harm. If the mechanism cannot repair the DNA, radiation induces apoptosis by either stimulating death receptors such as DR4 (death receptor 4) or CD95 (Fas) at the cell surface or halts cell cycle progression at distinct phases [19, 21]. The effect is most pronounced during M (mitosis) and G₂ (Gap-2) phases of the cell cycle [22, 23]. Failure to undergo apoptosis may contribute to resistance of cancer cells to the therapeutic modalities.

Low dose rates of radiation can also be toxic as the oxygen reacts with the free radicals (reactive oxygen species (ROS)) formed during the ionization of water producing more toxic byproducts that make the cell sensitive to ionization radiation [23]. Solid tumors contain regions

with low blood supply resulting in reduced oxygen concentration (hypoxia) thus making these regions more resistant to ionization radiation [21]. Even though improvements in radiotherapy regimens are available the efficacy is still disappointing with regards to solid tumors.

Radiation can be delivered internally through radioactive seed implants called brachytherapy. Implants can be precisely placed into a body cavity, into the tissue, into the lungs and into blood vessels. The radiation sources deliver high doses of radiation to the specific tumor while the radiation dose drops off within the adjacent normal tissue [19]. Zelefsky et al. [12] reported the 8-year relapse free survival rate of 74% and 61% for low and intermediate risk groups respectively using Phoenix ASTRO (American Society for Therapeutic Radiology and Oncology) criteria for a multi-institutional study following brachytherapy [6].

The most common form of RT is delivered externally through a beam called EBRT. In most PC cases, RT is accompanied with RP or androgen deprivation therapy (ADT) [24]. Adjuvant RT has shown to benefit men with adverse pathologic features with Gleason scores ≥ 7 at least in minimizing biochemical recurrence risk [25]. Thompson et al. from the Southwest Oncology Group (SWOG) showed an overall survival with adjuvant RT with 10 year estimates of 74% vs. 66% for patients with 60Gy to 64Gy and a metastasis free survival at 71% vs. 61% in adjuvant RT vs. no RT cohorts [25, 26]. Ten year survival rate following RT for well differentiated, moderately well differentiated and poorly differentiated PC is about 90%, 75% and 50% [27]. Along with the benefits seen with RT, complications such as rectal complications, urethral strictures and total urinary incontinence are common [25].

RT can be delivered in a fractionated dose of 1.8 - 2.0 Gy (Gray, unit of radiation) per day for 7-8 weeks (5 days per week) or until a total of 60 - 80Gy is delivered [28]. Pollark et al., showed that dosage has a direct impact on treatment effectiveness in a Phase III trial where they

compared 70Gy/2Gy versus 78Gy/2Gy, showing a significant difference (64% vs. 70% respectively) in the 6-year biochemical relapse free survival rate (bRFS) [29]. Similar results have been published in Phase III trial by Dearnaley et al., when comparing 64Gy/2Gy with 74Gy/2Gy in a 10-year bRFS [30]. Additionally, treatment strategy that employs less frequent and larger fractions, termed hypofractionated radiation, may be more efficacious. Moderate (<5 Gy/day) hypofractionated RT has shown similar efficacy with an improved side effect profile while extreme (≥ 5 Gy/day) hypofractionated RT is currently being evaluated but showing promising efficacy [28]. As dose is increased the risk of side effect increases as well.

Advances in imaging have raised the therapeutic ratio (the index between cytotoxic effects and normal tissue complications) and minimized damage to local tissue resulting in a decrease in the side effects seen due to RT. Advances in imaging has led to vast improvements in RT such as 3DCRT or IMRT and four dimensional RT (4D-RT) which splits the beam into several lower intensity beams sparing damage to surrounding normal tissue. With these advances more patients are being treated with doses exceeding 72Gy [31].

In this study we treated human DU145 PC tumors with EBRT from a clinical linear particle accelerator (LINAC) model 21EX and model 6EX that produced 8Gy X-rays for the cancer treatment. These particle accelerators at the Tri-State Regional Cancer Center in Ashland, Kentucky offer bremsstrahlung x-ray energy of 6 MV, which was used in these investigations as well as a rapid dose delivery to the targeted tumor at a rate of 6 Gy/MU [32].

High Intensity Focused Ultrasound

High Intensity Focused Ultrasound (HIFU) is used as a treatment for localized PC. It is a non-invasive and non-ionizing technique that induces coagulation, necrosis, cavitation and heat shock through intense US energy that thermally ablates a portion of the tissue situated at the focal point. US energy is delivered with a high-powered transducer, which is placed in the rectum to generate US waves that travel through the walls of the rectum and deposit energy to a focal zone in the prostate gland. There is no need for a surgical exposure or insertion of instruments into the lesion [6, 33].

The high powered US causes a rise in temperature up to 70 - 80°C [34]. This elevation of tissue temperature leads to melting of the lipid membranes and protein denaturation (>43°C) that results in irreversible tissue damage called coagulative necrosis [34, 35]. Similar tissue damage caused by a cavitation phenomenon can be achieved with bubble implosion and mechanical tissue disruption as a result of the interaction between US and MBs of water in the sonicated tissue enhancing tissue ablation [35].

In the past 15 years there have been 30,000 prostate HIFU treatments, mainly in Europe [35]. In most clinical trials [6, 35, 36], patients had a localized PC (stage T1/T2) with Gleason scores ranging from 2 to 10 and received HIFU because the patients were either unsuitable for or unwilling to undergo RP. Uchida et al. [6] reported that after HIFU the biochemical disease free 5 years rate was at 84%, 64% and 45% in low, intermediate and high-risk PC groups using Phoenix criteria. Pfeiffer et al. [36] also assessed the negative biopsy rates after HIFU at 84.2%, 63.6% and 67.5% for the low, intermediate and high-risk PC groups. Similarly after HIFU, 5-year biochemical free survival rates was reported to be 84.8%, 64.9% and 54.9% for aforementioned PC risk groups. Lastly, they also mentioned 5-year disease free survival rates as

81.7%, 53.2% and 51.2% for the respective PC risk groups [36].

HIFU has advantages over current treatment modalities as it is non-invasive and non-ionizing allowing for repeated treatments of the affected tissue as well as the ability to affect a distant tissue [35, 37]. The disadvantages include the inability of US to travel through air preventing treatment within lung or lumen of most hollow organs within the body and long (1-3hrs) exposure times depending on the size of the tumors [35]. Most common complications associated with HIFU are urinary retention, urinary tract infections, urinary incontinence and erectile dysfunction [35]. Presently, HIFU has some limitations and long-term clinical studies are needed to evaluate cancer specific and overall survival. Refinement of the HIFU and transducer technology will improve its therapeutic benefit making it an attractive treatment modality.

Currently, the cavitation phenomenon of microbubbles (MB) is being explored in relation to different US intensities as a potential drug delivery vehicle. The underlying mechanism is yet to be fully understood but there is growing evidence that suggest MB cavitation can elicit biological and mechanical changes that allow for the temporary uptake of drugs. Our lab has further explored this area of drug delivery with the intent to translate this technology from bench to bedside.

Gene Therapy

Gene therapy is a therapeutic drug delivery and vaccination method that can be used to treat a large array of genetic and non-genetic diseases. It uses genetic materials such as DNA and RNA to rewrite or reverse the pathological conditions that account for the transformation of normal cells to a malignant or diseased phenotype. There have been significant improvements in the treatment of a variety of different malignancies including PC.

Different strategies include the use of non-viral and viral vehicles that are suitable for integrating the genetic material into the host cell. There are distinct advantages and disadvantages for each delivery vehicle. Non-viral vehicles are suitable for their simplicity, packaging capacity, potential for large scale production and inducing fewer immunological responses. These vehicles have poor transfection and transduction efficiency to elicit a therapeutic benefit. Viral vehicles on the other hand can be engineered and finely tuned while retaining the capacity to deliver genetic material at a high transfection and transduction efficiency. However, our immunological system has evolved to counterattack against these viral pathogens by forming neutralizing antibodies that hamper its therapeutic potential.

Gene transfer can be done *in vivo* or *ex-vivo*. *In vivo* gene transfer is performed in the host via an intratumoral (IT) injection. It is cost effective and tailored to a class of patients rather than an individual. But the gene transfer efficiency is poor due to the mode of delivery and the stimulation of the hosts' immune system. *Ex-vivo* gene transfer is performed on surgically harvested cells that are genetically engineered and re-introduced back into the host [15]. *Ex-vivo* gene transfer is typically done on clonal expansive cells such as dendritic cells, macrophages, monocytes, etc. for vaccination based gene therapy.

There have been several gene therapy clinical trials, which have shown potential towards treating prostate cancer. These therapies include vaccine therapy that uses various cytokines such as interleukin 2 (IL2) or granulocyte-macrophage colony-stimulating factor (GM-CSF), suicide cytotoxic therapy such as HSV-thymidine kinase or certain toxins, transfection of suppressor genes such as p53 or retinoblastoma (Rb), oncolytic viruses such as CV787 or CN-706 that have been designed specifically to replicate preferentially in prostate cancer cells and anti-sense therapy such as bcl-2 and C-myc to block oncogenes [15, 38-40]. In this study we have

performed gene therapy with melanoma differentiated associated gene 7 or interleukin 24 (mda-7/IL-24), p53, retinoblastoma (Rb), retinoblastoma like protein 2 (p130) on PC models.

Adenoviruses

Adenoviridae are icosahedral non-enveloped viruses with a 30 to 40kb linear double stranded-DNA genome [41]. Ads have been isolated from a number of different species with over 100 reported serotypes [42]. Human adenoviruses (HAdVs) consist of more than 55 serotypes that are divided according to haemagglutination and genome sequences into seven species, HAdV-A, B, C, D, E, F and G. Members of species C, serotypes 2 and 5 Ads, are commonly used as vectors for gene therapy [42-44].

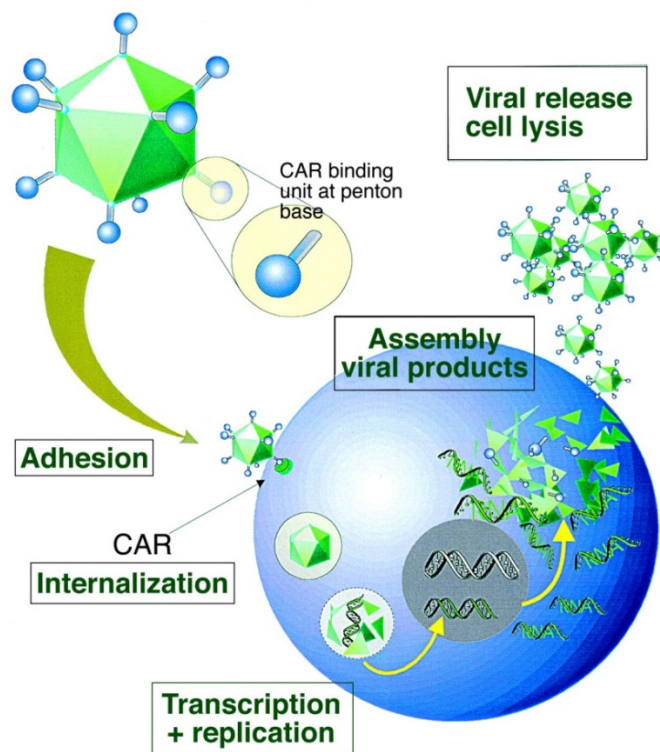


Figure 1. Life cycle of adenoviruses. Replication-defective adenoviral vectors express the proteins encoded on their DNA but do not enter the lytic phase. (Adapted from Vorburger and Hunt, *The Oncologist*, 2002 [42].)

The life cycle of an adenovirus can be divided into several stages (Fig. 1). During the infection stage, virus surface proteins, such as hexon proteins, penton base proteins, and fiber proteins attach to cellular receptors such as the coxsackie adenovirus receptor (CAR), integrins $\alpha V\beta 1/2/3$, membrane cofactor protein (CD46), desmoglein-2 (DSG2), coagulation factor IX and X (FIX/FX), heparan sulfate proteoglycan (HSPG), etc. [45]. After entry into the nucleus, genes from the early region 1 (E1a and E1b) are quickly transcribed (Fig. 1); these affect cellular proteins that modulate several cellular processes, such as preventing apoptosis or inducing cell cycle entry [46]. Four non-contiguous regions of the genome are expressed (E1 to E4) during the early phases of viral replication. These regions serve as master transcriptional regulators that start the process of viral gene expression leading unto genome replication. During genome replication, the major late genes (L1 to L5) drive the viral replication and code for proteins that make up components of the viral capsid or are involved in assembly of the capsid. Other viral elements (cis or trans genes) are responsible for the origin of replication or the packaging signal that condenses the DNA but these must be carried out by the virus itself [42].

The trans genes can be complemented or replaced by foreign or therapeutic DNA. At least three such regions of the viral genome can accept insertions or substitutions of DNA: a region in E1, E3, and between E4 and the end of the genome. The E1 deletion renders the recombinant virus replication-defective, and thus provides an important safety feature [47]. The first-generations of non-replicating ads are derived from E1/E3 deleted wild type (wt) Ads [41]. Newer generations of Ads have deleted or inactivated entire coding regions (E2, E3 or E4 regions) to increase DNA capacity and to alleviate antiviral host adaptive immunity [41]. However, to achieve a significant antitumor response Ads needs to be administered multiple times, which can still provoke an immune response that mediates viral clearance [44, 48].

Ad vectors have several advantages: first, they rapidly infect a broad range of human cells; second, they yield high levels of gene transfer; third, they have low pathogenicity in humans, fourth, they can accommodate relatively large (~7.5 kilobase (kb)) segments of DNA; fifth, they can transduce non-proliferating (quiescent) cells; sixth, the viral genome does not undergo rearrangement; seventh, they allow for the transmission of their genes into the host nucleus but do not insert them into the host chromosome; eighth they are easy to manipulate and finely retuned because the technology of Ad production at high titers is well established and the Ad structure, genome and replication cycle is well characterized [42, 48, 49]. Ads are the most commonly used vector in clinical trials (~471 clinical trials or ~23% of all clinical trials initiated until January 2015) and approximately 75% of the 471 clinical trials have been initiated to treat PC (51 clinical trials) [45, 50].

Conditionally Replication-competent Adenoviruses (CRCAs)

Replicating Ads or oncolytic Ads have the ability to infect a small portion of the tumor and kill the tumor cells at the end of their lytic cycle. Their resulting progeny are now capable of infecting the neighboring tumor cells ensuring a significant increase in the efficacy of gene delivery coupled with cytolytic activity (Fig. 2). The replication competence of Ads can be made conditional on the biology of the cells being infected. These replicating viruses are called conditionally replicating Ads.

CRCAs can be made by modifying the adenoviral proteins to enable the virus to replicate only in cells that bear the cancer related phenotypes [51]. For example, Ads deficient in E1B (ONYX-015) contain a deletion of 827 base pairs (bp) in the E1B region that allows the virus to replicate only in tumor cells lacking functional p53 [52]. In normal adenovirus, E1B codes for a

55kDa protein that binds and inhibits p53 in normal cells which in turn blocks viral replication. The ONYX-015 infected normal cell would exhibit p53 mediated growth arrest or apoptosis. Thus functional ONYX-015 is restricted to p53 deficient cells, resulting in tumor selective destruction [51].

CRCAs can also be made by placing key viral proteins under the regulatory control of cell-specific gene promoters that restrict the viral lytic cycle to only the target cells [51]. For example, Ad named CN706 contains a human PSA promoter gene that is cloned upstream of the E1A viral gene which starts the early viral replication phase. In this study, we used cancer terminator viruses (CTVs) that contained progression elevated gene-3 (PEG-3) promoter. This promoter drives the expression of E1A and E1B genes thus ensuring cancer specific replication. The CTV also contains cytomegalovirus (CMV) promoter that regulates the expression of melanoma differentiated associated gene 7 or interleukin 24 (mda-7/IL-24) [53].

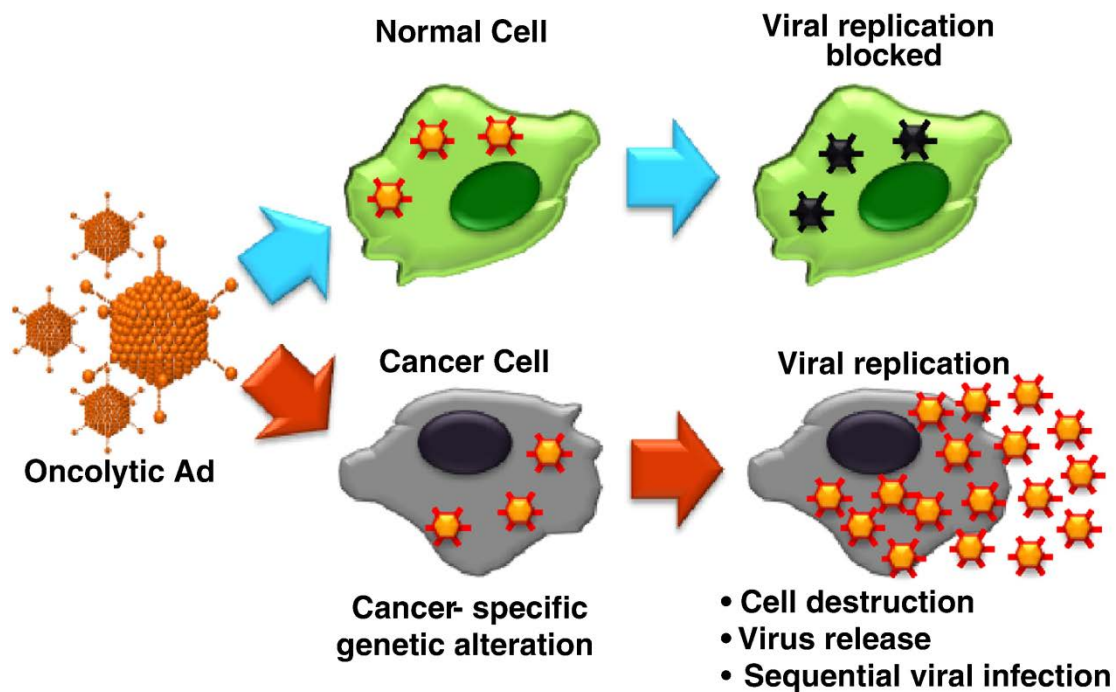


Figure 2. Schematic diagram of the cancer-selective killing efficacy of oncolytic Ads. Oncolytic Ads specifically kill tumor cells at the end of their lytic cycle, while sparing normal cells.

Replicated viral progeny then spread throughout a tumor, infect, and lyse surrounding cancer cells, ultimately leading to improved antitumor efficacy over non-replicating Ads. Moreover, the amplification and propagation of therapeutic genes using replicating viruses in infected neighboring cancer cells highlights the potential of replicating virus-based therapy. (Adapted from Choi, et al. *Advanced Drug Delivery Reviews*, 2012 [54].)

Barriers to Virotherapy

Gene therapy makes efficient use of targeting viruses for cancer therapy, but several barriers exist that limit the delivery of viruses from reaching and spreading throughout the tumor. These barriers forces an increase in dosage of the viral particles thus increasing the possibility of adverse events [55].

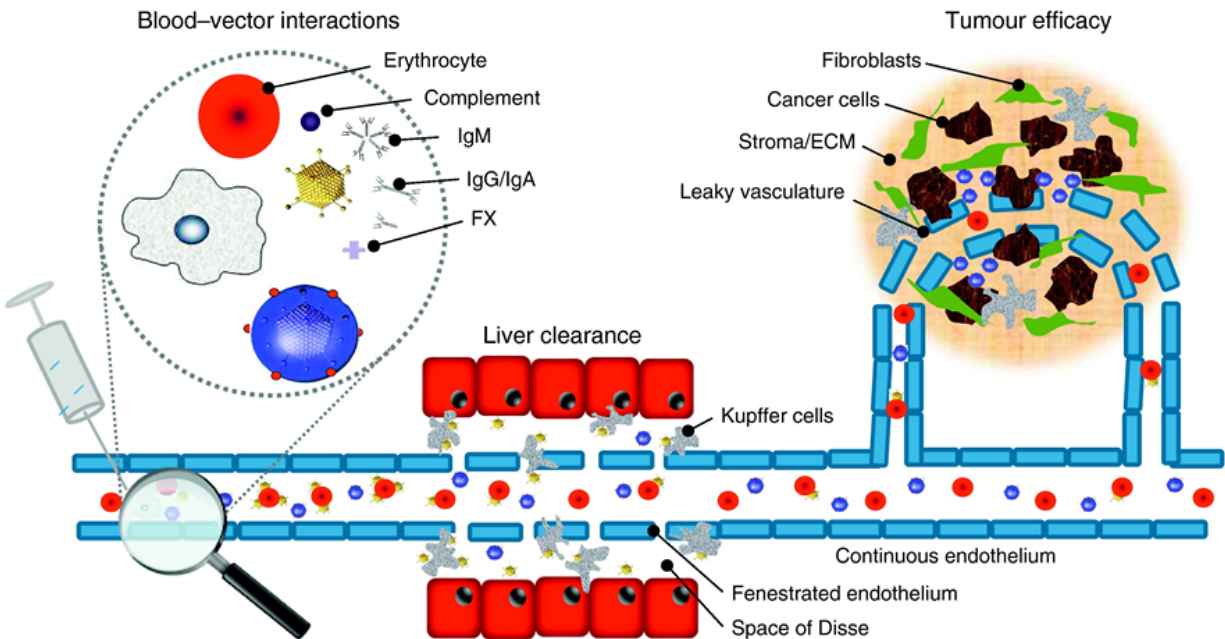


Figure 3. Barriers to systemic delivery of oncolytic viruses. There are three main areas that must be addressed to enable systemic delivery of virus particles, namely (i) avoiding neutralization by components of the blood stream including complement, FactorX, leukocytes, erythrocytes and

antibodies, (ii) minimizing unwanted infection of irrelevant cells, notably hepatocytes, which are usually present in vast excess, and avoiding premature scavenging by phagocytes, such as hepatic Kupffer cells, (iii) maximizing extravasation within tumor vasculature and penetration to infect all viable tumor cells whilst avoiding other components of the interstitium. Polymer coated viruses present one promising approach to address these barriers, although several other technologies are also under development. Abbreviations: ECM: extracellularmatrix, IgA: ImmunoglobulinA, IgG: ImmunoglobulinG, IgM: ImmunoglobulinM, FX: FactorX. (Adapted from Tedcastle, et al. Drug Discovery Today, 2012 [56].)

Current clinical trials in gene therapy are limited to intratumoral injections. This delivery method has the advantage of delivering large payloads to the tumor site and minimizing interactions with other cells but the viral spread is often limited to the needle track due to pressure gradients, binding to extracellular matrix (ECM) components, and limited convection [57, 58]. For massive tumor regression, infection must spread to cover a large volume of the tumor mass. Poorly organized leaky vasculature (Fig. 3) increases the interstitial fluid pressure (IFP) resulting in the loss of convection throughout the tumor making macromolecular transport dependent on passive diffusion [55, 59]. However, in a solid tumor, the complicated structure of the ECM (Fig. 3), which is composed of proteoglycans formed by both neoplastic and normal stroma, acts as a physical barrier against the penetration of the viruses [54]. Thus passive diffusion is limited due to the composition and organization of the tumor microenvironment. In addition, both specific (e.g., neutralizing Abs or cytotoxic T cells) and nonspecific (e.g., phagocytes or anti-viral cytokines) immune response mechanisms may also limit spread of viral particles [57].

The other major hurdle is to successfully use systemic virotherapy to deliver viral particles into tumor nodules [56]. Virus arriving at the tumor site must extravasate into the tumor. Extravasation is dependent on the adequate blood supply, tissue perfusion and tumoral enhanced permeability and retention (EPR) for transvascular transport. Tumor vasculature is chaotic in terms of microvessel length, diameter, spatial distribution, blood flow velocity and direction causing heterogeneous blood perfusion throughout the tumor [55]. The tumor vasculature causes regions of low-oxygenation leading to hypoxic tumor environments that become inaccessible to the virus. These regions are important as they house tumor stem cell niches and treatment resistant cells that trigger relapses in patients [55, 60, 61]. On the contrary, leaky tumor-associated vasculature can sometimes enable limited extravasation of virus particles through passive diffusion [56]. The passive diffusion is mediated by EPR but it is not consistent because of the differences in pore size and the abrupt changes in blood perfusion [55, 62, 63], thus extravasation into the tumor site is a limiting factor of systemic delivery. Lastly, once injected into the vasculature, the viruses undergo various interactions with the immune system, thereby reducing viral efficiency.

Ads are regarded as pathogens by the body and are attacked by the host immune system. They mostly induce the innate arm of the immune system resulting in the inactivation of the Ads, the inflammation of the transduced tissue due to T- and B-cell targeting the transduced tissue[64] and efficient clearance of Ads by the immune cells [41]. In fact, within 24 hours after IV administration, 90% of the Ad vector is eliminated from the mouse liver [65]. Systemic delivery of Ads into the bloodstream also exposes the virus to plasma proteins and blood cells (Fig. 3) [58]. The resulting interactions include the neutralization and/or opsonization by antibodies and complement (C3a)[66], phagocytosis by neutrophils and macrophages, sequestration on

erythrocytes as well as others [56, 58]. The innate immune response also involves the induction of cytokines by the viral capsid proteins and interactions with leukocytes, epithelial and endothelial cells resulting in signal transduction via MAP (Mitogen-activated protein kinases) and NF- κ B (nuclear factor kappa-light-chain-enhancer of activated B cells) [41] as well as through Toll-like receptors and lectins in the plasma membrane and endosomes [44]. The adaptive arm of the immune response is seen in patients with pre-existing immunity. This immunity leads to a high prevalence of virus neutralization antibodies against Ads, preventing the vector from transducing cells efficiently and lowering the overall effect [67]. Lastly, non-specific uptake by other tissues such as the lung, Kupffer cells in the liver, spleen and tissue resident macrophages all contribute to the rapid clearance of Ads. Thus these immune reactions severely limit the benefit of systemic delivery, intratumoral delivery, repeated administration and administration of high-titer Ads.

CHAPTER II : ULTRASOUND CONTRAST AGENTS IN CANCER THERAPY

This manuscript is a revised version of Chapter 13 from *Cutting Edge Therapies for Cancer in the 21st Century* (2014)

Nande R¹ and P.P. Claudio^{1,2,3} (2014) Ultrasound Contrast Agents in Cancer Therapy
In: Claudio, P.P., Vogiatzi, P., editor. *Cutting Edge Therapies for Cancer in the 21st Century*.
Bentham Science Publisher.

Marshall University School of Medicine, Huntington, WV

¹Department of Biochemistry and Microbiology

²Department of Surgery, Joan C. Edwards School of Medicine

³Corresponding author

Marshall University School of Medicine – McKown Translational Genomic Research Institute

Department of Biochemistry and Microbiology

1600 Medical Center Drive, Huntington, WV, 25701

Phone: 304-696-3516

FAX: 304-696-3713

Email: claudiop@marshall.edu

ABSTRACT

The field of ultrasound has expanded since the discovery of ultrasound contrast agents (UCAs) from diagnostics to therapeutic use. UCAs are known as microbubbles (MBs), which can be chemically and physically manipulated to improve their therapeutic potential. MBs can be tailored to bind to specific diseased tissues and act as carriers of different chemo-drugs and genetic materials. These engineered MBs can behave differently to ultrasound intensities resulting in different cavitation methods. Though the underlying mechanism is yet to be fully understood, there is evidence to suggest that mechanical pore formation of cellular membranes allows for the temporary uptake of drugs. The cavitation of MBs can induce temporary and reversible enhancement in the permeability of both individual cells as well as the endothelium including the blood brain barrier. There are too many side-effects and immune responses to current cancer and diseased treatments. MBs protect the immunogenic drugs from eliciting a detrimental response when delivered through the vasculature. They also help reduce the drug dosage by improving drug targeting and drug response. Thus, MBs can be used as vehicles for localized drug delivery and gene therapy allowing us to further develop the potential of curing cancer and other diseases.

Keywords: Microbubbles, ultrasound, ultrasound contrast agent, chemotherapy, adenovirus, Polyethylene glycol, perfluoropentane, phospholipid, sonoporation, cavitation, Blood Brain Barrier (BBB), Gene Therapy, Chemotherapy, DNA, RNA, Protein, siRNA, miRNA, Drug delivery.

INTRODUCTION

Historical Overview

Ultrasound (US) is the most widely used diagnostic imaging modality. This modality provides a safe, non-invasive, and portable real-time imaging at a low cost [68]. US sound waves have a frequency between 20 Hz to 20 kHz that is inaudible to the human ear [69]. Typically, in ultrasonography the diagnostic frequency ranges from 1-10 MHz [70]. To produce a US image a transducer that broadcasts the US wave pulses is placed on the skin or inside the body. These waves are reflected by the interfaces between different tissues or structures in the body. The imaging software system converts these reflected waves into electrical pulses and digitizes them [68]. Imaging is possible because the speed of sound in the tissue ($\sim 1500\text{m/s}$) is known [71]. Biological tissues (except lung or bone) mainly consist of water, which has low compressibility, and sound waves propagate without significant scattering or reflection [71]. Thus the backscatter energy from tissue contains less or no harmonics [72]. Blood, a liquid phase material, has low compressibility and scatters US poorly, but the infusion of ultrasound contrast agents (UCAs) or microbubbles (MBs) can increase the scattering and reflection of the ultrasonic waves [68]. Thus, harmonics can be used to differentiate between blood flow with UCAs and the surrounding tissue [72].

The discovery of microbubble (MB) agents came from an accidental observation by Dr. Charles Joiner, a cardiologist in the late 1960s. Dr. Joiner performed an M-mode echocardiogram by injecting a patient with indocyanine green through the left ventricle to measure cardiac output. He observed a transient increase in the US signal from the ventricle after each injection [73, 74]. It was later shown that small bubbles forming at the catheter tip caused the increase in the signal, but subsequent research into duplicating the results was not successful [74]. In 1968,

Gramiak and colleagues observed a cloud of echoes after the injection of agitated saline in the aortic root [73]. They showed that the backscatter of the US for the blood pool can be increased by adding the gas bubbles that exist in agitated saline [72, 73]. Agitated saline is still used for the detection of right to left shunts in the heart [75]. These bubbles were large and unstable and had a short half-life and did not persist in the blood for long periods of time which limited their use [72]. Only right heart imaging was achieved because the first generation of UCAs that entrapped air and carbon dioxide in agitated saline and hydrogen peroxide could not pass through the pulmonary circulation [76].

Mixing some of the patient's blood with saline was found to markedly increase and prolong the stability of the bubbles [74]. Dr. Feinstein [77] found that albumin was the blood component improving MB stability [74]. Later on Feinstein developed the sonication method that produced more stable MBs, whose size could be controlled [78]. In 1994, Albunex (Molecular Biosystems, San Diego, CA) became the first commercially available contrast agent approved for human use in the United States. Albunex has a coating made of human serum albumin [72]. Coating of MBs resulted in the stabilization of MBs with different substances such as phospholipid, albumin, or polymers. Coated MBs formed the second generation UCAs that had a mean diameter less than 8 μm , which guarantees that the UCA could pass through the pulmonary circulation and reach various organs. MBs survived longer in the blood stream due to their lower solubility in water and had a strong harmonic response [76].

The making of more stable, more effective UCAs revolutionized the pharmaceutical industry. The second commercially available contrast agent, Levovist, became available in Europe and Japan in 1996. Levovist like its forerunner Echovist [74] (Bayer Schering Pharma AG, Berlin, Germany) consists of galactose microcrystals whose surfaces provide absorption

sites on which air bubbles form when suspended in water [72]. Echovist performed poorly in the right heart because its intravenous (IV) injected MBs were not stable and failed to cross the lung capillaries [74]. Levovist MBs were further stabilized with a trace amount of palmitic acid [72], thus making it stable in the blood for 1-4 min, which increased the US signal by ~20 dB [74]. Levovist MBs formed in the blood flow while EchoGen® (Abbot Laboratories, Chicago, IL, USA) achieved MB formation through a totally different mechanism. EchoGen® consists essentially of a perfluoro-compound (perfluoropentane), which is liquid at room temperature but becomes a gas at body temperature. EchoGen® is prepared as an aqueous emulsion with surfactants that change to gas on injection, with the formation of MBs as small as 2–8 microns [74].

Since 1997, contrast agents (CAs) are further stabilized by replacing the air core with high-molecular-weight inert gases such as perfluorocarbons, which have a lower solubility and diffusivity in aqueous liquids compared with air [72]. Clinically proven agents based on this principle include SonoVue (SF₆ gas), Definity/Luminy (C₃F₈), Imagent (C₆H₁₄), Sonazoid (C₄F₁₀) (these materials possess a lipid stabilizer shell), and Optison (C₃F₈ has a shell of denatured human serum albumin) [71]. These became the third generation of UCAs.

The history of UCA development has been long and difficult. Luck and astute observations helped develop and make US imaging the most cost effective technology available in the world. UCAs have opened up new opportunities in molecular imaging [71], drug delivery systems, high focused US (HIFU) surgery [79], and atherosclerosis [80].

Ultrasound Contrast Agents or Microbubbles

Ultrasound contrast agents are also known as microbubbles (MBs). MBs enhance the quantification of perfusion and blood flow [81]. MBs are very echogenic and they resonate like a musical instrument [74]. The physical and chemical design of contrast agents (CAs) are manipulated such that synthetic surfactant, tuning of size, composition, degradability, surface properties and bio-functionality make them very echogenic [81]. Typically, MBs are comprised of surfactant shell made from proteins, lipid and biodegradable polymers with an inner gas core, either of air or inert gases (Fig. 4). MBs have an average diameter of ~ 2 to $3\mu\text{m}$, and the combined mass of the shell and gas core (Fig. 4) of each MB does not exceed a picogram [71].

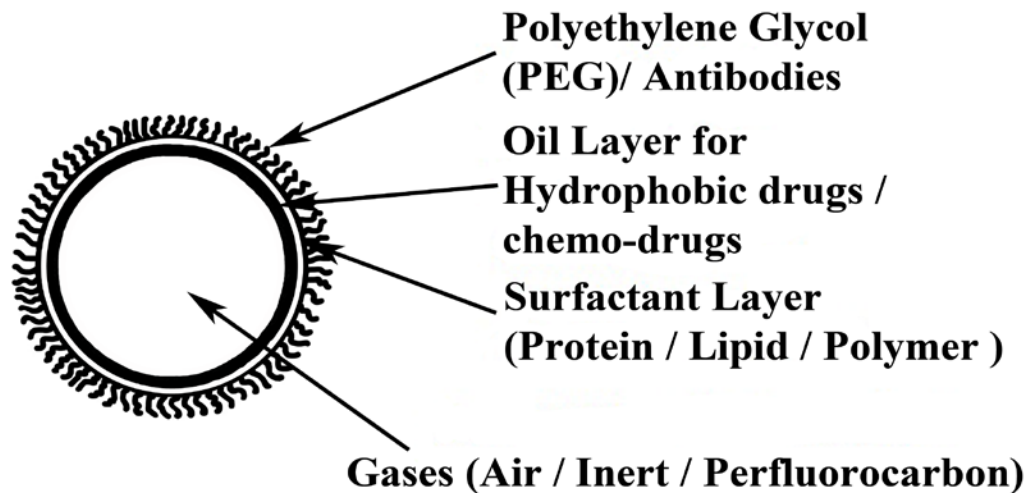


Figure 4. Schematic representation of a coated microbubble.

The particle size of MBs for intravenous injection plays a significant role and needs to be carefully controlled. MBs must be small enough to cross the capillary bed (7.5 micron). Indeed, large bubbles are unable to pass through the capillaries, whereas small bubbles are considerably less effective scatterers [81]. It is now accepted that the size must be in the range of $1-7\mu\text{m}$, preferably around $3\mu\text{m}$, with as narrow size distribution as possible. The critical resonance frequency required to destroy the bubble depends on the diameter [74]. The rigidity of the shell

determined by the thickness of the surfactant would also determine its resonating potency and its echogenicity. It has been determined that US reflectivity is proportional to the fourth power of a particle diameter, but also directly proportional to the concentration of the particles themselves. The resonance frequency of MBs 1–7 μ m in diameter lies within the 2–15 MHz range, which is the US frequency used for clinical diagnosis [74].

Echogenic liposomes and various nanoparticle (NP) dispersions are being evaluated as CAs. Most liposomes have a multi-lamellar structure with embedded air pockets that are responsible for acoustic backscatter signal [82, 83]. Without an enclosed gas core the US signal from these particles is low. NPs dispersions are mostly liquid perfluorocarbon-based emulsions [84]. These NPs are also characterized as contrast agents for MRI, optical imaging, and drug delivery. US imaging using these materials requires a high frequency (multi-MHz) or high degree of target surface coverage with a CA [71, 85].

MBs do not diffuse across the endothelium and thus there is no interstitial enhancement. Essentially, MBs act as blood pool markers, or markers of any other body space into which they have been injected and their behavior is, in many respects, similar to that of labeled red blood cells. Vascular enhancement usually lasts a few minutes and the MBs are then dissolved. However, this model is complicated by evidence that some MBs are taken up by the reticuloendothelial systems [74].

Single-bubble detection is possible *in vitro* in normal saline or blood with older imaging equipment. However, echoes from normal tissue can be nonlinear with non-fundamental frequency. To reduce these signals from tissues multi-pulse techniques such as phase inversion and power modulation are applied [71]. However, to detect MB vibration current imaging

systems use harmonic imaging, both in free-flow conditions [86] and when attached to a solid target [71, 87]. MBs are known to emit US at different frequencies such as sub-harmonic, second and third harmonic frequencies. This large discrepancy in the echoes between MBs and tissue allows for enhanced imaging with quantification of perfusion, blood flow, tumor and tissue vascularization [81], thus MBs are essential for diagnosing modality.

MBs are used not only for diagnostic applications but also for molecular imaging and therapeutic applications [68, 88-90]. Molecular imaging targets the molecular changes associated with diseases and improves the efficiency of *in vivo* imaging [72]. However, in this chapter we will focus on its therapeutic applications in treating cancer. Initial applications of MBs depended on the rate of bubble collapse and their bio-effects such as inducing cell damage, vascular injury [91], and the lysis of thrombus [92]. Interestingly, oscillating MBs can increase membrane permeability and open up tight junctions in endothelial cells [93-97], thus the therapeutic potential of drug delivery and drug action is increased. Based on chemical and physical nature of drugs, some MBs are known to have drugs encapsulated in liposomes, polymeric micelles, hollow particles and emulsion droplets with the aim to reduce non-specific drug resistance and side-effects associated with traditional cancer therapies [81].

Types of Microbubbles

MBs can be divided into several categories depending on their physical and chemical properties which are crucial in the design of a contrast agent for US guided drug delivery [81]. There are a few characteristics that are important when designing an MB. First, the intensity of the backscatter or echo caused by the MB is determined by Rayleigh scattering regime [81, 98]. The intensity depends on the surface properties or shell material, gas content and colloidal properties of MBs [81, 99]. Shell and gas components (Fig. 4) should be biodegradable, i.e. readily metabolized and/or excreted with minimal side-effects [81]. Additionally, MBs shouldn't aggregate into large clusters which could result in non-specific and undesired adhesion to cells [99]. MBs should be effective at low doses [81]; for instance, the typical US Food and Drug Administration (FDA) approved dose of MBs for a patient is approximately 10^9 - 10^{10} MBs given for a 1-2 mL bolus intravenous injection [99]. Additionally, pre-formed drug loaded MBs or MBs alone should be sterilizable and stable with a shelf-life of two years [81, 99]. Other requirements include backscattering proficiency, fragility and cavitation properties of MBs [81]. US or acoustic pressure required to cause cavitation is measured as mechanical index (MI), a relative quotient computed as a peak negative acoustic pressure divided by the square root of the frequency [71]. MBs behave differently at various acoustic pressures, for example, at $MI > 0.2$ MBs behave in a nonlinear manner that allows some systems to detect smaller MBs [71]. At higher pressures ($MI > 0.4$ and up to 1-1.9, depending on the frequency), MBs are completely destroyed [86]. Acoustic pressure depends on the diameter of the shell and its material, for example, thin lipid monolayered bubbles are flexible and vibrate in response to low-pressure US (e.g., $MI = 0.06$) [71], whereas, thick-shelled polymer bubbles don't crack unless at critical pressure, or vibrate resulting in low acoustic echo response [100].

Agitated Gas Microbubbles (First Generation)

First generation MBs were prepared at patient bedside with two syringes connected via a stopcock valve that contained air and saline [101]. When liquid and gas are rapidly transferred from one medium to another the resulting high shear flow causes air bubbles to form of varying sizes [71]. These bubbles produced by agitation are called agitated-saline and are both large and unstable [71, 72]. The surface tension between the gas core and surrounding liquid causes the gas to diffuse into the surrounding liquid decreasing the size of the bubble [71]. MB requires a stabilizer shell to prolong its circulation time. The rate can be calculated using the equation by Epstein and Plesset [102] and Chen et al. [103] that an air bubble with a diameter of 5 μ m in air-saturated water disappears in approximately 125 ms and an air bubble with a diameter of 3 μ m disappears in approximately 32 ms at room temperature and ambient pressure [72].

There are several limitations in using these bubbles such as the size of bubble, circulation time and gas core. These bubbles are effectively removed by the lungs [72]. Additionally, these bubbles have a size greater than 10 μ m and are unable to traverse the pulmonary circulation [68]. MBs larger than 6-8 μ m are trapped in the lung capillaries and bubbles smaller than 1 μ m are less stable and less ultrasound responsive [81]. These bubbles need to be administered by intracoronary or aortic root injection to visualize the left cardiac chambers [72]. Additionally, because it takes at least 12 sec for a contrast agent to pass from a peripheral vein (i.e., the site of injection) to the end-organ [104], to be useful these bubbles need to persist for several minutes [72]. In 1984, Feinstein et al. introduced the use of sonication to create MBs that were stable and small enough to transit through the pulmonary microcirculation from right to left heart [77].

Since the introduction of saline MBs, other agitated contrast agents (hydrogen peroxide, dextrose, indocyanine green dye, iodinated contrast) have been used [68].

Coated Microbubbles filled with Air (Second Generation)

The biggest dilemma facing scientists was the circulation time of bubbles. It was found empirically that a small admixture of the patient's blood to the saline improves the stability and effectiveness of the agitated saline as a contrast agent [105]. Surfactants from the blood form a coating around the gas core and promote the lifetime of the MB by greatly reducing the surface tension at the interface [72]. The first stable MB marketed was Albunex (Table 1). Albunex had a short shelf-life after intravenous injection (tens of seconds) [71].

An encapsulating shell is necessary to sustain the gas cavity and to reduce both the diffusion of gas leaving the core and the surface tension [81]. The encapsulating shell increases the shelf-life (days to months) of the bubbles. The albumin coating forms an elastic solid shell around the gas core and is relatively stiff. Coating enhances the bubble's stability by supporting a strain to counter the effect of the surface tension [72]. The transpulmonary passage of contrast particles became possible only after the addition of a MB shell, i.e., a surfactant (lipid, protein, e.g. denatured albumin or polymer, e.g. poly-butyl-cyanoacrylate [69]) coat, which stabilized the bubbles so that they did not attach to the extensive surface of lung endothelium capillaries [71, 106]. Bubble size is a critical parameter that must be controlled in the range of 1-7 μm preferably around 3 μm [81]. At that point, intravenous administration of contrast became a feasible option for delivering contrast to left heart chambers [106], with some contrast reaching the myocardium vasculature. To circulate freely and avoid entrapment in the microvasculature, MB particles need to be smaller than red blood cells (typically <4.5 μm in mean diameter) [71].

The compressibility of gaseous particles is many orders of magnitude higher than that of liquids and solids. As a result, the scattering efficiency from gaseous particles is many orders of magnitude higher than that from other objects. According to Rayleigh Scattering the intensity of

MB increases as the fourth power of frequency [81]. For such small MBs, the surface-to-volume ratio is high, and air can easily escape and dissolve in the surrounding medium (as a result, ultrasound contrast is lost). Therefore, transpulmonary air-filled MBs with these first-generation shells did not circulate long after intravenous injection (tens of seconds) [71]. Air consists mostly of nitrogen that is able to move easily out of the thin-shelled bubbles, especially in cases of oxygen inhalation that had reduced blood levels of dissolved nitrogen [107, 108]. In physiological conditions, the blood is saturated with air under atmospheric pressure, whereas the air pressure inside the bubbles is larger than atmospheric pressure due to Laplace pressure. When air-filled MBs are infused intravenously they dissolve spontaneously [99]. Surfactants such as lipid (~3nm thick), protein (15-150nm thick) or polymeric shell (200-500nm thick) eliminates the driving force for dissolution of MBs in saturated media as the elastic response of the interface arrests the shrinkage of the gas core [99, 109]. To improve MBs' stability, currently used strategy is to fill them with a sparingly water soluble gas (perfluorocarbons act as osmotic agent) instead of air [110].

At present Levovist (Table 1) is the most widely studied MB contrast agent and the only one commercially available in several countries. Levovist (Table 1), like its forerunner Echovist (Table 1) (also by Schering), is made of galactose microcrystals generating air in the vial [74]. Adding water to the galactose powder forms a suspension in which air MBs adhere to the fine irregularities of the surface of the microcrystals remaining in the solid state, which dissolve after injection, releasing the gas MBs into the blood. Levovist and Sonovue (Table 1) have half-lives of 78 seconds and 5 minutes, respectively [81].

MBs are manufactured by two general techniques: self-assembly stabilization of dispersed gas particles, and double-emulsion preparation with core extraction. The first

technique is for lipid or protein-based bubbles. Gases (air or fluorinated gas with low solubility) are dispersed in the aqueous medium that contains a lipid or surfactant micellar mixture or a protein that is denatured by sonication. Those components are deposited on the gas-liquid interface and stabilize the MB. Some preparations are stable on storage in the aqueous phase for many months. Alternatively, MBs can be rapidly frozen and lyophilized for extended storage in dry state. The addition of water results in a reformation of the MB aqueous dispersion immediately before use [72].

Table 1: Comparison of Commercially Available Contrast Agents

| Agent | Bubble Size mean (range) | Gas | Shell Composition |
|-------------------------------|-------------------------------|---------------------|---|
| Albunex | 4.5 μ m (1-10 μ m) | Air | Albumin |
| Levovist | 2-3 μ m (2-8 μ m) | Air | Galactose/ palmitic acid |
| Echovist | - | Air | D-galactose |
| EchoGen | 2-5 μ m (1-30 μ m) | Dodecafluoropentane | Stabilized surfactant |
| Sonogen | 2-5 μ m (1-30 μ m) | Perfluoropentane | Anionically charged surfactant |
| Optison | 4.7 μ m(1-10 μ m) | Octafluoropropane | Albumin N-acetyltryptophan, Caprylic acid |
| Definity | 1.5 μ m(1-10 μ m) | Octafluoropropane | Lipids: DPPA, DPPC, MPEG5000 DPPE |
| Imagent | 6 μ m | Perfluorohexane | Lipid: DMPC |
| Sonozoid | 2.4-3.6 μ m (3.4 μ m) | Perfluorobutane | Phospholipids |
| Sonovist | 1-2 μ m | Air | Cyanoacrylate (polymer) |
| Sonovue | 2.5 μ m(1-10 μ m) | Sulfur hexafluoride | Lipids: Macrogol 4000, DSPC, DPPG, Palmitric acid |
| Sonidel MB101 | 2.7 μ m | Perfluorocarbon | Stabilized Lipid |
| BG1135 | 2.9 μ m(1-8 μ m) | Air | Polymer |
| BR14 | 2.5-3 μ m | Perfluorobutane | Lipid |
| BR38 | <10 μ m | Perfluorobutane | Phospholipids |
| PB 127 | 4.0 μ m(3-5 μ m) | Nitrogen | Biodegradable polymer bilayer |
| PESDA | 4.7 μ m | Perfluorocarbon | Albumin |
| Artenga | 2.5 μ m | Variable | Lipid |
| AI-700 | 2 μ m | Perfluorocarbon | Poly-L-lactide co glycolide |
| Cardiosphere/ Bisphere | 4 μ m | Nitrogen | Poly lactide/Albumin |
| Targeson | 2.5 μ m | Perfluorocarbon | Surface-modified Lipid |

Adapted from Liu, Y. et al. 2006 [69], Alzaraa, A. et al. 2012 [111] and Nomikou, N. and McHale, A.P. 2010 [112])

Coated Microbubbles filled with Inert Gases (Third Generation)

Since 1997, contrast agents have been further stabilized by replacing the air core with high-molecular-weight inert gases or water soluble fluorinated gases [71] such as perfluorocarbons [72] and sulfur hexafluoride [68] which have a lower solubility and diffusivity in aqueous liquids compared with air [104]. Perfluorocarbons act as osmotic agents and would dilute the other gases inside the bubbles thereby also reducing their partial pressure [81, 113]. This effect counterbalances the Laplace pressure and blood pressure [81].

The gas core is generally surrounded by a protein (albumin), lipid, surfactant, or biocompatible polymer surfactant with a diameter ranging from 2 to 500nm. This shell improves stability against gas loss, dissolution, and MB coalescence, and produces a more standard size distribution [68]. The gases such as perfluorocarbons are exhaled through the lungs. Examples of this kind of agent are Optison (GE Healthcare, Chalfont St Giles, UK), which contains octafluoropropane and an albumin shell; SonoVue (Bracco, Milan, Italy), which has a sulfur hexafluoride core and a phospholipid coating [72]; Definity/Luminity (C3F8), Imagent (C6H14) and Sonazoid (C4F10) which possess a lipid stabilizer shell [71] (Table 1).

Different types of Coated Microbubbles

Shell coating is critical for stabilizing MBs because the configuration and conformation of the shell material determines its stiffness which increases its resistance to rupture by US as well as its clearance efficiency by the reticuloendothelial system [68]. The shell can be stiff with albumin, lysozyme and polymers or more flexible with lipid or phospholipid. Its thickness can vary from 10 to 600nm [81]. Surface tension, shell viscoelasticity and permeability, surface charge density, biodegradability, ligand density and payload capacity are properties that largely

depend on the choice of the surface-active agent, i.e. lipid, protein or synthetic polymer. MBs' surface properties and size play a crucial role in prolonging the circulation life of MBs as phagocytic uptake depends on surface opsonization [114] and particle size. The larger sized MBs are eliminated more rapidly. Dendritic cells and macrophages are assigned to the clearance of MBs in the bloodstream [99]. The study of MBs' biodistribution carried out by Tartis et al.[115] using Positron emission tomography (PET) showed that MB shell material accumulates in the spleen through size dependent filtration mechanisms. Immunogenicity, targeting efficiency, availability, potential for imaging and drug release upon ultrasound irradiation are functional properties consequently correlated with MBs' structural features [99].

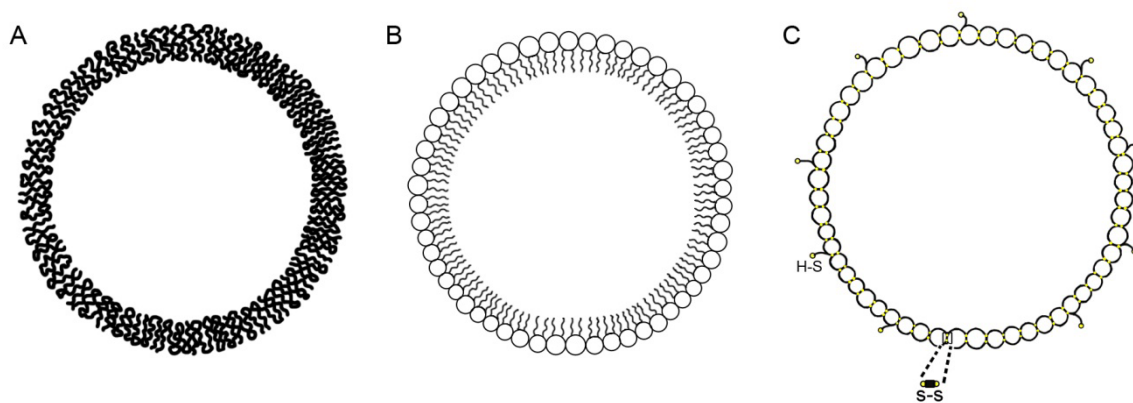


Figure 5. Schematic representation of different coated microbubbles. A) Polymer coated microbubbles. B) Phospholipid coated microbubbles. C) Protein coated microbubbles.

Interaction of Ultrasound and Microbubbles

Acoustic signals from MBs is dependent on the compressibility of the gas, bubble size, shell thickness, shell viscosity, shell density, properties of the surrounding medium, US frequency and power of the applied ultrasound [116, 117].

MBs owe their functionality to the gas core, which can compress and expand easily in response to the acoustic pressure change (Fig. 8) [72]. This change can result in 100-fold volume change and 4-5 fold diameter change [71]. Thus, when exposed to an ultrasound field, a gas bubble will undergo volumetric oscillations in response to the varying pressure (Fig. 8) [74, 118]. The MB oscillations also results in a high backscattering of the ultrasound wave. The amplitude of these oscillations will be much larger than those of a very weakly compressible body such as a red blood cell [79]. Thus, despite their similarity in size, the MB will produce much stronger US echoes [74, 118]. Moreover, the MBs can act as resonant systems with resonant frequencies within the same range as medical ultrasound frequencies [72].

Eventually with increasing pressure from the US the MBs will undergo violent collapse, releasing a shock wave and often fragmenting into smaller bubbles (Fig. 6, 7 & 8B) [119]. This process is variously referred to as inertial, unstable, or transient cavitation (Fig. 8B). Transient and unstable are both slightly misleading terms since a bubble can collapse repeatedly [120] without fragmenting, but inertial cavitation means the collapse of a gas cavity with significant amounts of energy being released (Fig. 8B) [72]. Broadband emissions are generated during inertial cavitation where bubbles undergo large radial oscillations that are dominated by the inertia of the surrounding liquid [121]. During compression of MB there is a rise in pressure and temperature within the bubble, but during an inertial collapse the temperature may reach several thousand degrees centigrade or more [122]. These extreme conditions are confined to the center

of the bubble; however, the bubble will have expanded again before any significant heat transfer can occur. Highly reactive chemical species may be produced such as free radicals and toxic chemicals such as hydrogen peroxide (H_2O_2) [123] at relatively high intensities [124].

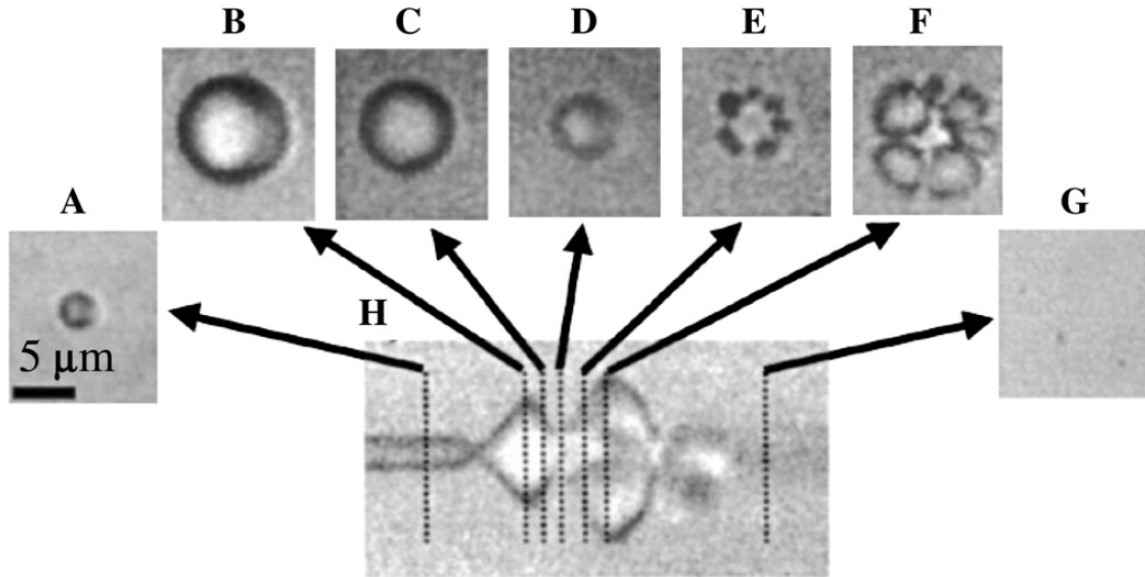


Figure 6. Optical frame images and streak image of ultrasound contrast agents. Optical frame images and streak image corresponding to the oscillation and fragmentation of a contrast agent microbubble, where fragmentation occurs during compression. The bubble has an initial diameter of $3 \mu\text{m}$, shown in A. The streak image in h shows the diameter of the bubble as a function of time, and dashed lines indicate the times at which the two-dimensional frame images in A–G were acquired relative to the streak image. (Adapted from Chomas et al. American Institute of Physics, 2000 [125].)

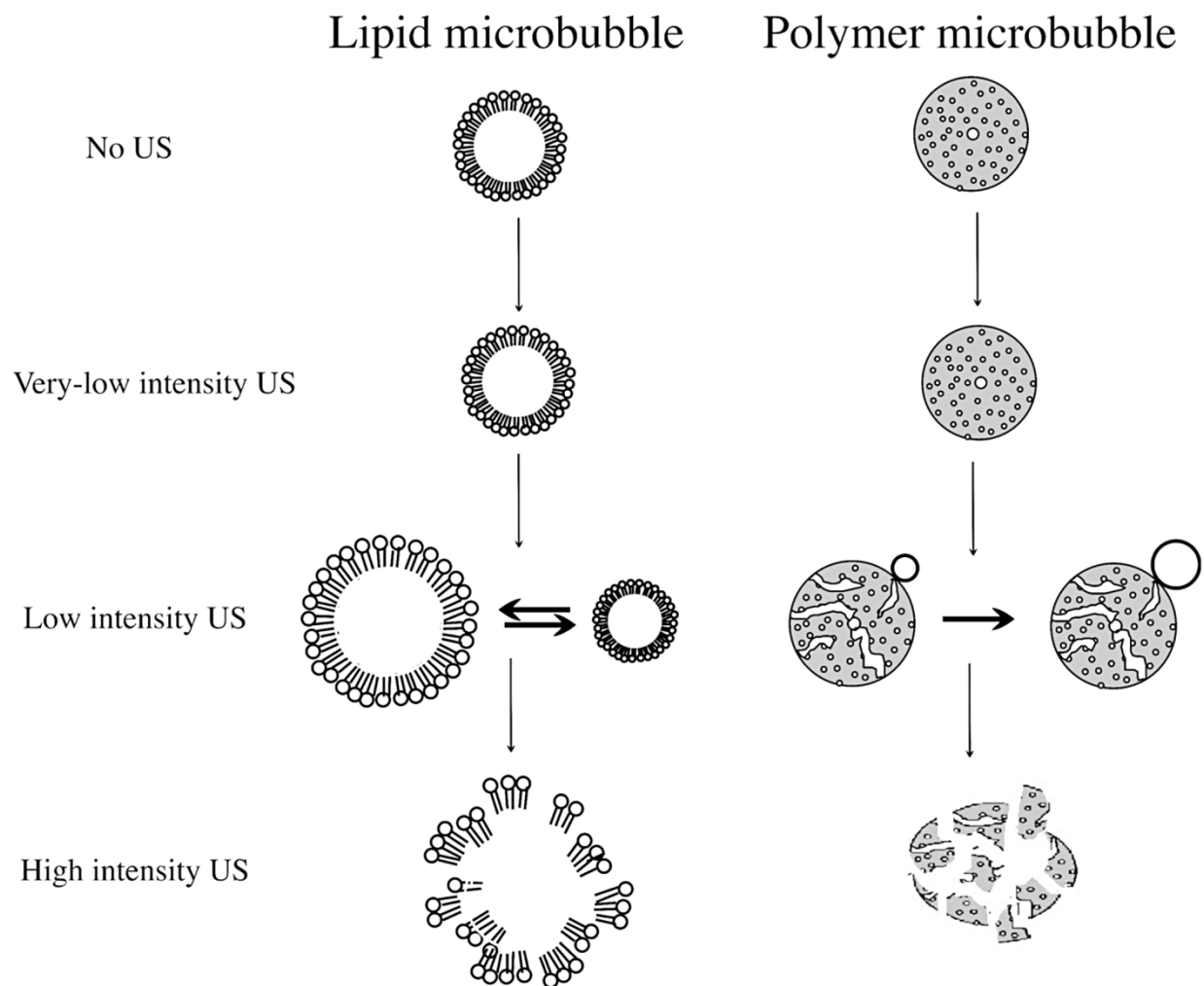


Figure 7. Schematic representation of lipid (left column) and polymer (right column) microbubble interaction with ultrasound of increasing intensity (top to bottom). (Adapted from Hernot and Klivanov, *Advanced Drug Delivery Reviews*, 2008 [68]).

In addition to a temperature rise, “streaming” currents may also be set up as ultrasound propagates through a liquid as a result of momentum transfer [126]. A similar effect can occur on a correspondingly smaller scale around MBs undergoing stable oscillations (Fig. 8A) [127]. If the bubble is sufficiently close to a surface, such as a cell membrane, these circulating flows may give rise to shearing stresses which have been hypothesized as the means by which uptake of therapeutic components is enhanced [128]. Micro-streaming (Fig. 8A) will also contribute to

circulating material in the target region, which is extremely important in the context of therapeutic applications [129]. At higher amplitudes of oscillation, microstreaming can cause significant damage to cells and produce mechanical erosion [79, 130, 131]. In addition when a bubble rapidly collapses near a boundary, this collapse is asymmetrical. A high-speed liquid jet may form projecting through the bubble towards the boundary. This phenomenon is known as microjetting (Fig. 8C) [81]. Microstreaming and microjetting generate moderate shear stress on inducing hyperpolarization of the cell membrane by modifying the electrophysiologic cell activities and enhancing the cell's permeability (Fig. 8) [132]. For drug-loaded MBs, microjetting would be the ideal release mechanism (Fig. 8C), since it effectively produces small holes within a cell membrane (sonoporation) which facilitates the drug uptake [133]. The rupture size is large enough to allow the passage of non-deformable particles up to 0.5 μ m in diameter, that depends on several parameters including the MB size, shell composition, acoustic pressure, and intravascular pressure [81].

MBs and ultrasonic waves undergo a scattering interaction by absorbing the acoustic energy [81]. MBs in a liquid are forced to oscillate with only a relatively small to moderate increase and decrease of radius. The mechanical biological effect is estimated by certain ultrasound parameters and is called mechanical index (MI). At low $MI < 0.1$, MBs undergo alternate equal expansion and contractions symmetrically and in a linear manner [81]. At a slightly higher MI of 0.1 to 0.3, the bubble becomes somewhat resistant to compression than to expansion which results in stable or non-inertial cavitation (Fig. 8A & B) and leads to non-linear oscillations and backscatter at a variety of frequencies (harmonics, sub-harmonics and ultra-harmonics) [68, 80]. When the bubbles are collapsing the kinetic energy of the bubble surpasses its surface energy and fragments into a number of smaller bubbles. Fragmentation (Fig. 6, 7 &

8B) has been exclusively observed with contrast agents with thin, elastic shells [134]. At even higher acoustic pressures (MI 0.3–0.6), MBs undergo forced expansion and compression that lead to its destruction by different methods such as outward diffusion of the gas during the compression phase, diffusion via large shell defects, or complete fragmentation of the shell and the gas core (Fig. 6, 7 & 8B)[125, 135]. MBs' fragmentation can instead produce violent effects which causes cell membrane permeability [136] and lysis [133](Fig. 8B). Acoustical experiments are performed on a population of MBs, therefore they do not show how individual MBs respond in an acoustic field. Experimental evidence is obtained with high-speed camera microscopy of insonated bubbles [68]. These optical frame or streak images show the oscillating and fragmentation changes of a 3 μ m MB (Fig. 6) [125].

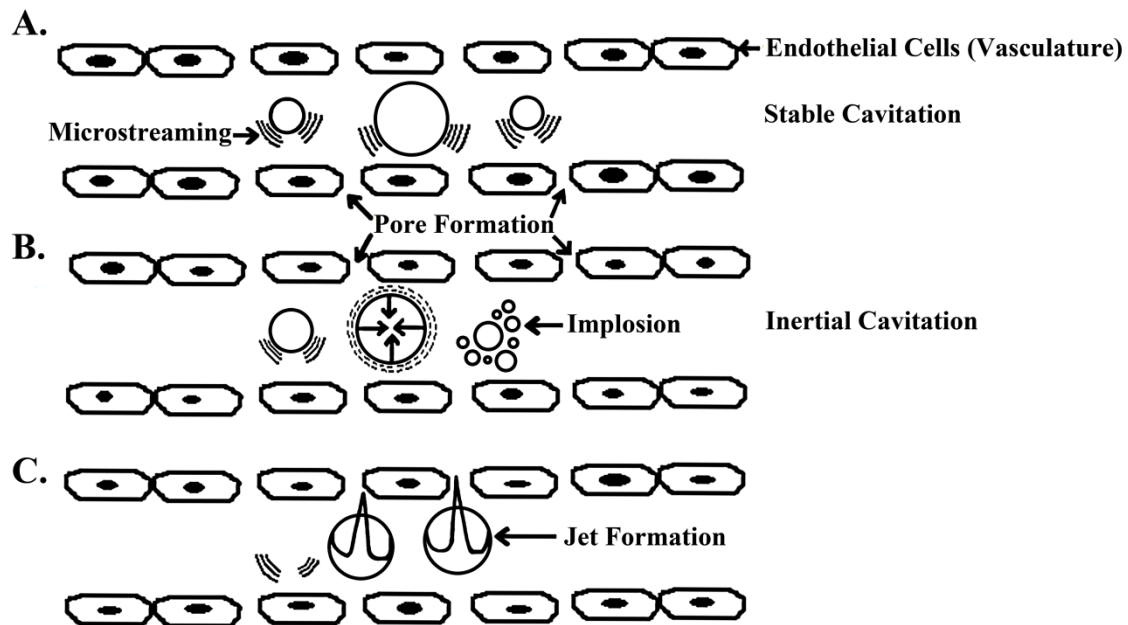


Figure 8. Schematic representation of ultrasound causing microbubbles to behave in different ways that leads to endothelial pore formation and increase vascular permeability. A) Stable cavitation leads to expansion and contraction of microbubble that generates shear stress known as microstreaming. B) Inertial cavitations lead to implosion of the microbubbles that allow for

the release of the bubble contents or fragment into smaller microbubbles. C) Bubbles generate microjets when the resonance diameter is larger than the blood vessels that damage the endothelial lining.

Coated MBs undergo damping as dissipation of viscous energy. Damping reduces the amplitude of the bubble oscillations and it widens the resonance curve of the bubble [72]. MB shell material and stiffness also play a major role in determining the type of explosion or implosion that may occur when exposed to acoustic energy. Lipid or protein MBs and polymer MBs behave differently and depend on the amplitude of ultrasound to which they are exposed [68, 134]. The regime of phospholipid coated MBs depends on bubble radius and the concentration of phospholipid molecules. Phospholipid MBs exist in buckled, elastic and ruptured regime. The bubble is compressed when the coating is condensed which leads to buckling, and with the bubble coating in such a tensionless state, the resulting surface tension is zero (Fig. 6D) [72]. When the bubble is expanded (Fig. 6B), the coating may be ruptured and the gas core will be exposed to the surrounding liquid, changing the surface tension of the gas–liquid interface. In the intermediate elastic regime, the coating is assumed to behave elastically where it is relatively stiff. During the elastic regime, its resonance frequency is high and it will not easily oscillate when driven below resonance [137]. An increasing acoustic pressure can modify the concentration of lipid molecules on the bubble’s surface, forcing the bubble into the buckling regime, which suddenly reduces its stiffness [72].

An oscillating phospholipid MB would most likely lead to stable or non-inertial cavitation (Fig. 8A & B). For MBs with a thin shell such as Optison (albumin shelled MBs) fragmentation is the major mechanism for bubble destruction [116]. Microjets (Fig. 8C) are also generated during cavitation of thin-shelled MBs [91] which produce vessel wall ruptures *in vivo*

and extravasation of nanoparticles into the interstitial space. Polymeric shells are stiff and will not oscillate actively at low US intensity (Fig. 7). The shell cracks as US pressure is increased above the threshold value resulting in the escape of the encapsulated gas (Fig. 7) [68]. This type of MB destruction is called sonic cracking (Fig. 7). However, thick shelled rigid albumin MBs also undergo sonic cracking [116, 138]. For bubbles containing drugs in the gas phase (anesthetic gases, nitric oxide, oxygen) [139, 140], sonic cracking is a suitable mechanism. Fragmentation (Fig. 7), microjetting (Fig. 8) and sonic cracking (Fig. 7) can be effective mechanisms in drug delivery and therefore their occurrence should be finely predicted and tuned [81, 141].

Bio-Effects

US assisted drug delivery is a very complex process that relies on biochemical and mechanical processes that occur during sonoporation which is defined as mechanical disruption of the plasma membrane [80, 81] (Fig. 9).

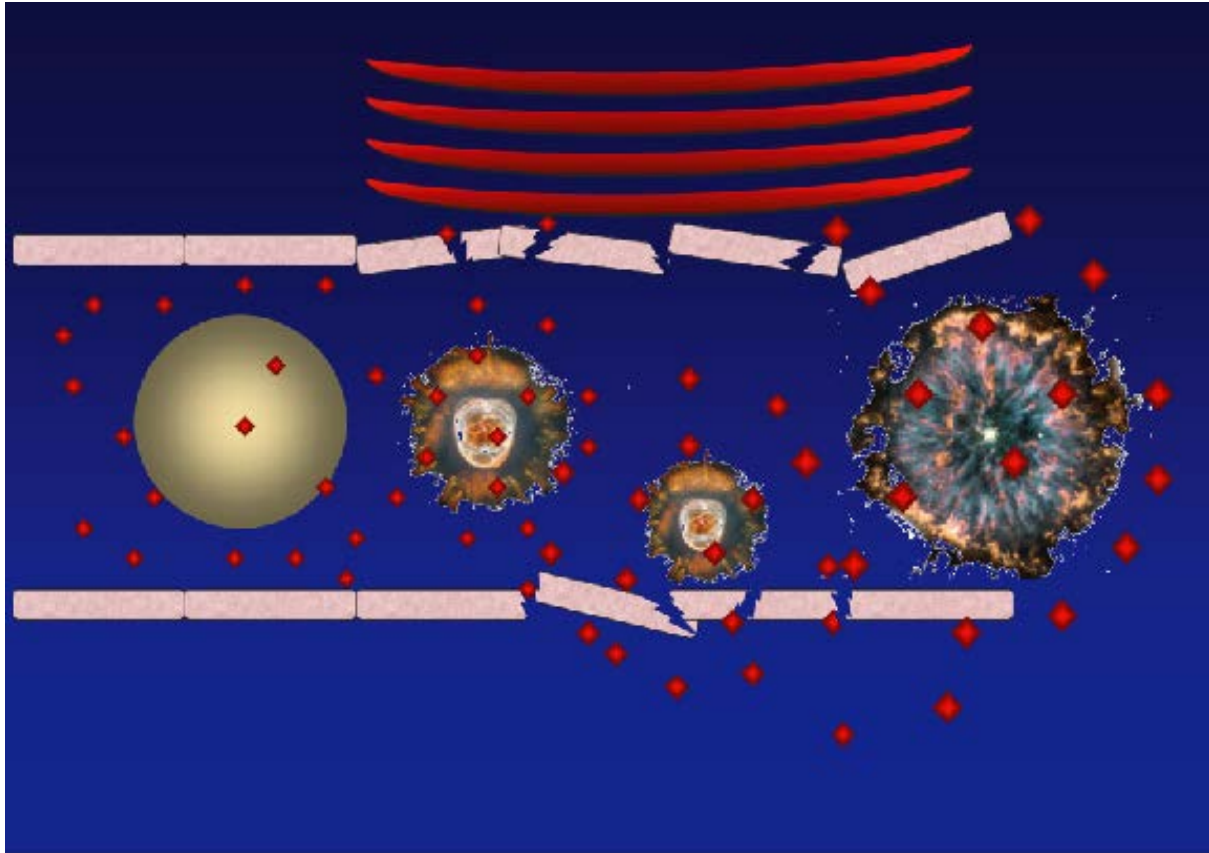


Figure 9. Ultrasound interacts with the microbubble, causing oscillation and eventual destruction, leading to the release of genetic material. The accompanying cavitation produces a local shockwave that increases cellular permeability, allowing transcapillary passage of macromolecules through small endothelial perforations. (Image courtesy of C.R. Merritt, MD, Thomas Jefferson University Hospital, Philadelphia, PA.) (Adapted from Howard, Applied Radiology, 2004, [142].)

US energy can penetrate or “push” materials into skin, blood clots or other tissues [143]. Shear stress can be generated on the membrane of an endothelial cell through the destruction of MBs that causes high-energy microstreams and microjets which increases the permeability of blood vessels promoting the extravasation (Fig. 10) of high molecular weight drugs [99]. This increase in permeability is probably due to transient holes in the plasma membrane and possibly the nuclear membrane [69]. Thus, acoustic cavitation is a pre-requisite in promoting the physical or chemical release of drugs from carriers (MBs), or in promoting the transport of drugs into cells (Fig. 10). US-induced passage of materials from the luminal to the adventitial side of vascular tissue (Fig. 9 & 10) have been proposed in the literature such as paracellular widening of inter-endothelial clefts and tight junctions, free passage through injured endothelial lining and transcytosis via fenestration and channel formation [94] (Fig. 11).

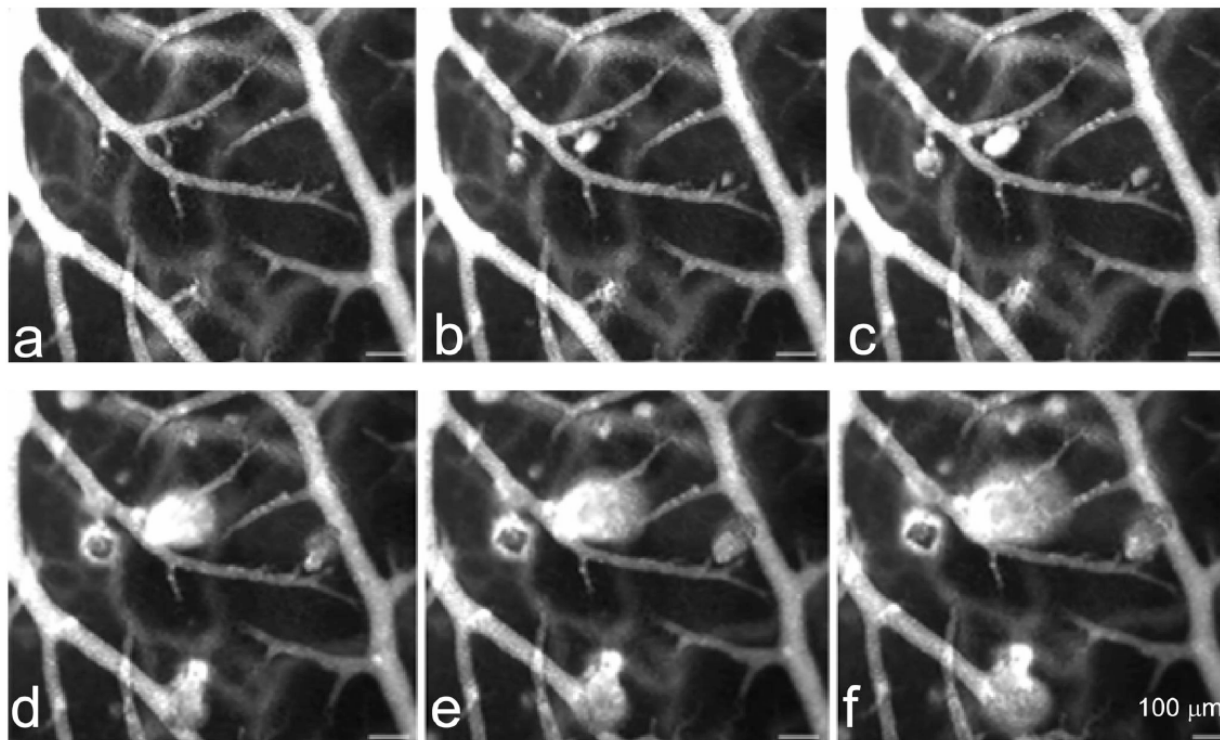


Figure 10. Enhanced drug and gene delivery achieved with the combination of particles and ultrasound. Insonation of circulating microbubbles in the chorioallantoic membrane model

results in small vascular defects, through which a fluorescent dye is transported, reproduced with permission from (27). (a)–(f) are a sequence of images acquired from 1.00-MHz center frequency insonation at a peak negative pressure of 1.3 MPa. (a) was acquired before insonation, (b)–(f) were acquired 0.06, 0.12, 1.24, 2.24 and 3.24 seconds after insonation began, respectively, demonstrating the transport of the fluorescent probe from the vasculature to the tissue interstitium. (Adapted from Ferrara et al., American Chemical Research, 2009[144].)

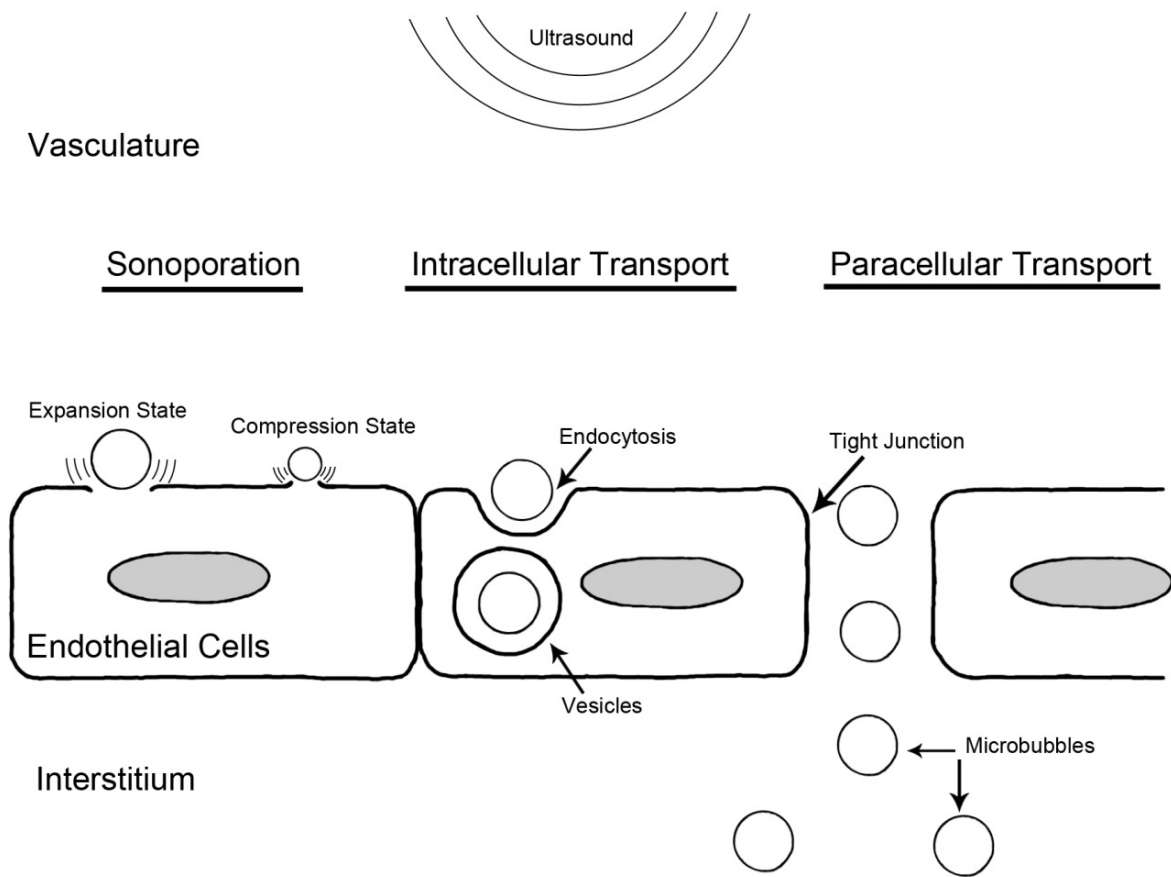


Figure 11. Ultrasound mediated drug delivery through different means of transport.

Sonoporation allows for the mechanical disruption of the endothelial cell membrane.

Intracellular transport allows for the uptake of microbubbles through endocytosis that transports the microbubble through to the interstitium. Paracellular transport allows for the opening of the

tight junctions or separation of bonds that hold the endothelial cells together which causes pore formation in the blood vessel wall.

In vivo studies suggest that a MI of 0.4 has been shown to be detrimental to the plasma membrane and microvasculature [145]. However, low intensity stable cavitation may not be adequately effective in triggering the drug delivery [81]. Reported bio-effects *in vivo* include hemolysis, damage to the microvasculature, opening of the blood brain barrier, effects on cardiac rhythm and thrombolysis [146]. The vessel wall structure has also been found to influence the degree of rupture [147]. The fore mentioned mechanisms have been proposed for the blood brain barrier (BBB)[148], but are also supported by studies in other tissue beds, including renal [149], prostate [150] and skeletal muscle [147] tissues.

Sonoporation

Sonoporation refers to the localized, mechanical disruption of plasma membrane (Fig. 11) [80]. Van Wamel et al., [151] using high speed imaging, showed transport of propidium iodide (PI) against endothelial cells as a direct correlation between cell deformation and resulting cell membrane permeability with *in vitro* studies. According to van Wamel et al. [93] poration is a transition of hydrophobic to hydrophilic pores. This transition creates cylindrical pores when a rotation of the polar heads brings a hydrophilic surface to the pore (Fig. 12). When US is applied, the adhered MBs on the transmembrane generate a critical 'shear' force, which leads to formation of pores once the membrane breakdown force is exceeded. Rapidly oscillating MBs undergo rapid expansion and compression (Fig.12) due to changes in the volume of the gases inside the bubble. The oscillating MBs generates fluid flow over the cell surface and is termed as microstreaming (Fig.13), which is responsible for the disruption of cell membrane by tearing the

lipid bilayer membrane open [130]. Cells can withstand compression better than elongation, which may act as the main component that determines pore formation. Scanning electron microscopy studies have already shown that membrane poration occurs after US and MBs treatment [152]. Mehier-Humbert et al. [152] showed an efficient delivery of FITC-dextran (77-164 KDa) or particles of 25nm. They showed cell membranes with a pore size distribution up to 75nm with ~60% of cells being positive for delivery of the particle. Pore formation allows for direct transfer of molecules into the cytoplasm. Van Wamel et al. [151] have also shown that PI does not enter a cell 1 min after the US exposure. These results support the general idea that the pores reseal quickly upon termination of US. Mehier-Humbert et al. [152] showed that almost all the routes of entry had closed 5 seconds after termination of US. The action of MBs on cells is a mechanical one and can be as important as chemical stimuli in determining vascular fate or pathological state. The most important biomedical application of the sonoporation technique is that it allows the introduction of membrane-impermeable xenomolecules (synthetic molecules) such as dyes, hormones, proteins, plasmids, etc. into living cells [93].

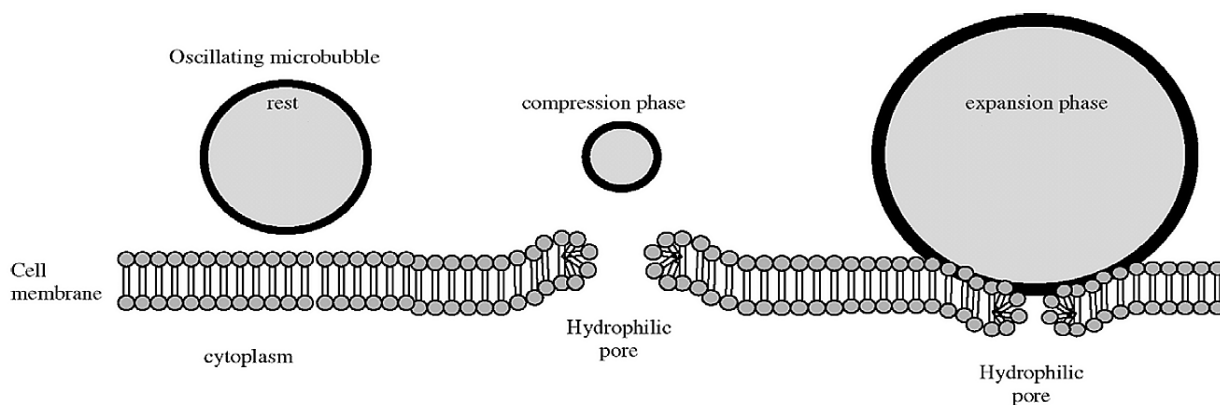


Figure 12. Proposed model of the oscillating microbubble enforced pore formation in the cell membrane. The pushing and pulling behavior of the microbubble causes rupture of the cell membrane creating a hydrophilic pore allowing trans-membrane flux of fluid and macromolecules. (Adapted from van Wamel et al., Journal of Control Release 2006 [93]).

Paracellular transport

Drugs can be delivered by paracellular transport between functional endothelial cells with MBs. Transport by low-frequency US is strongly supported in the literature [153]. When a sound wave is propagated through a liquid medium, steady currents (Fig. 13) are set up in the direction of beam as a result of momentum transfer [126]. This acoustic streaming (Fig. 13) occurs around MBs undergoing stable bubble oscillations (Fig. 13) within the US field growing in size via rectified diffusion [154]. These eddying flows may, in turn, impose shear stresses on nearby surfaces, such as cell membranes, and it is thought that this may promote the uptake of therapeutic components [130, 155]. When a MB oscillates near a vessel wall (Fig. 13), its shell is estimated to travel at speeds on the order of 250 m/s [156], either by directly perturbing nearby structures or by causing local fluid convection [157]. The acoustic radiation forces cause bubbles to move in the direction of the wave propagation by bringing them in contact with vessel endothelium [158]. Radiation pressure may be involved in Focused US + MBs-based blood brain barrier opening through activating the stretch-sensitive or mechanosensitive (MS) ion channels in the vascular endothelium [159]. MS channels are now known to be implicated in many basic cell functions [160]. During localized elongation of cell membranes the MS channels are activated by the conformational changes [161, 162]. The resulting openings are reversible [163].

Endothelial cell morphology can vary significantly between normal and diseased organs. The tissue microenvironment surrounding blood vessels seems to control the endothelial cell phenotype *in vivo* [164]. Thus the blood vessels or microvasculature in the brain differs from other organs. BBB is known to restrict the paracellular translocation of large hydrophilic macromolecules and toxic compounds into the brain via specific membrane located transport systems [165]. When MB oscillations occur in the cerebral microcirculation, the BBB is

disrupted, causing drug extravasation due to breakdown of transmembrane tight junction proteins that regulate the paracellular permeability of the endothelial cell layer [166].

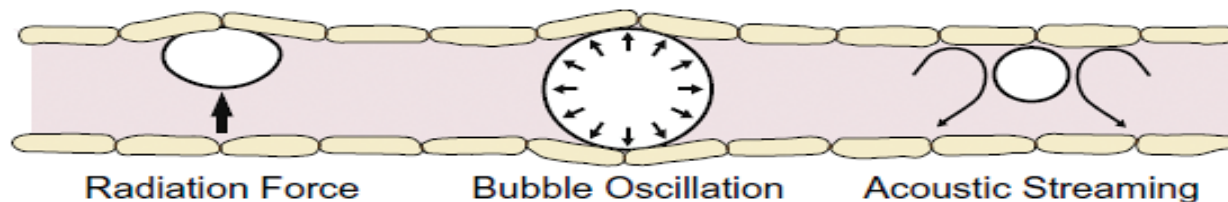


Figure 13. Possible mechanisms for blood–brain barrier disruption via ultrasound + microbubbles. Assuming that the effect is not due to bubble collapse (inertial cavitation), possible effects include stimulation of the endothelial cells via radiation force on the bubbles, bubble oscillation or from microstreaming of the fluid around the bubbles. (Adapted from Vykhodtseva et al, Ultrasonics, 2008 [159].)

Transcytosis/Intracellular transport

MB cavitation can also provoke drug transport through a vascular endothelial cell. Transcytosis or intracellular transport (Fig. 11), in the context of drug delivery, consists of the drug being endocytosed at the luminal surface of the endothelial cell membrane [80]. Transcytosis can be achieved through either a receptor-mediated fashion [167] or by invagination caused by cavitation with US [168]. Ghitescu et al. [167] showed specific adsorptive binding of albumin complexes to plasmalemmal vesicles and clustering in uncoated pits. Plasmalemmal vesicles allow endothelial cells to transport molecules, such as proteins, from the blood that are too large to diffuse through cell junctions or fenestrae, and this transport takes place both by vectorial transcytosis (vesicles) and by connective transcytosis (channels) (Fig. 11). Ghitescu et al [167], also demonstrated that albumin can stimulate endocytosis and transcytosis (Fig.11) in

mouse pulmonary and myocardial endothelium. Thus, albumin coated MBs could potentially undergo endocytosis through similar process. Subsequent transportation through several intracellular compartments and secretion from the cell at the basolateral aspect [169] results in delivery to vascular tissue. MBs could undergo endocytosis via caveolar, an alternative pathway for targeted drug delivery [170]. Endocytosis through caveolar is a receptor-mediated process via receptor-targeted drug vesicles [80, 171].

According to Chen et al. [168], invagination occurs when bubbles collapsed near the vessel wall that results in the vessel wall being pulled inward toward the lumen. Invagination causes higher strain on the vessel wall than distention resulting in vessel rupture [168]. This localized mechanical destruction of the endothelial membrane results in endocytosis and subsequent transcytosis (Fig.12). Cavitating MBs near the cell membrane can create a pore for increased membrane permeability to macromolecules, genes such as wt-p53 (plasmid vector) [172] and extracellular ions such as Ca^{+2} [173], which is repaired by cellular mechanisms within seconds [174]. Meijering et al. [95] demonstrated that endocytosis plays a key role in UMTD of macromolecules sized between 4 and 500 kDa. Dextran molecules of 155 and 500 kDa were mainly localized in vesicle-like structures after UTMD as a result of macropinocytosis, clathrin-mediated and caveolin-mediated endocytosis. MBs also showed increased membrane permeability to extracellular ions is upregulated by endocytosis due to the calcium flux into the cell [95]. The types of MB oscillations required to observe these effects have also been investigated. Inertially cavitating MBs near the cell membrane form 1 - 200 nm pores due to localized tensions [175]. These pores are capable of resealing bifunctionally by either rapid phospholipid rearrangement or gradual, exocytosis-mediated membrane tension changes, which restore membrane integrity [173]. Thus, US enhanced endocytosis is an important pathway for

targeting drug delivery by UTMD [80].

Enhanced Permeability and Retention Effect

UCAs are typically used to study the vasculature in animals and humans, thus employing them to study the aberrant tumor vasculature due to angiogenesis is a natural transition. Perfluoropentane filled silica nanoshells and microshells have been used to selectively image a tumor in a mouse ovarian tumor model [176]. Tumor angiogenesis is characterized by branching vessels with irregular diameters ranging from 10 to 200 μm [177] and a lack of defining structures such as arterioles, capillaries, or venules [178]. Tumors induce angiogenesis to increase their nutrient and oxygen supply. The particular property of angiogenic vessels is their rapid growth from established vessels renders them “leaky” and defective. According to Pasqualini et al. [179] and Li [177], the tumor microvasculature has a vascular pore cutoff size from as low as 380nm up to 780nm, and the endothelial cells are misaligned or have large fenestrations. This phenomenon, which is generally referred to as the Enhanced Permeability and Retention (EPR) effect, can achieve high local concentrations of nano-encapsulated drugs at a tumor site (10- to 50- fold higher than in normal tissue) [99]. US exposure can enhance the size of these leaky vascular pores allowing for micron sized bubbles to collect at the tumor site. At the breast cancer (SK-BR-3) tumor site Zhao et al. [180], with phospholipid MBs, showed membrane pore diameter of 1-2 μm with US exposure of 30 sec, diameter of 2-3 μm with US exposure of 60 seconds and diameter of 3-5 μm with US exposure greater than 60 seconds. Thus the EPR effect seen in tumors can be extremely beneficial in treating cancer.

Submicron bubbles could show higher intracellular uptake than microsized bubbles, allowing drug-release in different cellular compartments such as cytoplasm and nucleus [99]. The ability to synthesize nanobubbles has opened up further opportunities to deliver therapeutic

agents which require targeted extravasation into the tissues as micrometer sized MBs are typically too large to exit the vasculature. A prerequisite for this process is that the nanocarrier stays in the blood long enough to slowly accumulate in the tissue of interest with affected and leaky vasculature [99]. Nanometer sized bubbles can potentially exhibit an improved circulating lifetime [178]. The radiation force generated by insonification [181] with the medical ultrasonography equipment can force the nanobubbles or MBs towards pores in these vessels and induce penetration of nanobubbles or MBs through the pores. The penetration of MBs results in a higher concentration of contrast in the tumor, a better visualization of the acoustic imaging and a targeted delivery of drug payload. In addition, the drug containing nanobubbles can be made slowly biodegradable, thus delivering their payload at a controlled rate [99]. These properties of the micro- or nano- bubbles make them an efficient drug delivery system for treating cancer. The most successful nano-bubble system consists of liquid paclitaxel loaded into perfluorocarbon emulsions that become echogenic when accumulated at the site of interest such as ovarian, breast and pancreatic cancer [182, 183].

Uses of Microbubbles

Cavitation of MBs and its subsequent bio-effects on the vasculature and tissue cells shows the potential of using MBs as delivery vehicles. The chemical, physical and structural properties of the MBs also enhance the notion of using them to deliver therapeutic agents. Drugs can be incorporated into the MBs in a number of different ways, including binding of the drug to the MB shell and attachment of site-specific ligands. Drugs can also be imbedded in the membrane or loaded internally with the therapeutic agents and gas (Fig. 14).

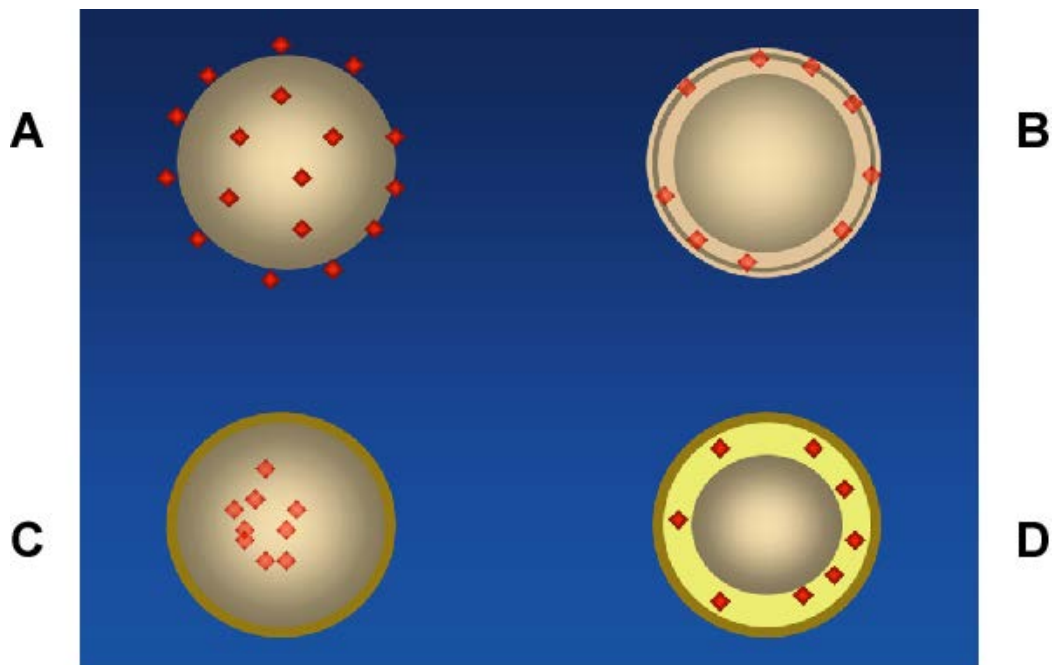


Figure 14. Manipulation of the microbubble shell for gene and/or drug delivery. (A) Drugs (red diamonds) may be attached to the surrounding microbubble membrane. (B) Materials may be imbedded in the membrane. (C) Bubbles may be loaded internally with the therapeutic agents and gas. (D) Hydrophobic drugs may be incorporated into an oily emulsion that forms a film around the bubble, which is then surrounded by a stabilizing membrane. (Adapted from Unger et al., *European Journal of Radiology*, 2002 [184].)

Subsequently, hydrophobic drugs may be incorporated into an oily emulsion that forms a film around the bubble, which is then surrounded by a stabilizing membrane (Fig. 14).

Perfluorocarbon-filled MBs act as carriers of these agents until the site of interest is reached as they are sufficiently stable for circulating in the vasculature as blood pool agents [185].

Ultrasound applied over the skin surface can then be used to burst the MBs at this site, causing localized release of the drug [172, 186-188]. The use of US and MBs lowers the concentrations and reduces the systemic side effects of hazardous drugs like cytotoxic agents thereby improving the therapeutic index [185]. Thus, there is an increasing interest in developing noninvasive delivery methods for gene therapy and chemotherapeutics.

CHAPTER III : ULTRASOUND TARGETED MICROBUBBLE DELIVERY IN PROSTATE CANCER CELLS

ABSTRACT

Background

The use of human adenoviruses (hu-Ads) in gene transfer studies is limited because of their immunogenic nature. To circumvent this limitation we have developed a novel approach constituted of hu-Ads encapsulated inside microbubbles (MBs). The melanoma-differentiation-associated-gene-7 or interleukin-24 (mda-7/IL-24) is a tumor suppressor with pro-apoptotic activity against several cancers. However, to translate the site-specific gene transfer of Ad.mda-7 complexes by ultrasound-targeted microbubble destruction (UTMD) from the bench to the bedside, studies involving the use of immune-deficient animal and immune-competent mice models are required.

Hypothesis

It has been shown that transfer of genes to mouse cells using hu-Ads is dependent on the expression of Coxsackie and Adenovirus Receptor (CAR) and certain integrins, which mediate hu-Ad attachment and internalization. Our hypotheses are that the murine derived prostate cancer cells will express CAR and/or α , β integrins and will be transduced by hu-Ads. Microbubbles will protect the viruses from inactivating substances such as complement. UTMD will enhance gene transfer in both DU145 and murine PC cells regardless of complement rich FBS media.

Methods

We investigated the expression of CAR and α , β integrins in murine and control human DU145 PC cells by flow cytometry analysis. We tested the infectivity of Ad.GFP (green fluorescent

protein) and Ad.mda-7/IL-24 on both murine and DU145 prostate cancer cells. Viral burst assay was carried out on murine and DU145 PC cells with the CTV.Mda-7 oncolytic adenovirus to measure viral replication. We also tested the microbubble delivery of Ads with ultrasound in cell culture. Western blot analysis confirmed mda-7 protein expression following Ad-transduction. Annexin-V studies assessed the pro-apoptotic effect of the Ad.mda-7/IL-24.

Results

Our studies showed that cells express CAR receptor, α , β integrins and that Ad.GFP and Ad.mda-7/IL-24 transferred their transgene in the murine and human DU145 prostate carcinoma cells. Murine PC cells were unable to replicate the CTV oncolytic virus. Additionally, mda-7/IL-24 significantly increased the apoptotic rate of the murine and DU145 transduced cells. Microbubble delivery of Ads with ultrasound in cell culture enhances gene transfer into the cells regardless of the complement rich FBS media.

Conclusion

Our study demonstrated the feasibility of using human DU145 prostate adenocarcinoma cells and TRAMP-C2 cells derived from a murine model of prostate cancer to translate the ultrasound-mediated microbubble Adenovirus delivery system that we have developed.

INTRODUCTION

For more than four decades, human adenoviruses have served as an excellent model system to study molecular mechanisms controlling cell cycle progression and cell death. More than 60 types of HAdV have currently been identified and divided into eight species, designated A, B1, B2, C, D, E, F and G. Members of the different species use different receptors for virus–host interactions and some are currently characterized as potential viral vectors in cancer gene therapy. HAdV show strict host specificity. Murine cells lack some of the receptors needed for HAdV infection such as the Coxsackie and Adenovirus Receptor (CAR), thus, murine cells are generally refractory (non-permissive) for HAdV infection and replication, although a very low level of HAdV infection and replication has been described in some mouse cells [189, 190].

Melanoma differentiation associated gene-7 also called interleukin-24 (mda-7/IL-24) is well-known for its pro-apoptotic, anti-angiogenic, radio-sensitizing, immune-stimulatory properties and bystander activity on distant tumors [53, 191-197]. Mda-7/IL-24 is a multifunctional suppressor gene belonging to the IL-10 family of cytokines [198, 199]. When delivered by HAdV vector, mda-7/IL-24 induces apoptosis selectively in almost all cancer cells while leaving normal cells unharmed [195]. Mda-7/IL-24 can be expressed and secreted from naïve normal and cancer cells thereby enhancing its apoptotic activity against primary and metastatic cancer [194]. Thus, HAdV expressing mda-7 should provide both tumor selectivity and adequate induction of newly synthesized mda-7/IL-24 [53].

Gene therapy by adenoviral vectors has shown promising results in treating locally advanced cancers; however, due to their immunogenicity they trigger both adaptive and innate immune responses. The antigenic nature of Ads leads to their rapid inactivation by neutralization antibodies and clearance by the immune system. Ad vectors elicit an innate immune response

through the myeloid differentiating factor 88 (MyD88)/Toll-like receptor (TLR)-9 resulting in the production of type I interferons (IFNs), interleukin (IL)-6 and IL-12 inflammatory cytokines [200, 201]. Additionally, unmodified viruses are generally non-specific in their action and this limits their use to direct target tumor or organ injection [53]. To circumvent these limitations we developed a novel approach wherein Ads are encapsulated inside the shell of acoustically active, lyophilized, lipid-encapsulated, perfluorocarbon microbubbles (MBs) (ultrasound (US) contrast agents), which act as delivery vehicles for a site-specific gene transfer system. MBs protect the viral payload from detection and rapid degradation by the hosts' immune system allowing for an intravenous (IV) injection rather than intratumoral (IT) injection [53, 202]. US breaks open the MB/Ads complexes by inducing cavitation, which allows Ads to transfer their transgene only to the sonoporated region. Cavitation of the MBs creates small shockwaves that increase cell permeability by forming temporary micropores on the cell surface bypassing the receptor-mediated dependence of HAdV. Our novel viral delivery technique mediated by MB and US brings new hope to the frontier of gene therapy and its use in clinical settings.

In order to facilitate the translation of this technology into human application, we envision testing an adenovirus carrying mda-7 (INGN 241) that is already in phase-I and -II clinical trials in patients with multiple solid tumors (none of which is of prostate origin) in treating PC cells [203]. *In vivo* studies involving the use of immune-deficient and immune-competent PC mice models are required. Thus, we studied the capacity of human Ad.mda-7/IL-24 to infect mouse PC cells (TRAMP-C2) derived from immune-competent mice and compared it to human PC (DU145). We also studied the effect of Ad.mda-7/IL-24 to increase the apoptotic rate of TRAMP-C2 and DU145 prostate cancer cells following mda-7 gene transfer. Lastly, we tested US guided MB assisted gene delivery of reporter Ad.GFP in both murine and human PC.

MATERIALS AND METHODS

Cell Lines and Cell Culture

The DU145 (human prostate adenocarcinoma), TRAMP-C2 (mice prostate adenocarcinoma) and human kidney embryonic 293 cell lines were obtained from the American Type Culture Collection (ATCC, Rockville, MD). DU145 cells were grown in RPMI 1640 (Hyclone, Waltham, MA) supplemented with 10% fetal bovine serum (FBS) (Hyclone, Waltham, MA), and 100 units/mL penicillin supplemented with 1 mg/mL streptomycin (both from Hyclone, Waltham, MA). The 293 cells were grown with Dulbecco's modified Eagle's medium (Hyclone, Waltham, MA) supplemented with 10% FBS (Hyclone, Waltham, MA). TRAMP-C2 cells were grown with Dulbecco's modified Eagle's medium (Hyclone, Waltham, MA) supplemented with 5% FBS (Hyclone, Waltham, MA), and 100 units/mL penicillin supplemented with 1 mg/mL streptomycin (both from Hyclone, Waltham, MA). All cells were grown at 37°C, in a 5% CO₂/95% atmosphere incubator.

Cytological Observations

The cells were examined under an inverted Olympus IX70 microscope (Olympus America, Inc. Melville, NY). Fluorescence images were captured with Sensicam QE camera (Cooke Co., Auburn Hills, MI) and managed with the SlideBook 3.0 software (Intelligent Imaging Innovations Inc., Denver, CO).

Adenoviral Production and Purification

Ad-GFP, which expresses the green fluorescence protein gene under the strong cytomegalovirus (CMV) constitutive promoter was generated using the AdEasy system (Carlsbad, CA); the conditionally replication competent cancer terminator virus CTV.Mda-7 (Ad.PEG-E1A-mda-7) [18, 204, 205] and Ad.mda-7 [206] were amplified and purified with the BD Adeno-X virus purification kit (BD Biosciences, Mountain View, CA) following manufacturer's directions. Viral titers were determined by a plaque assay and the titer was adjusted to 1.2×10^{12} plaque-forming units (pfu)/mL as described [206]. CTV.Mda-7 (Ad.PEG-E1A-mda-7) and Ad.mda-7/IL-24 were provided by Dr. Paul Fisher (Virginia Commonwealth University, Richmond VA). Each viral stock was propagated and purified from 293 cell cultures. Cells were harvested 24-36 hours after infection, pelleted and re-suspended in heat-inactivated media. 293 cells were lysed by a three-freeze/thaw cycle method. Cell debris was removed. Viruses were purified by chromatography followed by dialysis. Viruses are aliquoted and stored at -80°C . Viral titers were determined by a plaque assay. Ad transductions were performed using 10, 25, 50 MOI Ads, in RPMI-1640 media with 2% Fetaclone-III heat-inactivated FBS (Hyclone, Thermo Scientific, Waltham, MA) and in with DMEM media with 2% Fetaclone-III heat-inactivated FBS (Hyclone, Thermo Scientific, Waltham, MA). Cells were collected after 24- or 48-hours.

Viral Burst Assay

HEK 293 cells were used as control. HEK 293 cells, DU145 cells, TRAMP-C2 cells were infected with replicative HAdV (CTV.Mda-7) at 100 pfu/mL and 1,000 pfu/mL. Filtered transfection supernatants and viral particles present in the cells were collected at both 24 and 48

hours post-transfection. Cells were harvested 24- and 48- hours after infection, pelleted and re-suspended in heat-inactivated media. 293 cells were lysed by a three-freeze/thaw cycle method. Cell debris was removed. Viruses are aliquoted and stored at -80°C. The collective viral particles were tittered and determined by a plaque assay.

Antibodies

The following primary antibodies were used in Western Blot studies: mouse monoclonal anti-Mda-7/IL-24 k101 (GenHunter Corporation) (1:2,000 incubation for overnight), GFP cat#632377 (1:500) (BD Bioscience) and β -actin cat#A3853 (1:1,500) (Sigma Aldrich) as a control. The following are used in the flow cytometry studies: Rabbit Anti-Coxsackie Adenovirus Receptor Polyclonal Antibody, Alexa Fluor® 488 Conjugated bs-2389R-A488, Rabbit Anti-Integrin Alpha V + Beta 5 Polyclonal Antibody, Alexa Fluor® 647 Conjugated bs-1356R-A647 and Rabbit Anti-Integrin Alpha V + Beta 3 (CD51+CD61) Polyclonal Antibody, Alexa Fluor® 488 Conjugated bs-1310R-A488 from Bioss Inc.

Western Blot Analysis

DU145 and TRAMP-C2 cells were transduced with 10, 25, 50 multiplicity of infection (MOI) of Ad.GFP and Ad.mda-7. Western blot analysis was conducted as previously described [53]. Cells were lysed on ice for 1hr with lysis buffer. Fifty μ g of total protein plus loading buffer were loaded in each well for western blot analyses. SDS-PAGE was run using 8-12% bis-acrylamide gel at room temperature. Samples were blotted onto a nitrocellulose membrane. To detect proteins the membranes was blocked with 5% Milk-TBST overnight at 4°C and reacted to primary antibodies for 2hr at room temperature with constant motion on an orbital shaker. The

membranes were washed with TBST to remove excess primary antibodies. Incubation for 45 minutes with appropriate secondary antibodies followed. Immunodetection was performed using the enhanced chemiluminescence (ECL) system (Amersham, IL) according to the manufacturer's instructions. Western blot analyses with antibodies against the targeted proteins were performed to validate successful viral transfection of the cells.

Flow Cytometry Assay

DU145 and TRAMP-C2 cells were checked for different surface Ad receptors such as CAR (coxsackie adenovirus receptor) and integrins $\alpha V\beta 3/5$. Each was compared against IgG control. 10 μ L of Boss primary conjugated antibody was added for 30 mins at 4°C, aashed several times with 2mL 1X PBS and resuspended in 100 μ L of 1X PBS. Samples were analyzed on BD Accuri C6 Flow Cytometry.

Adenoviral transduced DU145 and TRAMP-C2 cells were trypsinized and collected. Cells were centrifuged at 5000 rpm, washed and suspended in 1% FCS-PBS. This step was repeated three times. Samples were prepared and run by a BD Accuri C6 Flow Cytometer (BD Bioscience, San Jose, CA). Single cells population was gated and an FL1 & FL4 area histogram was drawn and formatted to show only the events inside the single cell region.

Annexin-V Assay

Apoptotic cells were analyzed with fluorescein isothiocyanate (FITC) conjugated to Annexin-V antibody and Propidium Iodide (PI) from the Annexin-V/FITC Kit (Bender MedSystems, Burlingame, CA) following manufacturer's instructions. Cells were trypsinized and washed with PBS. Cells were centrifuged and re-suspended in binding buffer. The samples were

analyzed with BD Accuri C6 Flow Cytometer (BD Bioscience, San Jose, CA). Annexin-V assay experiment was repeated three times and was run as triplicate of technical repeats. Statistical analysis was performed with GraphPad Prism 6 statistical software.

UTMD for Prostate Cancer Cells.

Human DU145 and murine TRAMP-C2 prostate cancer cells were grown in both Fetal Bovine Serum (FBS) rich media and Heat-inactivated FBS media. Targeson (Targeson, Inc. San Diego, CA) custom synthesis US contrast agent (perfluorocarbon microbubbles, encapsulated by a lipid monolayer and polyethylene glycol stabilizer) were prepared following manufacturer's instructions [53]. Cells were infected with Ad.GFP with 10MOI or with Ad.GFP complexed with microbubbles (Targeson) at 10MOI. US exposure was achieved with a Micro-Maxx SonoSite (SonoSite, Bothell, WA) US machine equipped with the transducer L25 set at 0.7 Mechanical Index (MI), 1.8 MPa for 1 min [53].

Statistical Analysis

Statistical analysis was performed using the GraphPad Prism 6 statistical software. Comparison of cell death by Annexin-V on adenoviral transduced groups was conducted using an ANOVA test with post hoc test Tukey's multiple comparison test. P-values of less than 0.05 were considered statistically significant.

RESULTS

Cytological Observations after Adenoviral Gene Transfer

The murine TRAMP-C2 and human DU145 prostate cancer cells were transduced with an Ad carrying the green fluorescence protein (GFP) (Ad.GFP) (Fig.15) with increasing doses of 10, 25 and 50 MOI (multiplicity of infection). TRAMP-C2 cells and DU145 cells infected with various doses of Ad.GFP showed a dose dependent increase of fluorescence. However, DU145 cells showed a higher transduction of GFP in comparison to TRAMP-C2 cells at each multiplicity of infection.

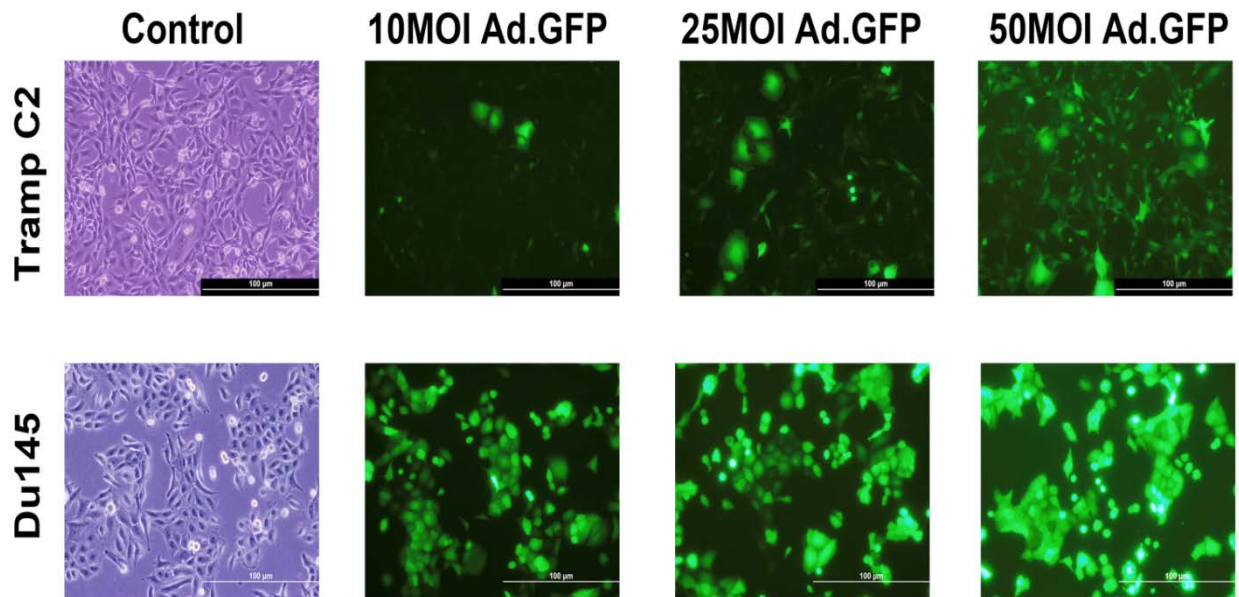


Figure 15. Fluorescence microscopy images of Ad.GFP (10, 25, 50 MOI) transduced TRAMP-C2 and DU145 cells. We effectively infected TRAMP-C2 cells with Ad.GFP and observed a dose-dependent expression of GFP, which was correlated to the increasing amount of Adenoviral MOI used.

Quantification of the Ad.GFP Viral Uptake

Ad.GFP uptake was determined for murine TRAMP-C2 and human DU145 prostate cancer cells by using FACS analysis after infecting the cells with 10, 25 and 50 MOI. A discrepancy is observed for TRAMP-C2 cells when infected with 10MOI, showing only a 90% uptake of Ad.GFP. A dose dependent increase in uptake of Ad.GFP is observed in TRAMP-C2 cells as the MOI is increased. DU145 cells on the contrary showed a 100% uptake regardless of MOI (Fig. 16).

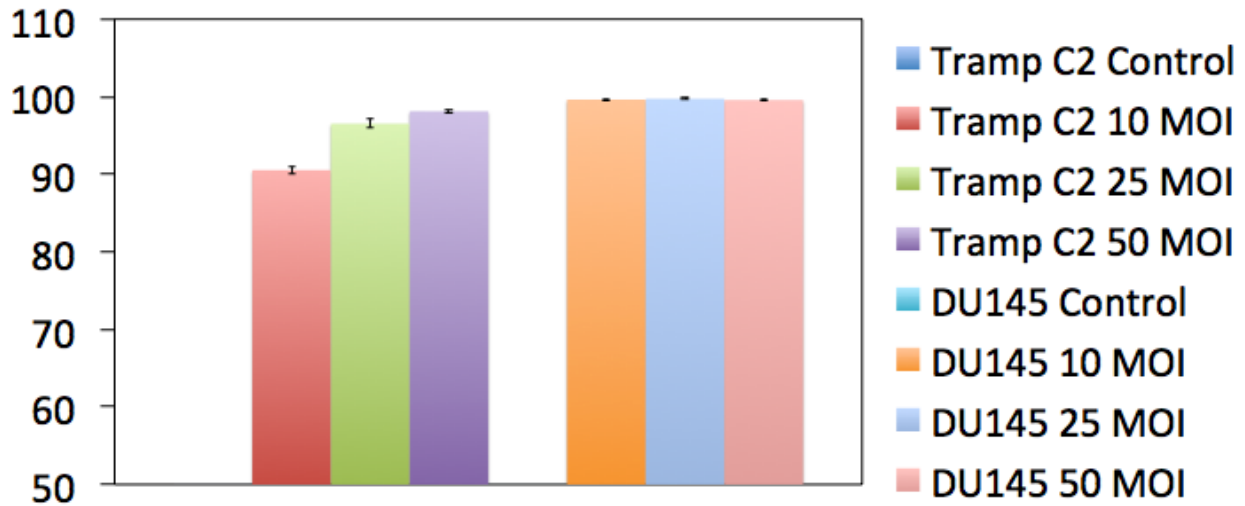


Figure 16. *In vitro* assessment of Ad.GFP uptake in murine and human carcinoma cell lines. Cells were infected at 10, 25 and 50 particles/cells (ppc) of Ad.GFP and harvested at 24 hours post-infection to determine the infectivity by FACS analysis.

Quantification of Ad Receptors Present on the Surface of the Cells

Surface Ad receptors were determined by Accuri C6 flow cytometry for the percentage of expression of Coxsackie Adenovirus Receptor (CAR), integrin $\alpha V\beta 5$ and $\alpha V\beta 3$ that are known to be responsible for the attachment of Ad5 to mammalian cells (Table 2). Both human DU145 and murine prostate cancer cells showed a similar expression profile for CAR and integrins

$\alpha V\beta 3/5$.

Table 2. Determination of the expression of surface Adenoviral receptors by flow cytometry.

| Cells | CAR | $\alpha V\beta 5$ | $\alpha V\beta 3$ |
|----------|------------|-------------------|-------------------|
| DU145 | 90.08±1.71 | 95.98±0.17 | 28.58±1.13 |
| TRAMP-C2 | 96.60±0.22 | 93.9±1.38 | 32.70±1.97 |

Verification of Protein Expression by Western Blots

The TRAMP-C2 cell line is generated from prostate tumors harvested from a 32-week TRAMP mouse. We carried out infection studies with Ad5 carrying mda-7 or GFP at different multiplicities of infection (MOI). Figure 17 shows dose dependent expression of GFP and mda-7 protein by western blot analysis (Fig. 17). The results show that we effectively transferred to murine PC cells a transgene (GFP or mda-7) with Ad5 viruses.

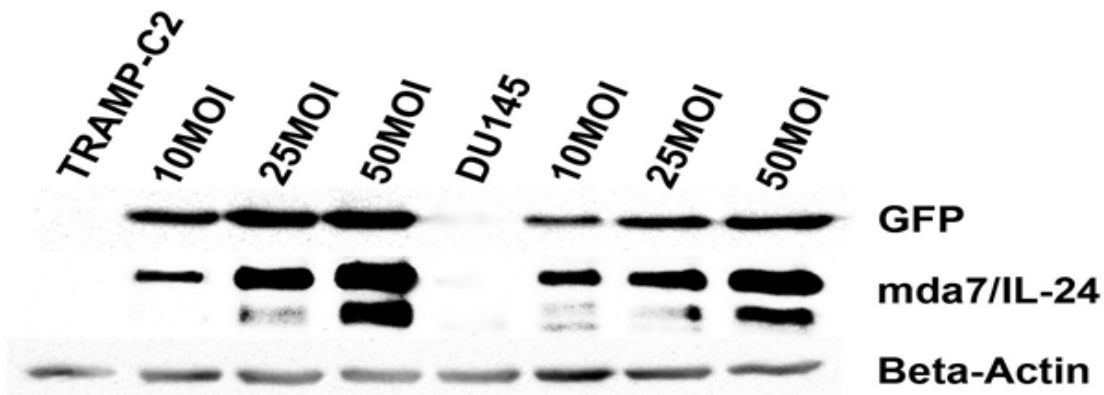


Figure 17. Western blot analysis of TRAMP-C2 and DU145 cells infected with different MOIs of Ad.GFP or Ad.mda-7/IL-24. Cell lysates were run on SDS-PAGE and reacted with appropriate specific primary and secondary HRP-conjugated antibodies. Beta actin was used as a loading control.

Viral Burst Assay to Assess the Capacity of Replicative HAd5 to Produce Viral Particles

The control HEK 293 embryonic kidney cells and human DU145 prostate cancer cells showed an increase in viral count at both 24 and 48 hours post infection of 100 pfu/mL and 1,000 pfu/mL replicative competent HAd5 (CTV). Thus, DU145 and HEK 293 are permissive for the replication of HAd5 and would make good animal models for testing the replicative and transfection ability of HAd5. However, TRAMP-C2 cells showed a decrease in viral count from 24 to 48 hours for both pfu of HAd5 indicating a lack of viral replication (Fig. 18). Thus TRAMP-C2 cells are non-permissive for replication of HAd5 and would make a good animal model only for the transfection ability of HAd5.

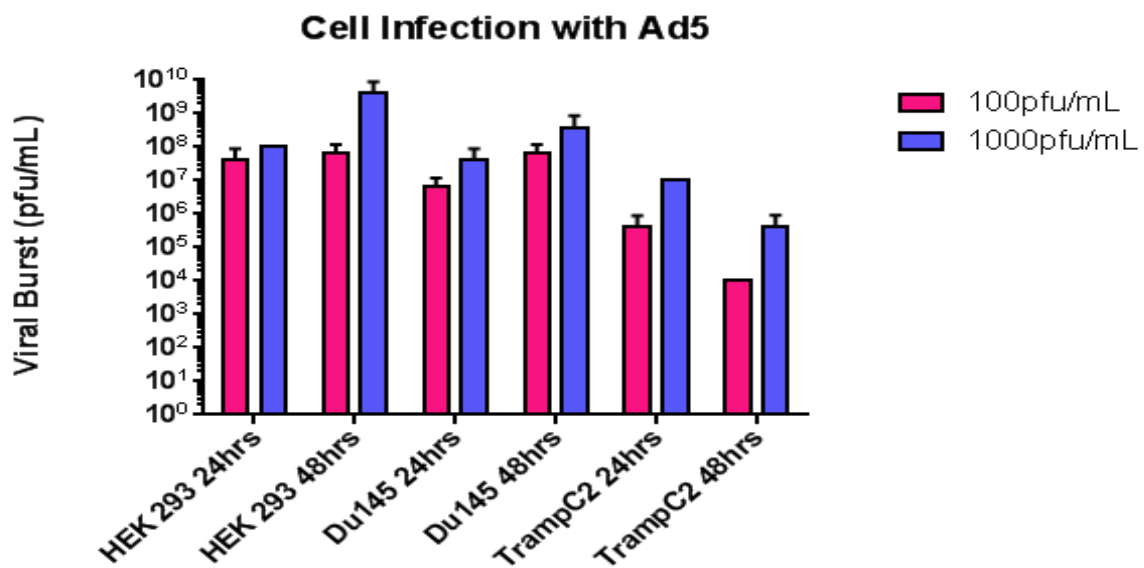


Figure 18. Subconfluent murine and human cell lines were infected with replicative competent HAdV at 100 pfu/mL and 1,000 pfu/mL and harvested 24- and 48-hours later.

Annexin-V Staining for Cell Death

The apoptotic rate of the transduced cells was quantified by assessing Annexin-V expression. The analyzed cells were allocated in a quadrant diagram according to their DNA

content and the presence of Annexin-V on the extracellular cell membrane during apoptosis. Statistical analysis was run on Annexin-V triplicates using Graphpad Prism 6 software for an ANOVA on dead cells with a post hoc test of Tukey's multiple comparison test (Fig. 19 and Table 3). TRAMP-C2 and DU145 cells were undergoing apoptosis and necrosis, collectively called as dead cells. Non-transduced cells were compared to Ad.mda-7/IL-24 transduced cells. Mean and standard deviation from Annexin-V experiment was calculated for each adenoviral treated group. There was an increase in the significance and percentage of cell death that was concentration dependent compared to the control. A significant percentage of cell death for TRAMP-C2 cells infected with 50MOI was observed in comparison to 10MOI of Ads (Fig. 19 and Table 3). Cell death observed for TRAMP-C2 cells infected with 10MOI and 25MOI did not show any significant difference in comparison to DU145 cells infected with 10MOI. However, overall DU145 cells showed more cell death with Ad.mda-7 at 25MOI and 50MOI in comparison to TRAMP-C2 cells infected with the same MOI.

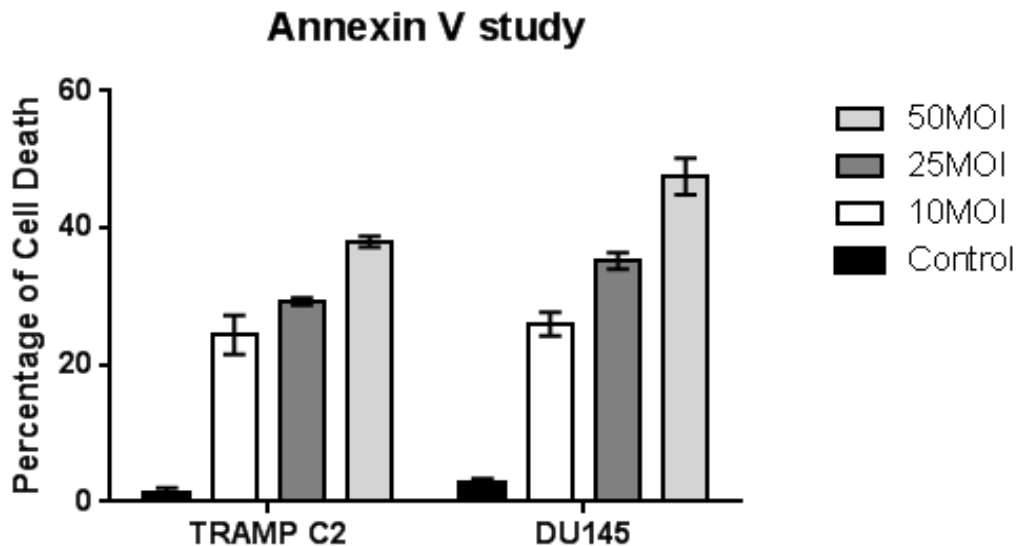


Figure 19. Annexin-V/PI staining of TRAMP-C2 and DU145 cells infected with Ad.mda-7/IL-24. TRAMP-C2 cells were transduced with Ad.mda-7/IL-24 at 10, 25 & 50 multiplicity of

infection (MOI) and harvested at 96 hours post infection and determined by FACS analysis. Bar graph represents sum of apoptotic and necrotic cells.

Table 3. ANOVA (Analysis of Variance) significance table with a Post Hoc Tukey's multiple comparison test for Annexin-V assay between TRAMP-C2 and DU145 cells transduced with Ad.mda-7/IL-24. * The mean difference is significant at the 0.05 level.

| Comparison between groups | | Significant? |
|---------------------------|----------------|--------------|
| TRAMP-C2:Control | TRAMP-C2:10MOI | Yes |
| TRAMP-C2:Control | TRAMP-C2:25MOI | Yes |
| TRAMP-C2:Control | TRAMP-C2:50MOI | Yes |
| TRAMP-C2:Control | DU145:Control | No |
| TRAMP-C2:Control | DU145:10MOI | Yes |
| TRAMP-C2:Control | DU145:25MOI | Yes |
| TRAMP-C2:Control | DU145:50MOI | Yes |
| TRAMP-C2:10MOI | TRAMP-C2:25MOI | Yes |
| TRAMP-C2:10MOI | TRAMP-C2:50MOI | Yes |
| TRAMP-C2:10MOI | DU145:Control | Yes |
| TRAMP-C2:10MOI | DU145:10MOI | No |
| TRAMP-C2:10MOI | DU145:25MOI | Yes |
| TRAMP-C2:10MOI | DU145:50MOI | Yes |
| TRAMP-C2:25MOI | TRAMP-C2:50MOI | Yes |
| TRAMP-C2:25MOI | DU145:Control | Yes |
| TRAMP-C2:25MOI | DU145:10MOI | No |
| TRAMP-C2:25MOI | DU145:25MOI | Yes |

| | | |
|----------------|---------------|-----|
| TRAMP-C2:25MOI | DU145:50MOI | Yes |
| TRAMP-C2:50MOI | DU145:Control | Yes |
| TRAMP-C2:50MOI | DU145:10MOI | Yes |
| TRAMP-C2:50MOI | DU145:25MOI | No |
| TRAMP-C2:50MOI | DU145:50MOI | Yes |
| DU145:Control | DU145:10MOI | Yes |
| DU145:Control | DU145:25MOI | Yes |
| DU145:Control | DU145:50MOI | Yes |
| DU145:10MOI | DU145:25MOI | Yes |
| DU145:10MOI | DU145:50MOI | Yes |
| DU145:25MOI | DU145:50MOI | Yes |

UTMD for Prostate Cancer Cells.

Human DU145 and murine prostate cancer cells were infected either with Ad.GFP or complexed Ad.GFP/MB at 10MOI and after 24hours images were taken with fluorescent microscopy. US application increased the expression of GFP in comparison to the control or Ad.GFP alone group for both DU145 and TRAMP-C2 cells (Fig. 20 and 22). US also allowed for the transfection of Ad.GFP in complement rich FBS media for both DU145 and TRAMP-C2 cells (Fig. 20 and 22).

MBs also facilitated the transfection of Ad.GFP in both FBS rich and Heat Inactivated-complement depleted FBS media (Fig. 21 and 23). Transfection increased further when Ad.GFP was complexed with a MB (Ad.GFP/MBs) and US was applied to both DU145 and TRAMP-C2 cells (Fig. 21 and 23). Similar GFP expression was observed for DU145 when complexed Ad.GFP/MBs were incubated with FBS and US was applied regardless of media being used (Fig.

21) because FBS contains a complement, which binds to the free Ads on the surface of the bubble thereby inactivating the Ads. Similar observation was also recorded for TRAMP-C2 cells (Fig. 23). Lastly, unclean complexed Ad.GFP/MBs showed similar GFP expression compared to cleaned (FBS incubated) complexed Ad.GFP/MBs in complement rich FBS media (Regular media). Highest transfection was observed for DU145 cells that received the unclean (FBS untreated) Ad.GFP/MBs and US (Fig. 21).

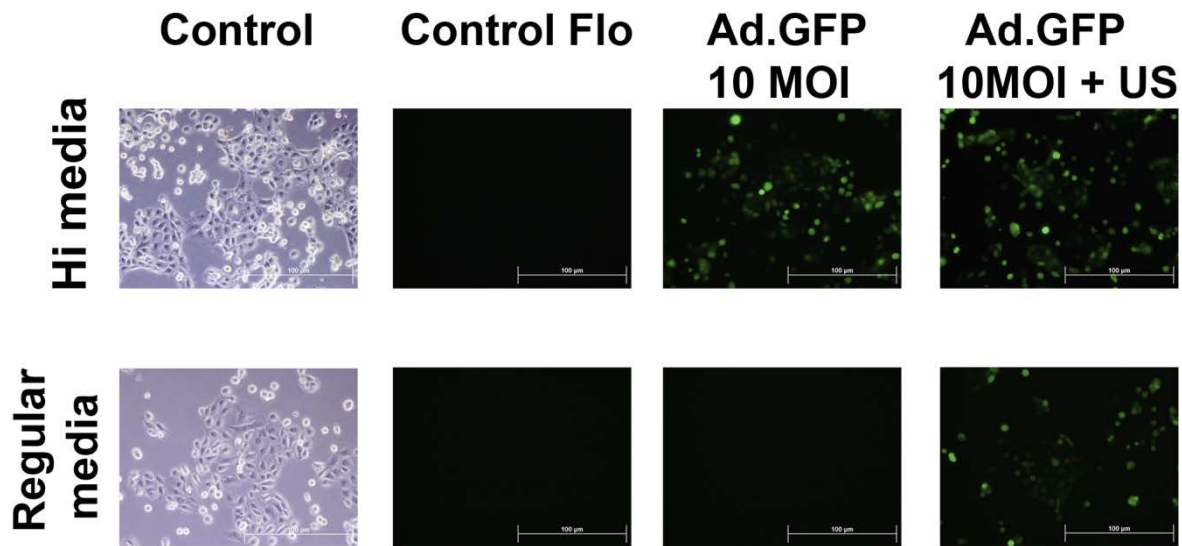


Figure 20. DU145 cells infected with Ad.GFP at 10MOI and Ultrasound application.

*Flo:Florescence, HI:heat inactivated, US: Ultrasound, Regular media: contains fetal bovine serum (FBS).

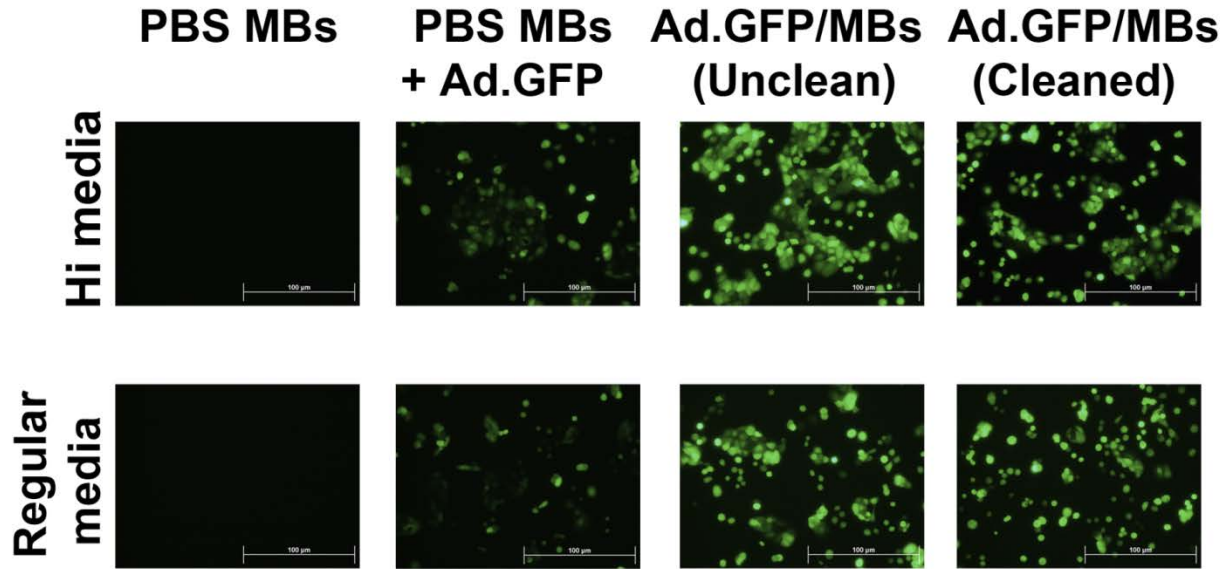


Figure 21. DU145 Cells infected with Ad.GFP/MBs at 10MOI and Ultrasound application. In second column MBs rehydrated with PBS was added separately with Ad.GFP at 10MOI. In the third column Ad.GFP/MBs were complexed but not cleaned with FBS before adding it to the cells. In the fourth column Ad.GFP/MBs were complexed and cleaned with FBS before adding it to the cells. *Flo:Florescence, HI:heat inactivated, US:Ultrasound, Regular media: contains fetal bovine serum (FBS).

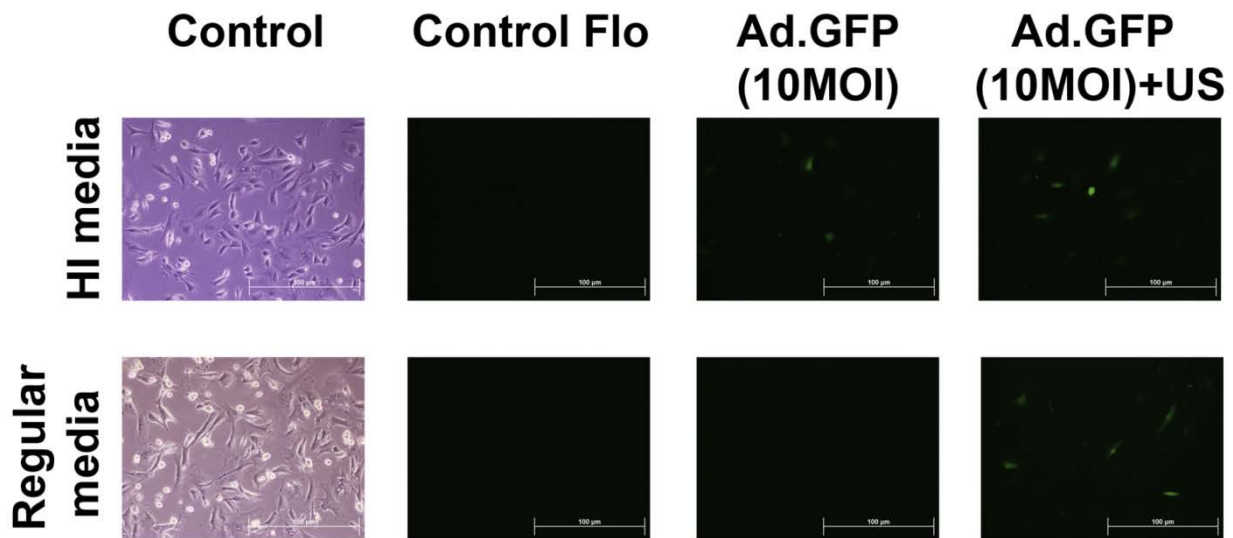


Figure 22. TRAMP-C2 cells infected with Ad.GFP at 10MOI and Ultrasound application.

*Flo:Florescence, HI:heat inactivated, US: Ultrasound, , Regular media: contains fetal bovine serum (FBS).

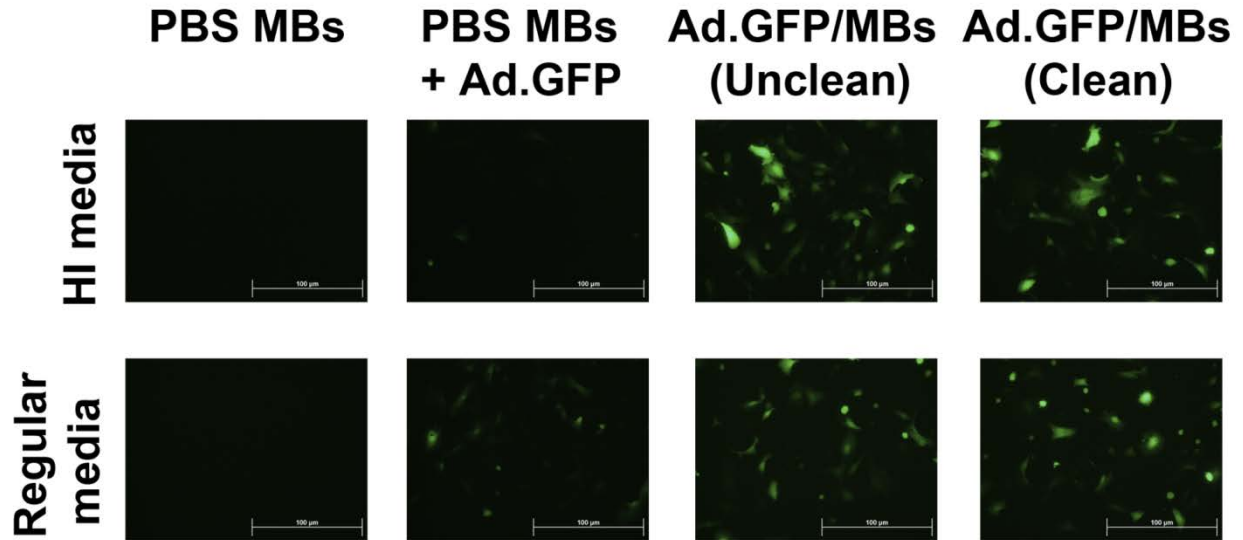


Figure 23. TRAMP-C2 cells infected with Ad.GFP/MBs at 10MOI and Ultrasound application.

In second column MBs rehydrated with PBS was added separately with Ad.GFP at 10MOI. In the third column Ad.GFP/MBs were complexed but not cleaned with FBS before adding it to the cells. In the fourth column Ad.GFP/MBs were complexed and cleaned with FBS before adding it to the cells. *Flo:Florescence, HI:heat inactivated, US: Ultrasound, Regular media: contains fetal bovine serum (FBS).

DISCUSSION

There are many obstacles to successful virotherapy that have become apparent from clinical studies, including problems associated with the use of replicating human Ads that are species-specific as the non-human (animal) model systems rarely predict the outcome seen in humans. For example, human tumor xenografts in nude mice can provide a ‘permissive’ preclinical model for Ads but nude mice are by definition immune-compromised [190], thus the immune responses due to Ads cannot be fully studied in this pre-clinical model. Additionally, due to species specificity, Ads do not replicate in normal mouse tissues thereby preventing any relevant off-target effects in such systems. Lastly, immune-compromised mice have a deficient immune system thus making it difficult to observe the effects of immune modulatory viruses [56], thus more suitable animal models need to be selected for the desired effect to be observed.

In this study, the ability of both replicating (CTV.mda-7) and non-replicating (Ad.GFP and Ad.mda-7/IL-24) human Ad5 was tested by infecting human DU145 and murine prostate cancer cells. The goal of this study was to test if human DU145 PC cells that are radio-resistant, androgen receptor ablated, p53 mutated cells and isolated from a brain metastasis would make a good pre-clinical model for the use of microbubble assisted gene delivery with US. This delivery system has several components that needed to be tested to ensure successful translation from bench to bedside. The infection studies on DU145 cells with Ad.GFP, Ad.mda-7 and CTV.mda-7 showed successful transduction with different MOI of replication permissive HAd5 and demonstrated a therapeutic response to gene therapy with mda-7. Lastly, US greatly enhanced the transgene expression of GFP when delivered with complexed Ad.GFP/MBs regardless of the presence of FBS, thus ensuring a proper penetration of the encapsulated Ads into the cell. FBS acted as a complement protein system inactivating the Ads from infecting

DU145 cells. US and MBs cause temporary pore formation on the plasma membranes and increase the permeability of the membrane to allow an increased Ad uptake. These factors make DU145 xenografts an attractive immune-compromised animal model to test the delivery of microbubble assisted gene delivery with US.

Similarly, TRAMP-C2 PC cells that are radio-resistant, possessing wild-type (wt) p53, isolated from 32-week old C57BL6 immune-competent mice with poorly differentiated prostate carcinoma were tested for the delivery of MB assisted gene therapy with US to verify if they would make a good pre-clinical immune-competent model. Similar results to DU145 studies were observed using TRAMP-C2 cells except that infection studies using TRAMP-C2 cells showed a reduced GFP expression in comparison to the transfected DU145 cells. However, a dose dependent increase in transgene expression was observed as the MOI were increased. The transgene expression could not be explained by the Ads surface receptor expression in TRAMP-C2 cells, as they are similar to DU145. Also, a reduced therapeutic response was observed for Ad.mda-7 transfected cells in comparison to DU145 cells, however still statistically significant in comparison to the control. Thus, murine immune-competent TRAMP-C2 prostate cells that can be syngeneically implanted into immune-competent C57BL6 would make an attractive model to study the immune-modulating, immune-responses due to the Ads and the therapeutic benefit of microbubble assisted US guided gene transfer. Additionally, the TRAMP mouse model of prostate cancer can be used to demonstrate the validity of UTMD mda-7 gene delivery approach in immune competent animals.

Successful completion of the immune competent animal studies will open the possibility to translate from the bench to the bedside the targeted mda-7 gene delivery method by performing clinical studies on metastatic prostate cancer patients.

**CHAPTER IV: ERADICATION OF THERAPY-RESISTANT HUMAN PROSTATE
TUMORS USING AN ULTRASOUND-GUIDED SITE-SPECIFIC CANCER
TERMINATOR VIRUS DELIVERY APPROACH**

This is a revised version of a manuscript published in *Molecular Therapy* (2010) 295-306.

Greco A¹⁻⁴, Di Benedetto A^{1,5}, Howard CM^{1,6}, Kelly S¹, Nande R¹, Dementieva Y⁷, Miranda M⁵, Brunetti A^{2,4}, Salvatore M^{2,3}, Claudio L⁸, Sarkar D⁹, Dent P¹⁰, Curiel DT¹¹⁻¹⁴, Fisher PB⁹, Claudio PP¹⁻¹⁵. Eradication of therapy-resistant human prostate tumors using an ultrasound-guided site-specific cancer terminator virus delivery approach. *Molecular Therapy*, 2010 Feb; v18 (2): 295-306.

doi:10.1038/mt.2009.252

¹Department of Biochemistry and Microbiology, Joan C. Edwards School of Medicine, Marshall University, Huntington, West Virginia, USA

²Department of Biomorphological and Functional Science, University of Naples "Federico II", Naples, Italy

³IRCCS SDN Foundation, Naples, Italy

⁴CEINGE-Advanced Biotechnology, s.c.ar.l., Naples, Italy

⁵Department of Basic and Applied Biology, Faculty of Sciences, University of L'Aquila, L'Aquila, Italy

⁶Department of Orthopedic Surgery, Marshall University, Huntington, West Virginia, USA

⁷Department of Mathematics, Marshall University, Huntington, West Virginia, USA

⁸Urology Department, National Cancer Institute "Fondazione Senatore Pascale", Naples, Italy

⁹Department of Human and Molecular Genetics, VCU Institute of Molecular Medicine, VCU Massey Cancer Center, Virginia Commonwealth University, School of Medicine, Richmond, Virginia, USA

¹⁰Department of Biochemistry and Molecular Biology, VCU Institute of Molecular Medicine, VCU Massey Cancer Center, Virginia Commonwealth University, School of Medicine,

Richmond, Virginia, USA

¹¹Division of Human Gene Therapy, Department of Medicine, University of Alabama at Birmingham, Birmingham, Alabama, USA

¹²Division of Human Gene Therapy, Department of Pathology, University of Alabama at Birmingham, Birmingham, Alabama, USA

¹³Division of Human Gene Therapy, Department of Surgery, University of Alabama at Birmingham, Birmingham, Alabama, USA

¹⁴Division of Human Gene Therapy, the Gene Therapy Center, University of Alabama at Birmingham, Birmingham, Alabama, USA

¹⁵Department of Surgery, Joan C. Edwards School of Medicine, Marshall University, Huntington, West Virginia, USA

Corresponding Author,
Pier Paolo Claudio,
Department of Biochemistry and Microbiology,
Department of Surgery, Joan C. Edwards School of Medicine,
Marshall University, Huntington, West Virginia 25755, USA.
E-mail: claudiop@marshall.edu

ABSTRACT

Intratumoral injections of a replication-incompetent adenovirus (Ad) expressing melanoma differentiation–associated gene-7/interleukin-24 (Ad.mda-7), a secreted cytokine displaying cancer-selective, apoptosis-inducing properties, profoundly inhibits prostate cancer (PC) growth in immune-incompetent animals. In contrast, Ad.mda-7 is ineffective in PCs overexpressing antiapoptotic proteins such as Bcl-2 or Bcl-xL. However, intratumoral injections of a conditionally replication-competent Ad (CRCA) in which expression of the adenoviral E1A gene is driven by the cancer-specific promoter of progression-elevated gene-3 (PEG-3) and which simultaneously expresses mda-7/interleukin (IL)-24 in the E3 region of the Ad (Ad.PEG-E1A-mda-7), a cancer terminator virus (CTV), is highly active in these cells. A major challenge for gene therapy is systemic delivery of nucleic acids directly into an affected tissue. Ultrasound (US) contrast agents (microbubbles—MBs) are viable candidates for gene delivery/therapy. Here, we show that MB/Ad.mda-7 complexes targeted to DU145 cells using US dramatically reduced tumor burden in xenografted nude mice. Additionally, US-guided MB/CTV delivery completely eradicated not only targeted DU145/Bcl-xL-therapy-resistant tumors, but also nontargeted distant tumors (established in the opposite flank), thereby implementing a cure. These findings highlight potential therapeutic applications of this novel image-guided gene therapy technology for advanced PC patients with metastatic disease.

Key Words: CTV; mda-7/IL-24; bystander anti-tumor activity; systemic targeted viral gene delivery; apoptosis induction

INTRODUCTION

Prostate cancer (PC) is the most common cancer and the second leading cause of cancer-related deaths in men in the United States [1]. At present, no effective therapy is available for metastatic PC [207]. Advanced PC is refractory to conventional anticancer treatments because of frequent overexpression of antiapoptotic proteins Bcl-2 and/or Bcl-xL [208, 209]. The Melanoma differentiation associated gene-7/interleukin-24 (mda-7/IL-24), is a secreted cytokine having broad-spectrum, cancer-selective, apoptosis-inducing properties that profoundly inhibits prostate cancer cell growth [210]. Adenovirus (Ad)-mediated delivery of mda-7/IL-24 (Ad.mda-7) has shown dramatic anti-tumor effects in animal models and in clinical trials [195, 196, 211, 212]. However, forced overexpression of Bcl-2 or Bcl-xL renders prostate cancer cells resistant to Ad.mda-7 [209]. In contrast, a conditionally replication-competent adenovirus (CRCA) (a cancer terminator virus- CTV), which expresses mda-7/IL-24 (Ad.PEG-E1A-mda-7) can abrogate acquired resistance of prostate cancer cells mediated through Bcl-2 and/or Bcl-xL overexpression causing growth arrest and apoptosis and selectively replicating in prostate cancer xenografted cells in athymic nude mice. Moreover, the CTV completely eradicates not only primary tumors but also distant tumors following repeated intratumoral injections into the primary tumor site [18, 213].

A major challenge for effective gene therapy is the ability to specifically deliver nucleic acids and potentially toxic gene products directly into diseased tissue. Progress in gene therapy has been hampered by concerns over the safety and practicality of viral vectors, particularly for intravenous delivery, and the inefficiency of currently available non-viral transfection techniques [214]. Viruses are appealing delivery vectors because of their ability to efficiently transfer genes with sustained and robust expression. Recombinant Ads are one of the most common gene

transfer vectors utilized in human clinical trials, but systemic administration of this virus is thwarted by host innate and adaptive antiviral immune responses which can limit and/or preclude repetitive treatment regimens [215].

The quest for novel, safe and more efficient systemic gene delivery systems has recently highlighted ultrasound (US) contrast agents (microbubbles) as a potential candidate for enhancing delivery of molecules to target tissue [136, 216-218]. Currently used US contrast agents (microbubbles) contain high-molecular weight gasses with less solubility and diffusivity, which improves microbubble persistence and allows passage through the microcirculation. Microbubbles (MB) can be injected in peripheral veins, because the more robust bubbles can recirculate through the systemic circulation numerous times, surviving for several minutes within the bloodstream [218, 219]. The ideal MB diameter most likely is between 2.5 to 4 μm . MB is small enough to prevent entrapment within the pulmonary capillary bed (ranging from 5 to 8 μm in diameter), but big enough to entrap and protect viral vectors such as Ad from the environment.

We previously demonstrated the feasibility of site-specific gene delivery mediated by diagnostic US using Ad-GFP encapsulated in commercially available US contrast agents *in vitro* and *in vivo* [214]. An additional goal of our previous study was to determine if incubation of the microbubbles with complement could improve specificity of viral transgene transduction to the target tissue/organ allowing a simplified approach to encapsulation of the viral vectors with commercially available contrast agents. In the current investigation we tested a US contrast agent provided by Targeson, Inc (San Diego, CA) and the portable SonoSite Micro-Maxx ultrasound platform (SonoSite, Inc., Bothell, WA) equipped with a L25 linear array transducer. Targeson's agents are lipid-encapsulated perfluorocarbon microbubbles with a mean diameter of 2.5 μm that can be used in a wide variety of animal models, and are compatible with virtually all ultrasound

scanners. The gas-filled microspheres effectively lower the energy threshold for non-thermal cavitation, thus allowing diagnostic transducers operating within the energy levels mandated by the FDA to be used for drug/gene delivery. Ultrasound-targeted microbubble destruction (UTMD) enables focal release of entrapped materials as well as the creation of small shock waves that increase cellular permeability [220]. In addition, the microbubbles protect the viruses from rapid degradation by the immune system, thus allowing for intravenous (IV) injection rather than direct target organ delivery by catheter-based approaches or operative bed injection [214, 218]. The IV injection is particularly important in cancer gene therapy of potentially inaccessible tumors because the microbubbles may also limit the amount of inflammatory response to the viruses and may allow repeated injections.

The ultimate goal of our research programs is to develop efficacious therapies for cancer. A primary focus is to engineer effective and safe delivery systems for viruses, chemotherapeutic agents and small molecule drugs. In the present study, we provide proof-of-principle for two essential components of this process, a site-specific gene delivery approach mediated by diagnostic US generated by a portable platform that works efficiently *in vivo* in combination with Ads delivering a highly effective, broad-based cancer gene therapeutic mda-7/IL-24. Evidence is provided that this combination has profound effects in animal models containing therapy-resistant human prostate cancer cells.

MATERIALS AND METHODS

Cell Lines, Cell Culture and Adenovirus Production

The DU145 (human prostate adenocarcinoma), cell line was obtained from the American Type Culture Collection (ATCC, Rockville, MD) and the DU-Bcl-xL cell line, which constitutively expresses elevated levels of Bcl-xL has been described previously [209]. The cell lines were grown at 37 °C, in a 5% CO₂/95% atmosphere, in Dulbecco's modified Eagle's medium (Mediatech Inc., Herndon, VA) supplemented with 10% fetal bovine serum (FBS) from Hyclone, Inc., (Logan, UT). Ad-GFP, which expresses the green fluorescence protein gene under the strong cytomegalovirus (CMV) constitutive promoter was generated using the AdEasy system (Carlsbad, CA); the conditionally replication competent cancer terminator virus CTV (Ad.PEG-E1A-mda-7) [18, 204, 205] and Ad.mda-7 [206] were amplified and purified with the BD Adeno-X virus purification kit (BD Biosciences, Mountain View, CA) following manufacturer's directions. Viral titers were determined by a plaque assay and the titer was adjusted to 1.2×10^{12} plaque-forming units (pfu)/mL as described [206].

Preparation of Microbubbles and Ultrasound Platform

Targeson (Targeson, Inc. San Diego, CA) custom synthesis US contrast agent (perfluorocarbon microbubbles, encapsulated by a lipid monolayer and polyethylene glycol stabilizer) were prepared following manufacturer's instructions. Microbubbles were reconstituted in the presence or absence of 1 mL of 1.2×10^{12} pfu of Ads and unenclosed, surface associated Ads were inactivated as previously described [214]. For *in vivo* experiments US exposure was achieved with a Micro-Maxx SonoSite (SonoSite, Bothell, WA) US machine equipped with the transducer L25 set at 0.7 Mechanical Index (MI), 1.8 MPa for 10 min.

Antibodies and Western Blot Analysis

DUI45 cells were transduced with 50 MOI of Ad.mda-7 or Ad-CMV as a control and 24 or 48-hr post transduction 50 μ g of total cell extracts were subjected to Western blot analysis using a mouse monoclonal anti-MDA-7/IL-24 (GenHunter, Inc, Nashville, TN) (1:2,000 incubation for 1 hr) or the mouse monoclonal anti-GAPDH sc-0411 (1:5,000 incubation for 1 hr) (SantaCruz, Santa Cruz, CA), as control. Western blot analysis was also conducted on protein extracts from microbubble/US assisted *in vivo* transfer of Ad-GFP or mda-7/IL-24 using antibodies that specifically recognized GFP sc-53882 (SantaCruz, Santa Cruz, CA), MDA-7/IL-24 (GenHunter, Nashville, TN), and β -actin sc-47778 (SantaCruz, Santa Cruz, CA). Briefly, 96 hr following targeted microbubble/US assisted *in vivo* transfer of Ad-GFP, mice were sacrificed and fresh tumor (right and left flank), heart, lung, liver, and kidney tissues were harvested and snap frozen in liquid nitrogen. Mice receiving mda-7/IL-24 gene-microbubble US guided therapy were sacrificed at the endpoint of the study (5-6 wks after gene therapy injections). Tissues were homogenized and equal amounts of proteins were run on a SDS-PAGE and transferred to a nitrocellulose membrane. The membrane was then incubated with the monoclonal anti-GFP 1:2,000 for 1 hr at room temperature and then washed three times in TBS-T. Monoclonal anti-MDA-7/IL-24 (GenHunter, Inc, Nashville, TN) was incubated 1:2,000 for 1 hr at room temperature and then washed three times in TBST. Monoclonal anti β -actin (1:5,000) was incubated 1 hr at room temperature and then washed three times in TBST. Appropriate secondary HRP-conjugated antibodies 1:20,000 were incubated 45 min at room temperature and washed three times with TBS-T. Signals were developed on an X-ray film after reaction with an Electrogenated Chemiluminescence (ECL) Supersignal kit (Pierce, Rockford, IL).

Animal Study and Ultrasonic Bubble Destruction

Animal studies were performed in accordance with NIH recommendations and the approval of the institutional animal research committee. Animal care and humane use and treatment of mice were in strict compliance with (1) institutional guidelines, (2) the Guide for the Care and Use of Laboratory Animals (National Academy of Sciences, Washington, DC, 1996), and (3) the Association for Assessment and Accreditation of Laboratory Animal Care International (Rockville, MD, 1997). All the animals used in these studies were 8- to 12-week-old female/male congenitally athymic BALB/c nude mice, homozygous for the *nu/nu* allele, bred in our laboratory. The colony of the mice was developed from breeding stock obtained from Charles Rivers Laboratories, Wilmington, MA. The mice were maintained in isolation in autoclaved cages with polyester fiber filter covers, under germ-free conditions; all food, water, and bedding were sterilized. A total of about 420 nude mice (n=10 each experimental point) were implanted with the human prostate adenocarcinoma cell lines (DU145 or DU-Bcl-xL) as a xenograft model (injecting 1.5×10^6 or 2.5×10^6 cancer cells on each flank of the animal). After ~30-days, mice were sedated in an IMPAQ6 anesthesia apparatus (VetEquip Inc, Pleasanton, CA) that was saturated with 3-5% Isoflurane and 10-15% oxygen with the aid of a precision vaporizer (VetEquip Inc, Pleasanton, CA) to deliver the appropriate amount of anesthetic and to induce anesthesia. The mice were placed on a warmed mat with 37°C circulating water for the entire procedure. A27-gauge needle with a heparin lock was placed within a lateral tail vein for administration of contrast material. The nude mice received injections of 100 μ L of microbubbles with/without Ads through the tail vein for 5 wks/once a wk. The mice were split into two control groups (one control group receiving 100 μ L of microbubbles and US, and another control group receiving both microbubbles/Ad-GFP and US) and eight active groups of

10 mice each (all receiving microbubbles and Ad.mda-7 or CTV and US). Six additional control groups were set up which received direct i.v. injections of 100 μ L of the Ads (Ad-GFP, Ad.mda-7/IL-24, or CTV) in the presence or not of US. Grayscale US imaging was performed with a SonoSite scanner (SonoSite, Bothell, WA) equipped with the transducer L25 set at 0.7 Mechanical Index (MI), 1.8 MPa for 10 min. Ultrasound images were recorded as digital clips. In every experiment, 10 animals for each treatment or control group were used to study tumor regression. Every experiment was repeated at least twice. Tumor volumes were determined by measuring the tumors twice a wk with either a caliper or by ultrasound measurements of the tumor axes. Tumor volumes were determined using the following formula: $V = (\pi/8) a X b^2$, where V is the tumor volume, a is the maximum tumor diameter, and b is the diameter at 90° to a [221]. The mice were humanely sacrificed by placing them in a CO₂ gas jar placed in a ventilated fume hood. The tumors (right and left flank), heart, lungs, kidneys, and liver were harvested. Tissues to be sectioned were dry snap frozen or placed either in OCT (Sakura Finetek USA, Inc., Torrance, CA), frozen in liquid nitrogen, and stored at -80°C or were preserved in neutral buffered formalin at 4°C prior to embedding in paraffin for immunohistochemical analysis.

Statistical Analysis

All statistical analyses were performed by using SAS version 9.1. Comparisons of tumor volumes were done separately three times: before the treatment, two weeks after the treatment, and at the end of the study. Statistical analyses for comparisons of different types of treatments were done using one-way ANOVA followed by Tukey-Kramer multiple adjusted pair wise tests. P-value < 0.05 was considered significant.

RESULTS

Targeson Microbubbles and a SonoSite Portable Micro-Maxx Ultrasound (US) Platform Efficiently Targets Ad-GFP Viruses to Tumors

We previously documented the feasibility of *in vivo* gene delivery mediated by diagnostic US using Ad-GFP encapsulated in a series of commercially available US contrast agents [214]. In the current investigation, we tested a different US contrast agent available from Targeson, Inc (San Diego, CA) and the portable SonoSite Micro-Maxx ultrasound platform (SonoSite, Inc., Bothell, WA) equipped with a L25 linear array transducer. Targeson's agents are lipid-encapsulated perfluorocarbon microbubbles with a mean diameter of 2.5 μm that can be used in a wide variety of animal models, and are compatible with virtually all ultrasound scanners [222]. Targeson agents are normally sold as already reconstituted contrast agents that are stable for three months from arrival, and for this study we obtained a custom made freeze-dried Targeson contrast agent (perfluorocarbon microbubbles, encapsulated by a lipid monolayer and polyethylene glycol stabilizer) to be reconstituted with the viruses as previously described [214].

To confirm the ability of the lyophilized Targeson US contrast agent to deliver viruses efficiently and specifically to defined sites *in vivo*, we performed a pilot study in which tumor xenografts were established in both flanks of athymic nude mice by injecting each site with 2×10^6 DU145 human prostate carcinoma cells (Figure 24A). The DU145 tumor-bearing nude mice (n=10) were then injected in their tail vein with 100 μL of US contrast agent that was reconstituted with Ad-GFP or water as control. A portable SonoSite Micro-Maxx ultrasound platform (SonoSite, Inc., Bothell, WA) equipped with a L25 linear array transducer set at 0.7 Mechanical Index (MI), 1.8 MPa for 10 min was used to sonoporate only the tumor implanted on

the right side (Figure 24A). Mice were sacrificed 96 hr after treatment and tumors (right and left side), lung, heart, liver and kidney were harvested and snap frozen. Figure 24B shows the specific delivery to the right tumor as evidenced by expression of the green fluorescence protein (GFP) in an immunoblot in which total protein extracts were run on a 10% SDS-PAGE. As a GFP control, we ran a GST-GFP fusion protein. Protein gel loading was normalized using β -actin as a control. US-targeted microbubble destruction (UTMD) enables focal release of entrapped materials as well as the creation of small shock waves that are visualized as an enhancement of the image on the US scanner. Figure 24, panel C depicts the B-mode US imaging of a sonoporated tumor before injection with the microbubble/Ad-GFP complex contrast agent. Figure 24, panel D shows the B-mode ultrasound imaging of the same sonoporated tumor following microbubble/Ad-GFP complex injection. The image enhancement of the targeted tumor from cavitation of the microbubbles within the US field of view is clearly discernable indicating that the US settings are efficient in targeting microbubble destruction.

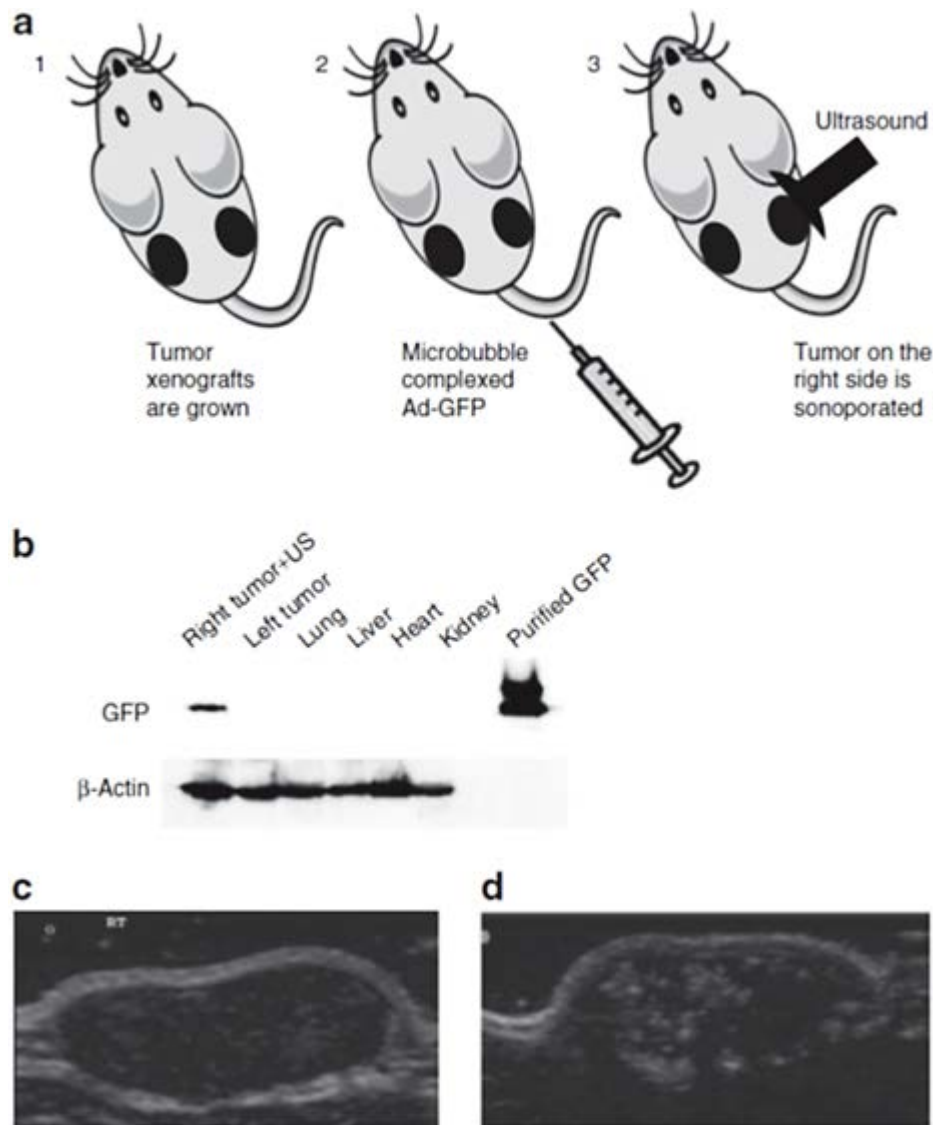


Figure 24. (a) Schematic representation of the microbubble delivery of Ad-GFP complexes and ultrasound (US) release in a tumor target site of the mouse. (b) Western blot analysis of Ad-GFP/microbubble–transduced DU145 tumor xenografts. Immunoblot showing the expression levels of green fluorescent protein (GFP) in DU145 cells following ultrasound-targeted microbubble/Ad transduction of GFP at 96 hours. Only the tumor on the right flank was sonoporated for 10 minutes resulting in the delivery and expression of GFP. The left tumor, heart, lung, liver, and kidney were negative for GFP expression. Purified glutathione-S-

transferase–GFP was used as a positive control. Protein gel loading was normalized using β -actin as a control. (c) Ultrasound imaging and US contrast enhancement of *in vivo* transduced DU145 tumor xenografts. B-mode US imaging of a tumor before MB contrast agent injection. (d) B-mode US imaging of the same tumor depicted in c following injection of microbubbles/Ad-GFP complexes. MBs cavitation within the targeted tumor dramatically enhances the tumor image within the US field of view. Ad, adenovirus.

Microbubble Assisted Ad.mda-7 Gene Delivery Inhibits DU145 Human Prostate Cancer Growth *In Vivo*

In vitro and *in vivo* Ad-mediated gene transfer of the human mda-7/IL-24 gene (Ad.mda-7) potently suppresses the growth of human cancer cells with no apparent toxicity to normal cells [195, 203, 206, 211, 212, 223-230]. Repeated intratumoral administration of Ad.mda-7 to tumor xenografts of various histological origin results in growth suppression via induction of apoptosis and anti-angiogenic mechanisms [195, 196, 209-212, 226, 228, 231]. Additionally, mda-7/IL-24 induces a profound “*bystander*” antitumor effect resulting in tumor growth suppression not only in the treated tumors, but also in untreated distant tumors [18, 194, 195, 197, 205, 211-213, 223, 224, 226, 227, 232, 233]. Although these results have been encouraging, this approach is limited since systemic delivery of Ad for treatment of disseminated cancer has not shown significant efficacy.

We have employed a novel systemic delivery approach to target Ad release in a site-specific manner that consists of Ad incorporated in microbubbles combined with diagnostic US [214]. Proof-of-principle for this strategy comes from studies using Ad to systemically deliver the GFP gene in a tissue specific manner [214]. Because mda-7/IL-24 has shown significant

potential as a selective and effective anticancer agent in multiple animal model studies and in a Phase I intratumoral gene therapy trial in patients with advanced solid cancers [195, 196, 203, 211, 212, 223, 224, 228], we tested the capacity of this approach to deliver Ad expressing this novel cytokine in prostate adenocarcinoma nude mouse xenograft models. For these studies, we used DU145 human prostate carcinoma cells and DU145 cells genetically engineered to express elevated levels of Bcl-xL (DU-Bcl-xL) [209], which is a common event in advanced prostate cancer and provokes resistance to multiple chemotherapeutic agents and to mda-7/IL-24 [207-210]. The therapeutic arm of this work included two different viral constructs to deliver mda-7/IL-24, Ad.mda-7, a nonreplicating Ad similar to the one used in Phase I clinical trials [206], and the CTV, a conditionally replication competent Ad capable of expressing mda-7/IL-24 that has been previously shown to completely eradicate not only primary breast, prostate and melanoma tumors but also distant tumors by intratumoral injections in a nude mouse model [18, 197, 204, 205].

To test this new therapeutic approach for tumor delivery, DU145 or DU-Bcl-xL tumor xenografts were established on both flanks of nude mice by injecting 2×10^6 cells in each side of the animals. DU145 and DU-Bcl-xL tumor bearing nude mice (n=10 each group) were then injected in their tail vein with 100 μ L of US contrast agent that was reconstituted with Ad-GFP or water as control. Additional DU145 and DU-Bcl-xL tumor control nude mice (n=10 each group) were injected in the tail vein with 100 μ L of Ad.mda-7 or the CTV (Ad.PEG-E1A-mda-7) without US contrast agent. Alternatively, tumor-bearing animals were injected in their tail vein with 100 μ L of US contrast agent that was reconstituted with Ad.mda-7 or the CTV. A portable SonoSite Micro-Maxx US platform (SonoSite, Inc., Bothell, WA) equipped with a L25 linear array transducer set at 0.7 Mechanical Index (MI), 1.8 MPa for 10 min was used to sonoporate

the tumor implanted on the right side. In this study, gene therapy treatments were started ten weeks after the injection of the cell lines, when tumors reached an approximate volume of 150-200 mm³. Mice were injected once a week for four weeks for a total of four treatments. Mice were sacrificed two weeks after the end of the treatments to determine whether tumor suppression was reversible or irreversible. At the end of the study tumors (right and left flank), lung, heart, liver and kidney were harvested and snap frozen using liquid nitrogen.

US of Ad-GFP microbubble complexes in the right side tumor resulted in progressive growth of the tumors on both flanks (Figures 25A and E). The results shown in Figure 25 represent the average tumor volumes measured in a minimum of 7 mice for each mda-7/IL-24 group and a minimum of 5 mice for each control GFP group. All the mice were injected in the tail vein with the microbubble/Ad complexes and only the tumor on the right flank was sonoporated. Interestingly, we observed that microbubble-mediated Ad.mda-7 gene therapy inhibited the growth of DU145 prostate tumor xenografts during the treatment regimen (Figure 25B), while the CTV microbubble-mediated gene therapy resulted in a steady progressive tumor regression that lasted an additional two weeks post-treatment (Figure 25C).

As predicted from previous studies [18, 209, 210], Ad.mda-7 was ineffective in causing a therapeutic response in tumor xenografts on either flank developed from DU-Bcl-xL cells (Figure 25F). In contrast, the conditionally replication competent CTV (Ad.PEG-Prom-mda-7) elicited a sustained growth inhibition of the therapy resistant DU-Bcl-xL tumor xenografts (Figure 25G). A Western blot analysis of total protein extracts from the harvested tumors showed expression of MDA-7/IL-24 protein in both the tumor samples implanted on the right and left flank (Figures 25D and H) validating the “*bystander*” effects of MDA-7/IL-24 previously reported [18, 194, 197, 204, 233]. In the case of the CTV, this amplified expression of MDA-

7/IL-24 in the non-injected left tumor may also reflect secondary viral infection by the CRCA [18]. GAPDH expression was used to confirm equal loading of the gel. No tumor regression was observed in mice bearing DU145 and DU-Bcl-xL control tumors when injected intravenously with comparable doses of unprotected Ad.mda-7 and CTV viruses (Figures 27 and 28).

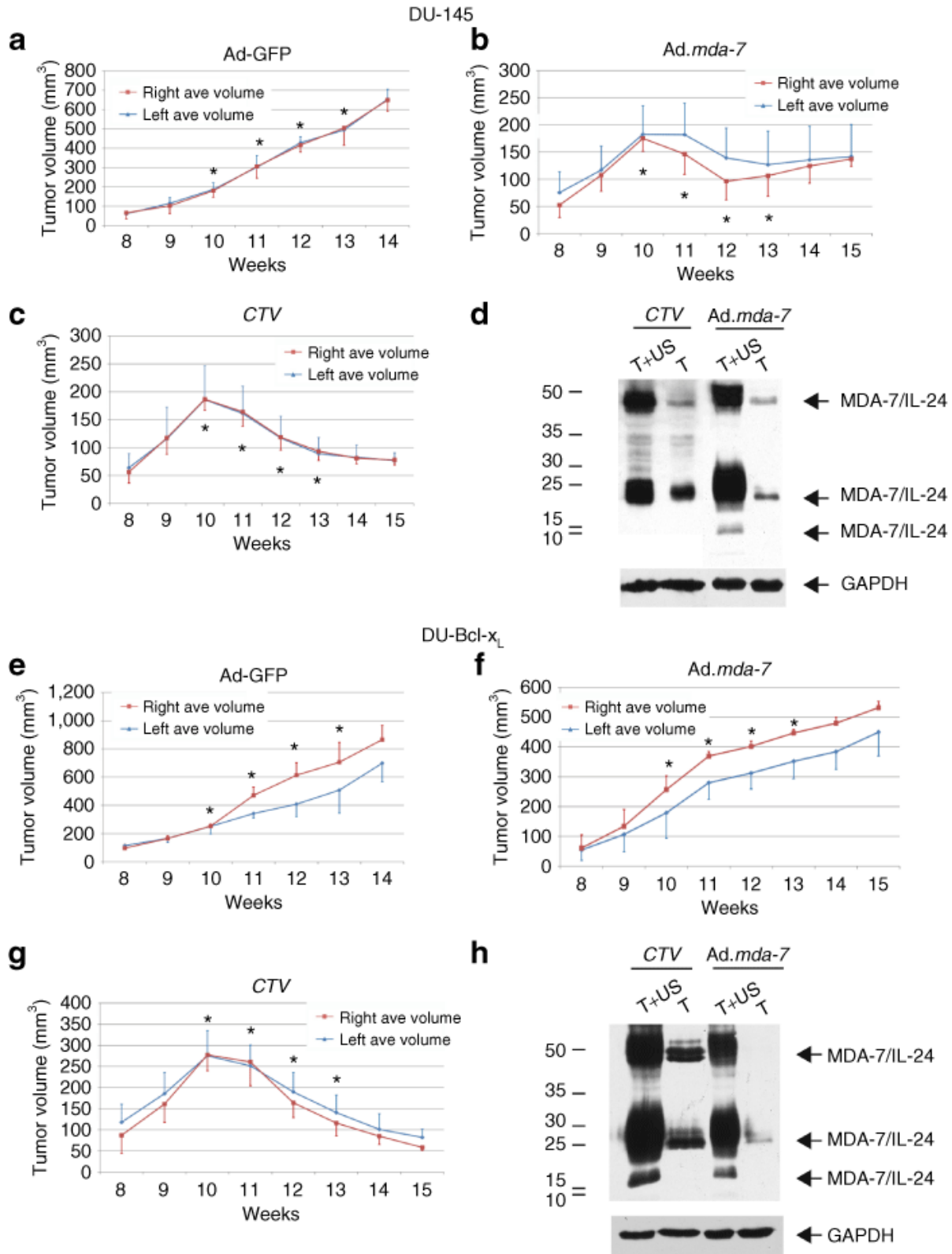


Figure 25. Growth curves and western blot analysis of large DU145 and DU-Bcl-x_L tumor

xenografts treated with microbubble encapsulated Ad-GFP, Ad.mda-7, or cancer terminator virus (CTV) (Ad.PEG-E1A-mda-7) and treated with ultrasound (US) in the right tumor. Subcutaneous tumor xenografts from DU145 and DU-Bcl-xL were established in athymic nude mice in both right and left flanks and only tumors on the right side were sonoporated following tail-vein injection of the indicated microbubble/Ad complexes during a course of 4 weeks. Tumor treatments were initiated when tumors reached a size of 250–350 mm³. Arrows point at tumors and asterisks point at treatment times. (a) Measurement of green fluorescent protein (GFP)-treated DU145 tumor volumes. The data represent mean \pm SD with at least 5 mice in each group. (b) Measurement of Ad.mda-7-treated DU145 tumor volumes. The data represent mean \pm SD with at least 7 mice in each group. (c) Measurement of CTV-treated DU145 tumor volumes. The data represent mean \pm SD with at least 7 mice in each group. (d) Western blot analysis of protein extracts from representative DU145 tumor samples treated with Ad.mda-7 or CTV. The immunoblot was reacted with anti-MDA-7/IL-24. Arrowheads point at the various glycosylated forms of MDA-7/IL-24. Protein gel loading was normalized using anti-GAPDH as a control. (e) Measurement of GFP-treated DU-Bcl-xL tumor volumes. The data represent mean \pm SD with at least 5 mice in each group. (f) Measurement of Ad.mda-7-treated DU-Bcl-xL tumor volumes. The data represent mean \pm SD with at least 7 mice in each group. (g) Measurement of CTV-treated DU-Bcl-xL tumor volumes. The data represent mean \pm SD with at least 7 mice in each group. (h) Western blot analysis of protein extracts from representative DU-Bcl-xL tumor samples treated with Ad.mda-7 or CTV. The immunoblot was reacted with anti-MDA-7/IL-24. Arrowheads point at the various glycosylated forms of MDA-7/IL-24. Protein gel loading was normalized using anti-GAPDH as a control. Ad, adenovirus; GAPDH, glyceraldehyde 3-phosphate dehydrogenase.

Microbubble Assisted CTV Gene Delivery Eradicates Prostate Cancer growth *In Vivo*

In our study, the size of the tumor was measured twice a week by caliper as well as by B-mode ultrasound scanning. Figure 26A shows the ultrasound image and measurements of a DU145 tumor before treatment with Ad.mda-7-microbubble complexes. Panels B and C demonstrate the volume reduction in the same tumor after 2 and 4 weeks of treatments with Ad.mda-7-microbubble complexes and US. Figure 26D shows the B-mode scan image and measurements of a DU-Bcl-xL tumor before treatment with CTV-microbubble complexes. Panels E and F emphasize the dramatic volume reduction in the same tumor after 2 and 4 wks of treatments with CTV-microbubble complexes and US leading to the eradication of the tumor xenograft. Additionally, no tumor regrowth in the primary or distant sites was evident CTV-microbubble complex and US-treated DU-Bcl-xL animals after an additional three weeks post-treatment. To investigate if the tumor would reappear after a longer period of time following the last treatment, three out of ten animals initially treated with CTV-microbubble complexes were not sacrificed at the endpoint of the study and were maintained for an additional 3 months. The mice were then sacrificed and dissected to look for potential tumor recurrence and/or eventual tumor spread. We did not observe any local tumor reappearance or distant metastasis in the lungs or liver in these mice that were treated with CTV-microbubble complexes and US indicating that this therapeutic approach could be suitable to target conditionally replication-competent adenoviruses (CRCA) to prostate tumors causing the eradication of localized as well as distant metastatic tumors. Future studies testing this approach in immune competent tumor bearing and transgenic animals would provide definitive support for exploring this strategy in the context of a Phase I clinical trial.

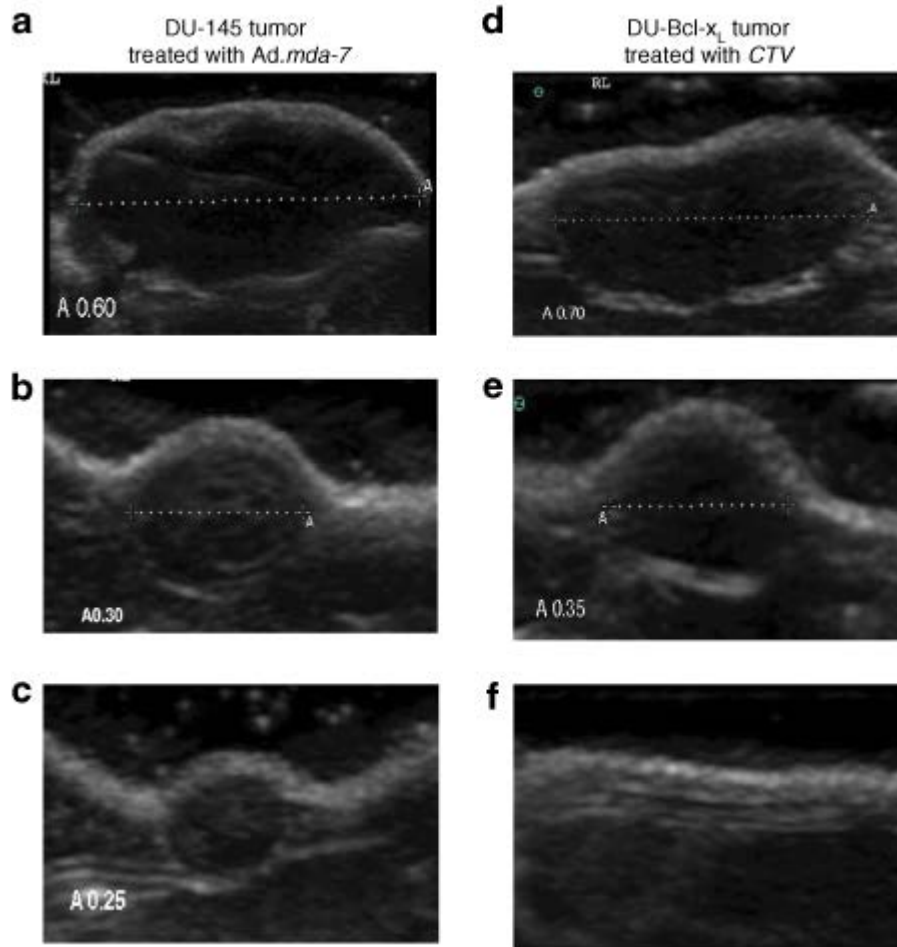


Figure 26. B-mode ultrasound (US) imaging of DU145 tumor xenografts treated with microbubble/US-guided Ad.mda-7 and therapy resistant DU-Bcl-xL tumor xenografts treated with microbubble/US-guided cancer terminator virus (CTV).

Subcutaneous tumor xenografts from DU145 and DU-Bcl-xL cells were established in athymic nude mice in both right and left flanks and only tumors on the right side were sonoporated following tail-vein injection of the indicated microbubble/Ad complexes during a course of 4 weeks. Tumor volumes were determined by measuring twice a week the tumors with either a caliper or by US measurements of the tumor axes.

(a) Ultrasound image and measurement of a DU145 tumor before treatment with Ad.mda-7/microbubble complexes and US.

(b) US image and measurement of the same DU145 tumor 2 weeks following treatments with Ad.mda-7/microbubble complexes and US.

(c) US image and measurement of the same DU145 tumor 4 weeks following treatments with Ad.mda-7/microbubble complexes and US.

(d) US image and measurement of a DU-Bcl-xL tumor before treatment with CTV/microbubble complexes and US.

(e) US image and measurement of the same DU-Bcl-xL tumor 2 weeks following treatments with the CTV/microbubble complexes and US.

(f) US image and measurement of the same DU-Bcl-xL tumor 4 weeks following treatments with CTV/microbubble complexes and US.

Complete eradication of the DU-Bcl-xL tumor occurs 4 weeks after initiating the therapeutic treatment protocol. Ad, adenovirus; GFP, green fluorescent protein.

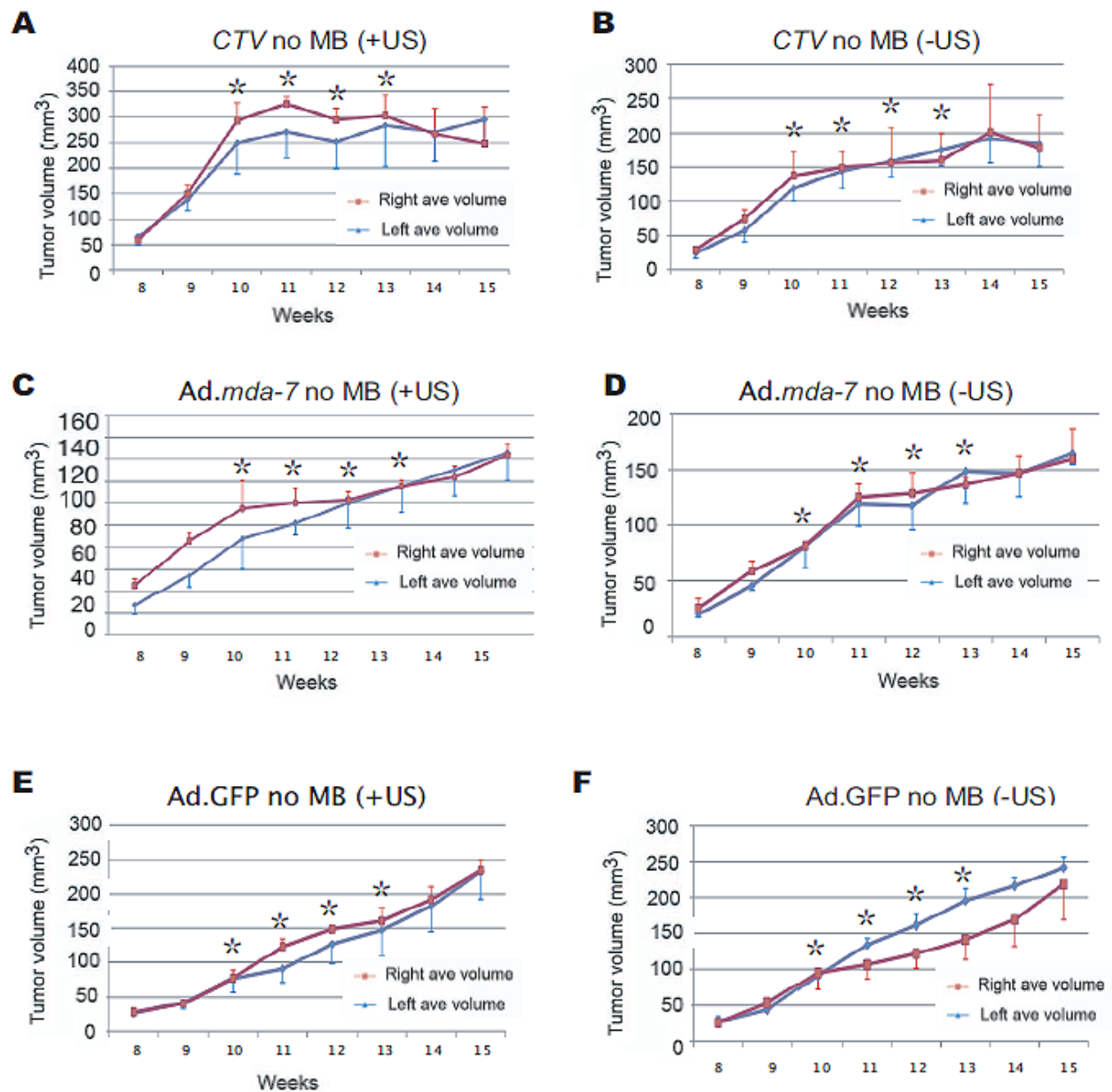


Figure 27. Growth curves of control DU145 tumor xenografts injected i.v. using unprotected Ad-GFP, Ad.mda-7, or CTV (Ad.PEG-E1A-mda-7) and treated or not with US. Subcutaneous tumor xenografts from DU145 were established in athymic nude mice in both right and left flanks and only tumors on the right side were sonoporated following tail vein injection of the indicated Ads during a course of 4 wks. Tumor treatments were initiated when tumors reached a size of 150 – 200 mm³. Asterisks point at treatment times.

A) Measurement of CTV-injected and sonoporated DU145 tumor volumes. The data represent

mean \pm s.d. with at least 5 mice in each group.

B) Measurement of CTV-injected, but not sonoporated DU145 tumor volumes. The data represent mean \pm s.d. with at least 5 mice in each group.

C) Measurement of Ad.mda-7-injected and sonoporated DU145 tumor volumes. The data represent mean \pm s.d. with at least 5 mice in each group.

D) Measurement of Ad.mda-7-injected, but not sonoporated DU145 tumor volumes. The data represent mean \pm s.d. with at least 5 mice in each group.

E) Measurement of Ad.GFP-injected and sonoporated DU145 tumor volumes. The data represent mean \pm s.d. with at least 5 mice in each group.

F) Measurement of Ad.GFP-injected, but not sonoporated DU145 tumor volumes. The data represent mean \pm s.d. with at least 5 mice in each group.

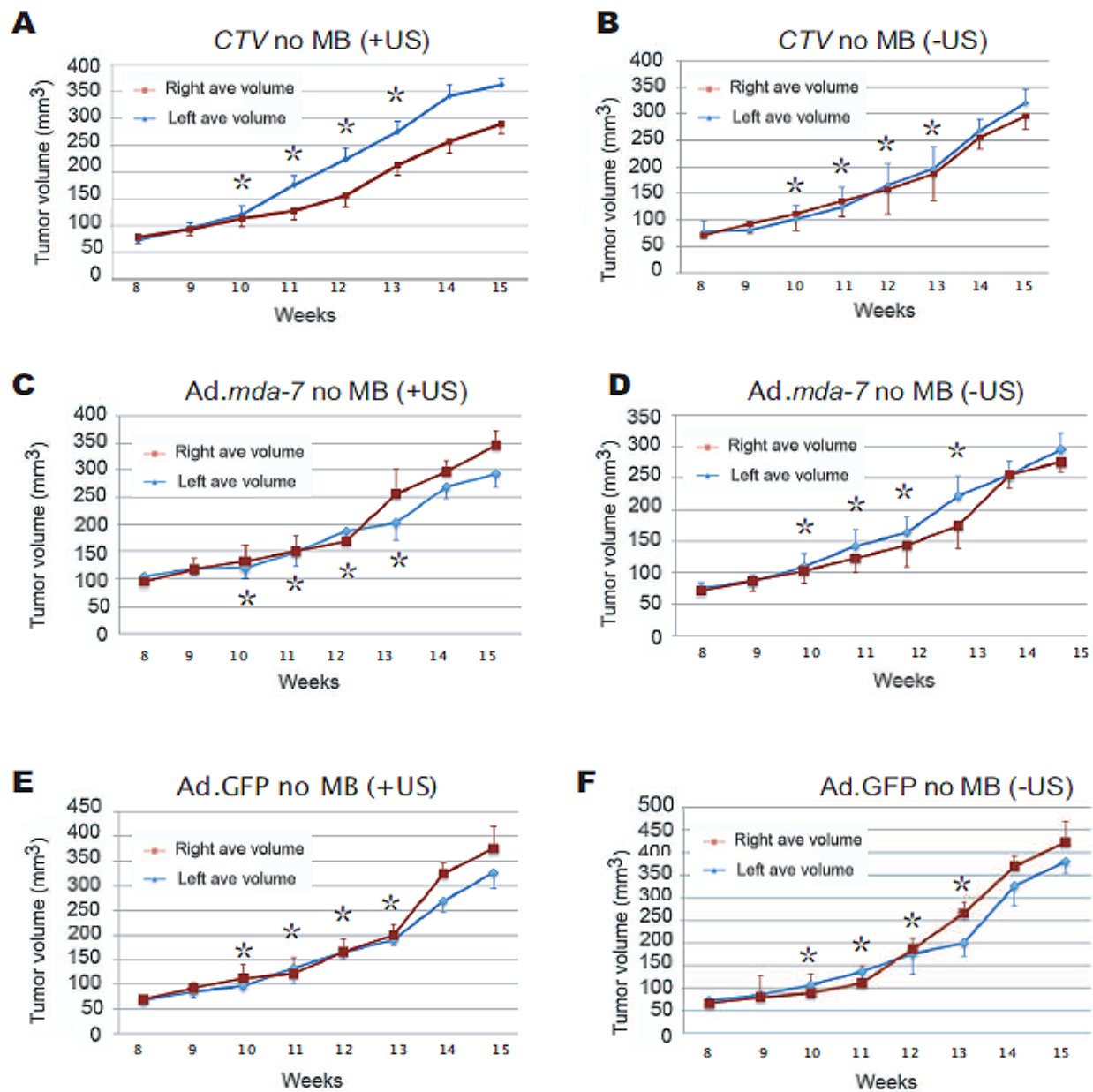


Figure 28. Growth curves of control DU-Bcl-xL tumor xenografts injected i.v. using unprotected Ad-GFP, Ad.mda-7, or CTV (Ad.PEG-E1A-mda-7) and treated or not with US. Subcutaneous tumor xenografts from DU-Bcl-xL were established in athymic nude mice in both right and left flanks and only tumors on the right side were sonoporated following tail vein injection of the indicated Ads during a course of 4 wks. Tumor treatments were initiated when tumors reached a size of 150 – 200 mm³. Asterisks point at treatment times.

A) Measurement of CTV-injected and sonoporated DU-Bcl-xL tumor volumes. The data

represent mean \pm s.d. with at least 5 mice in each group.

B) Measurement of CTV-injected, but not sonoporated DU-Bcl-xL tumor volumes. The data represent mean \pm s.d. with at least 5 mice in each group.

C) Measurement of Ad.mda-7-injected and sonoporated DU-Bcl-xL tumor volumes. The data represent mean \pm s.d. with at least 5 mice in each group.

D) Measurement of Ad.mda-7-injected, but not sonoporated DU-Bcl-xL tumor volumes. The data represent mean \pm s.d. with at least 5 mice in each group.

E) Measurement of Ad.GFP-injected and sonoporated DU-Bcl-xL tumor volumes. The data represent mean \pm s.d. with at least 5 mice in each group.

F) Measurement of Ad.GFP-injected, but not sonoporated DU-Bcl-xL tumor volumes. The data represent mean \pm s.d. with at least 5 mice in each group.

DISCUSSION

Microbubbles have been used to protect viruses from rapid degradation by the immune system, thus allowing intravenous injection rather than direct target organ delivery by catheter-based approaches or operative bed injection [234]. However, variable levels of non-targeted gene expression have been noted in other organs such as the liver and lungs [234]. We have recently shown that US imaging and US contrast agents can increase target specificity of Ads to tumors, achieving transient transgene expression with strict image-guided site specificity by selecting microbubbles which completely enclosed the Ads in their gas filled core [214]. In our prior experience, US-mediated microbubble destruction improved the efficacy and reduced the non-specific expression of gene therapy vectors providing a useful tool for manipulating gene expression in the living animal.

Genetic therapies for prostate cancer represent promising strategies for the treatment of this neoplasm. The prostate gland is accessible by US, and potential therapeutic genes can be directed to this organ using portable diagnostic US platforms such as the SonoSite MicroMaxx (SonoSite, Inc., Bothell, WA) after a simple intravenous injection. Importantly, because prostate cancer is commonly a relatively slow-growing disease, it may be necessary to use repeated gene therapy applications, with single or multiple genes, over the life span of the patient. In these contexts, gene therapy protocols that delimit virus exposure to the immune system and can be administered multiple times during a patient's lifetime are appealing. This possibility will need to be explored in the future using tumor-bearing immune competent animals. In the current work, we explored the ability of US-mediated microbubble destruction to specifically deliver in prostate adenocarcinoma xenografts the mda-7/IL-24 gene [235, 236], that has been successfully employed in a Phase I clinical trial in patients with advanced solid tumors [195, 196, 203, 211,

212, 223, 224, 228].

Potentially useful approaches for treating prostate and other cancers involve the use of a replication incompetent adenovirus (Ad.mda-7) or a conditionally replication competent Ad (Ad.PEG-E1A-mda-7; CTV) to administer the therapeutic cytokine mda-7/IL-24 to induce targeted therapy of tumors [18, 195-197, 204, 205, 211, 212, 237]. Although very effective in prostate cancer cell lines, no therapeutic benefit is observed with Ad.mda-7 in the context of prostate cancer cells displaying elevated expression of Bcl-2 and/or Bcl-xL [18, 209]. In contrast, administration of the CTV by direct intratumoral delivery in nude mice containing xenografted Bcl-xL overexpressing DU145 cells implanted on both flanks of the animal results in tumor eradication in both the primary injected tumor and the distant untreated tumor [18].

Conditionally replication competent Ads (CRCA), which induce oncolysis by cancer-specific replication, have been evaluated in several prostate cancer clinical trials [238, 239]. Most currently employed CRCA are based on the ONYX-015 backbone, which is dependent on the p53 status of the cancer cells and have shown only minimal objective clinical responses, thus limiting their universal applicability for the treatment of prostate or other cancers [240]. To this end, the novel CTV CRCA that employs the progression elevated gene-3 (PEG-3) promoter that functions in all types of cancer cells [18, 204, 205, 241, 242], irrespective of their p53 or Rb/retinoblastoma gene status, with very limited to no activity in normal cells has been constructed. In the cancer terminator virus (CTV), Ad replication through the E1A gene is driven by the cancer-specific promoter of progression elevated gene-3 (PEG-3) [243], which results in concomitant production of mda-7/IL-24 from the E3 region of the Ad. This CTV generates large quantities of MDA-7/IL-24 as a function of Ad replication uniquely in cancer cells that not only have cancer-selective apoptosis-inducing properties but also display a plethora of indirect

antitumor “*bystander*” activities, including distant tumor growth suppression and apoptosis, immune modulation and anti-angiogenesis [195, 196, 204, 211, 212, 223, 232, 233, 237].

A limiting factor in effective gene therapy when employing intravenous viral delivery and when using CRCA is the effect of the immune system in neutralizing Ads [215]. In this context, a means of shielding the initial viral delivery vector using microbubbles in principle permits enhanced delivery of the viral payload to tumors when coupled with US [214]. In the present study, we have employed this strategy using CTV-microbubble complexes coupled with US to treat both DU145 and therapy resistant DU-Bcl-xL established tumor xenografts on both flanks in nude mice. Systemic administration of the CTV-microbubble with US on the established right-side tumor resulted in robust transgene expression and apoptosis induction with complete eradication of both the injected right side primary and distant (opposite flank; potentially representative of metastasis) human prostate cancers. However, no tumor regression was observed instead in mice bearing DU145 and DU-Bcl-xL control tumors when injected intravenously with unprotected Ad.mda-7 and CTV viruses (see Figures 27 and 28), indicating that comparable doses of untargeted, unprotected viruses injected directly i.v. failed to elicit an antitumoral response. An exciting finding was that this protocol resulted in the indication of an enduring response in which no tumor regrowth occurred 3 months after cessation of the therapy protocol in the treated or untreated tumor site and additionally these animals had no signs of metastatic spread to the lungs or liver. Previous studies have indicated that the CTV when injected intratumorally will enter into the circulation, replicate and generate MDA-7/IL-24 protein in the primary and distant tumors in the nude mouse, predicting induction of a potential immune response [18, 204, 205, 237, 241]. Further studies are planned in the context of immune competent animals, which would be an important step toward developing clinical trials with the

CTV-microbubble approach and US.

Obvious questions are why mda-7/IL-24 serves as such an effective anti-tumor agent and why the CTV is superior to Ad.mda-7 as a viral-based therapeutic for primary and disseminated cancers. A noteworthy reason for the robustness of mda-7/IL-24 is the ability of this secreted cytokine to elicit a potent '*bystander*' anti-cancer effect [195]. Mda-7/IL-24 can directly induce apoptosis when expressed inside cancer cells and can also induce growth suppression, apoptosis and endogenous MDA-7/IL-24 protein expression and secretion when added as a purified protein through interactions with the IL-20R1/IL-20R2 and IL-22R1/IL-20R2 cell surface receptors [195, 211, 232, 233]. As a secreted cytokine, MDA-7/IL-24 also induces an array of potent immunomodulatory proteins from immune cells, including IL-6, IFN- γ , tumor necrosis factor- α , IL-1 β , IL-12, and granulocyte macrophage colony-stimulating factor [232]. These cytokines secreted by peripheral blood mononuclear cells can activate antigen-presenting cells to present tumor antigens, thereby triggering an antitumor immune response [244]. These observations have been recapitulated in a Phase I clinical trial involving intratumoral injection of Ad.mda-7 (INGN 241) in patients with advanced carcinomas and melanomas [203, 211, 228]. In principle, the '*bystander*' effects elicited by MDA-7/IL-24 are concentration dependent [233] and large amounts of this cytokine generated by the CTV would be predicted to have an enhanced therapeutic impact in the patient. Moreover, the immunomodulatory functions of mda-7/IL-24 would be particularly significant in a patient with an intact immune system where the generation of robust amounts of mda-7/IL-24 by the CTV might result in an amplified immune response against the cancer cells. The potent activity of the CTV compared to Ad.mda-7 suggests a need for only limited administration of this CRCA [18, 204, 205, 237], which would work extremely well in the context of microbubble-Ad complexes. In principle, the microbubble approach would

further minimize the activation of the immune system against the Ad that would normally promote viral clearance. We presently confirm for the first time that microbubble-assisted delivery of the CTV can serve as a valuable therapeutic tool to combat therapy resistant prostate cancer. As previously emphasized, the CTV-microbubble injected US treated mice appeared to be disease free 3 months after therapy cessation suggesting that a cure was established. We are planning to conduct long-term animal studies to verify this provocative observation in both immune incompetent and immune competent animals.

In summary, the present studies support the proposition that US-directed delivery of CTV-microbubble complexes might provide a nontoxic and effective alternative or complement to conventional adjuvant treatment modalities for patients with primary and metastatic prostate cancer. Based on previous studies of combinatorial therapy preclinical-trials in cell culture and in animal models, a combination of CTV-microbubble approach employing US with localized low-dose radiotherapy might promote an even more profound effect, potentially further enhancing mice survival [212, 245]. We are currently studying the effects of chemotherapy and/or radiation therapy combined with microbubble-enhanced delivery of the CTV on promoting a cure in a preclinical setting of prostate cancer.

ACKNOWLEDGEMENTS

We gratefully acknowledge the Marshall University Biochemistry and Microbiology & Surgery Departments for their support. The present studies were supported in part by the awards number CA131395 and CA140024 from the National Cancer Institute, and in part by NIH-COBRE 5P20RR020180, WV-INBRE 5P20RR016477, and the Cell Differentiation and Development Center (CDDC), Marshall University (to PPC). The content is solely the responsibility of the authors and does not necessarily represent the official views of the National Cancer Institute or the National Institute of Health. The authors also acknowledge support from: the Goldhirsh Foundation and the Dana Foundation (to DS); NIH grants P01 CA104177, R01 CA35675, and R01 CA097318 (to PBF); the Samuel Waxman Cancer Research Foundation (to PBF); and the National Foundation for Cancer Research (NFCR) (to PBF). Sarah Kelly is the recipient of a fellowship from WV NASA Space Grant Consortium. We also gratefully acknowledge SonoSite, Inc. for loaning the MicroMaxx, SonoSite ultrasound portable platform and Targeson, Inc. for the custom synthesis of the ultrasound contrast agent that were used in this study. DS is a Harrison Endowed Scholar in Cancer Research, VCU Massey Cancer Center. PBF holds the Thelma Newmeyer Corman Chair in Cancer Research, VCU Massey Cancer Center.

CHAPTER V: MICROBUBBLE-ASSISTED P53, RB, AND P130 GENE TRANSFER IN COMBINATION WITH RADIATION THERAPY IN PROSTATE CANCER

This is a revised version of a manuscript published in *Current Gene Therapy* (2013) 163-174.

Nande R¹, Greco A^{1,2,3}, Gossman MS⁴, Lopez JP⁴, Claudio L⁵, Salvatore M², Brunetti A², Denvir J¹, Howard CM¹, Claudio PP^{1,6,*}. “Microbubble-assisted p53, RB, and p130 gene transfer in combination with radiation therapy in prostate cancer” *Current Gene Therapy*, 2013 Jun 1;13(3):163-74.

doi: 10.2174/1566523211313030001.

¹Department of Biochemistry and Microbiology, Translational Genomic Research Institute, Joan C. Edwards School of Medicine, Marshall University, Huntington, WV25755, USA

²Department of Biomorphological and Functional Science, University of Naples “Federico II”, Naples, Italy

³CEINGE, Biotecnologie Avanzate, s.c.a.r.l

⁴Department of Radiation Oncology, Tri-State Regional Cancer Center, Ashland, KY, USA

⁵Urology Department, National Cancer Institute “Fondazione Senatore Pascale”, Naples, Italy

⁶Department of Surgery, Marshall University, Huntington, WV 25755, USA

*Corresponding Author,
Pier Paolo Claudio, M.D., Ph.D.
Department of Biochemistry and Microbiology,
Department of Surgery, Joan C. Edwards School of Medicine,
Marshall University, Huntington, West Virginia 25755, USA.
E-mail: claudiop@marshall.edu

ABSTRACT

Combining radiation therapy and direct intratumoral (IT) injection of adenoviral vectors has been explored as a means to enhance the therapeutic potential of gene transfer. A major challenge for gene transfer is systemic delivery of nucleic acids directly into an affected tissue. Ultrasound (US) contrast agents (microbubbles) are viable candidates to enhance targeted delivery of systemically administered genes.

Here we show that p53, pRB, and p130 gene transfer mediated by US cavitation of microbubbles at the tumor site resulted in targeted gene transduction and increased reduction in tumor growth compared to DU145 prostate cancer cell xenografts treated intratumorally with adenovirus (Ad) or radiation alone. Microbubble-assisted/US-mediated Ad.p53 and Ad.RB treated tumors showed significant reduction in tumor volume compared to Ad.p130 treated tumors ($p < 0.05$). Additionally, US mediated microbubble delivery of p53 and RB combined with external beam radiation resulted in the most profound tumor reduction in DU145 xenografted nude mice ($p < 0.05$) compared to radiation alone. These findings highlight the potential therapeutic applications of this novel image-guided gene transfer technology in combination with external beam radiation for prostate cancer patients with therapy resistant disease.

Keywords: Retinoblastoma, RB, p130, p53, tumor suppressor gene, microbubbles, ultrasound, systemic targeted viral gene delivery, radiation, external beam radiation, apoptosis induction, prostate cancer.

INTRODUCTION

Current gene transfer clinical trials for prostate carcinoma use adenoviral vectors as efficient gene transducing agents but these viral vectors have been shown to elicit an immune response [202]. Rapid inactivation of adenoviruses by anti-adenoviral and neutralizing antibodies in the blood limits the use of adenoviral gene transfer to intraprostatic injections for site-specific delivery. To circumvent this problem we previously demonstrated a unique intravenous site-specific delivery system for gene transfer both *in vivo* and *in vitro*, using adenoviral (Ad) mediated delivery of GFP [214] and melanoma differentiation associated gene-7/interleukin-24 (mda-7) encapsulated in commercially available ultrasound (US) contrast agents (microbubbles) [53]. The microbubbles (MBs) are able to entrap and protect viral vectors from the immune system and are small enough to flow freely in the pulmonary and liver capillary bed. MBs undergo cavitation in the sonification zone, and release their contents. Cavitation also creates shockwaves that increase cell permeability allowing for better uptake of the genetic material into the targeted cell [53, 68, 214].

Radiation therapy (RT) is commonly used in cancer management, with 40% to 60% of all cancer patients receiving radiation treatment [246]. RT stimulates death receptors at the cell surface, generates reactive oxygen species and activates several cell cycle regulatory proteins including p53 [247], pRB [248], and other proteins that trigger senescence, necrosis or apoptosis [249]. Additionally, factors such as location, size, and inadequate vascular supply (hypoxia) play a role in the lack of responsiveness of neoplasms to ionization radiation [250].

The human prostate cancer, DU145, displays genetic mutations in key cell cycle regulatory proteins, p53 and pRB. DU145 expresses a mutant p53 protein (mt-p53) due to mutations at codon 223 and 274 on both alleles [251], which is functionally inactive, stabilized,

and temperature sensitive [252]. Therefore, because functional p53 is required for ionizing radiation to activate p21^{cip/waf} and to induce a G1-cell cycle arrest, DU145 cells are radioresistant [251, 253]. In addition, pRB gene has a biallelic disruption in these cells; one allele is deleted while the other produces a truncated product of the RB gene resulting in the loss of another G1 cell cycle phase regulator required for apoptosis following irradiation [254]. Studies by Sasaki, et al. [255] and Bowen, et al. [256] showed that DU145 cell death following ionizing radiation is increased when p53 and pRb are restored.

Another cell cycle regulator, p130 is frequently altered in several human neoplasms including prostatic carcinomas. Previously we observed that p130 was expressed at low levels in more aggressive prostate tumors and hypothesized that the lack of p130 expression could be involved in the progression of the disease [257]. Additionally, we have examined the role of p130 in γ -radiation induced apoptosis by using a hamster tetracycline inducible glioblastoma cell line HJC12, and demonstrated that the cell cycle regulator p130 promoted radiation induced apoptosis by downregulation of the antiapoptotic BCl-2 gene and upregulation of pro-apoptotic transcription factor p73 [258]. These data suggest that cell cycle regulatory proteins play a significant role in the radio-sensitivity of prostate cancer cells.

In 1996, Stevens and colleagues demonstrated that ionizing radiation improves viral gene transfer efficiency with greater integration of the transgene into the host cells [259]. In addition, combined treatment with adenovirus p53 and radiation has been shown to enhance the proportion of apoptotic cells by greatly increasing the number of cells arrested in the G1-phase of the cell cycle [255]. We hypothesized that ultrasound guided targeted delivery of adenoviruses containing the cell cycle genes p53, RB and p130 in combination with external beam radiation can further enhance the incorporation of cell cycle transgenes in prostate cancer cells, resulting

in greater ablation of prostate tumors than x-ray radiation alone.

In the current investigation we used an ultrasound contrast agent provided by Targeson, Inc (San Diego, CA) and the portable SonoSite Micro-Maxx ultrasound (US) platform (SonoSite, Inc., Bothell, WA) equipped with an L25 linear array transducer. Targeson's agents are lipid-encapsulated perfluorocarbon microbubbles (MBs) with a mean diameter of 2.5 μm . The gas-filled microspheres effectively lower the energy threshold for non-thermal cavitation, thus allowing diagnostic transducers operating within the energy levels mandated by the FDA to be used for drug/gene delivery. Ultrasound-targeted microbubble destruction (UTMD) enables focal release of entrapped materials as well as the creation of small shock waves that increase cellular permeability [220]. In addition, the MBs protect viruses from recognition and rapid degradation by the immune system, thus allowing for intravenous injection rather than direct target organ delivery by catheter-based approaches or operative bed injection [214, 218]. MB protection of the viruses may also limit the inflammatory response to the viruses, potentially allowing for repeated injections of transgene containing MBs.

The ultimate goal of this research is to develop efficacious treatment modalities for therapy resistant prostate cancer. In the present study, we provide proof-of-principle for a site-specific gene delivery approach mediated by a standard, portable diagnostic US platform. This system worked effectively *in vivo* to deliver Ads carrying cell cycle regulatory genes (p53, RB, and p130). Evidence is offered that the combination of 8 Gy radiation therapy with US targeted gene transfer of p53 and RB reduced the tumor size in an animal xenograft model of radiation-resistant human prostate cancer cells.

MATERIALS AND METHODS

Cell Lines, Cell Culture, and Adenoviral Production.

The DU145 (human prostate adenocarcinoma), cell line was obtained from the American Type Culture Collection (ATCC, Rockville, MD). DU145 cells were grown in RPMI 1640 (Hyclone, Waltham, MA) supplemented with 10% fetal bovine serum (Hyclone, Waltham, MA), and 100units/mL penicillin supplemented with 1 mg/mL streptomycin (both from Hyclone, Waltham, MA). The human kidney embryonic 293 cells were obtained from the American Type Culture Collection (ATCC, Rockville, MD) and grown with Dulbecco's modified Eagle's medium (Hyclone, Waltham, MA) supplemented with 10% fetal bovine serum (Hyclone, Waltham, MA). All cells were grown at 37°C, in a 5% CO₂/95% atmosphere incubator.

The recombinant adenoviruses with wild-type p53, RB, p130 used in this study were serotype 5 adenovirus containing a cytomegalovirus (CMV) promoter. Non-coding empty Adenoviruses carrying only the CMV promoter were used as vector control. Each viral stock was propagated in and purified from 293 cell cultures. Cells were harvested 24-36 hours after infection, pelleted, resuspended in heat inactivated media and lysed by three-freeze/thaw cycles. Cell debris were removed and the viruses purified by chromatography followed by dialysis. Viruses were aliquoted and stored at -80°C. Viral titers were determined by a plaque assay. Ad.p53 viruses were generated using the AdEasy system (Carlsbad, CA), as previously described [260-263]. The Ad.RB viruses were generously provided by Dr. Juan Fueyo (M.D. Anderson Cancer Center, The University of Texas) and Ad.p130 viruses were purchased from Vector BioLabs (Philadelphia, PA). All adenovirus transductions were performed using 50 MOI Ads for *in vitro* studies, in RPMI-1640 media with 2% Fetaclone-III heat-inactivated FBS (Hyclone, Thermo Scientific, Waltham, MA).

Radiation

External beam radiation was provided using Varian Medical Systems, Inc. (Palo Alto, CA) Model 21EX and Model 6EX linear accelerators (LINAC), each owned and operated by Tri-State Regional Cancer Center in Ashland, KY. The machines were approved by the Inspector General of the State of Kentucky for irradiations to biological specimens and animals as desired by us. These particle accelerators offer a bremsstrahlung x-ray energy of 6 MV, which was used in these investigations as well as a rapid dose delivery to the targeted tumor at a rate of 6Gy/MU. Here, the number of monitor units (MU) is simply the internal timer of the LINAC. All dosages were pre-calculated for *in vitro* and *in vivo* studies as previously described [264].

For the *in vitro* studies, 2×10^6 DU145 cells were seeded in 75cm² flasks and irradiated at 10Gy or 20Gy, at room temperature. For one treatment of 10Gy, 965 MU were given at 600 MU/min for a run time of 1 min 37 seconds. For one treatment of 20Gy, 1,930 MU were given at 600 MU/min for 3 min 13 seconds. For a combination therapy, 2×10^6 DU145 cells were first radiated at 10Gy and 20Gy following by infection with Ad5CMV-p53 or Ad5CMV-RB or Ad5CMV-p130 viruses at 50 multiplicity of infection (MOI) units. The sensitivity to x-ray induced apoptosis was evaluated by phase contrast microscopy and flow cytometric analysis. Cells were collected at 24, 48, 72 and 96 hours after radiation to carry out Flow cytometric analysis and Western Blots.

For the *in vivo* studies, mice received irradiation in pie cages for a one-time dose of 8Gy (800 MU given at 600 MU/min for 80 seconds). An approved protocol concerning the Physics Policies and Procedures for handling of the mice and disposal of waste was used.

Flow Cytometry Analysis

Irradiated, adenoviral (Ad.p53, Ad.RB and Ad.p130) transduced and combination treated DU145 cells were harvested at 24, 48, 72 and 96 hours following treatments, to study the cell cycle phase of each group. After three washings in 1mL of 1% fetal calf serum (FCS)-PBS the cells were fixed in 70% ethanol and stored at -20°C. Cells were centrifuged, washed and resuspended in 1% FCS-PBS. The samples were then incubated at 37°C with propidium iodide (PI) and RNase A for 30 min. The DNA content was analyzed by a BD Accuri C6 Flow Cytometer (BD Bioscience, San Jose, CA). The proportions of G1, S, G2 phase cell cycle were determined as previously reported [255].

Apoptosis analysis was done using the Annexin-V assay on the Flow Cytometer. Apoptotic cells were analyzed with fluorescein isothiocyanate (FITC) conjugated to Annexin-V antibody and Propidium Iodide (PI) from the Annexin-V/FITC Kit (Bender MedSystems, Burlingame, CA) following manufacturer's instructions. The samples were analyzed with BD Accuri C6 Flow Cytometer (BD Bioscience, San Jose, CA). The Annexin-V assay experiment was repeated three times and was run as triplicate of technical repeats. Statistical analyses were performed with IBM SPSS statistic software.

Antibodies and Western Blot Analysis

Western blot analyses with antibodies against the targeted proteins were performed to validate successful viral transfection of the cells and of the *in vivo* tumors. DU145 cells were X-irradiated, transduced with 50 MOI of Ad.p53, Ad.RB, Ad.p130, or Ad.CMV (control) for 24, 48, 72 and 96 hrs post-irradiation/transduction. Cells were lysed on ice for 1 hr with lysis buffer. Fifty µg of total protein plus loading buffer were loaded in each well for western blot analyses.

SDS-PAGE was run using 8-12% bis-acrylamide gel at room temperature. Samples were blotted onto a nitrocellulose membrane. To detect proteins, the membranes were blocked with 5% Milk-TBST overnight at 4°C and reacted with primary antibodies for 2 hr at room temperature with constant motion on an orbital shaker. The membranes were washed with TBST to remove excess primary antibodies. Incubation for 45 minutes with appropriate secondary antibodies followed. Immunodetection was performed using the enhanced chemiluminescence (ECL) system (Amersham, IL) according to the manufacturer's instructions using x-ray films. The following primary antibodies were used: mouse monoclonal antibodies against p53 (DO-1) cat#sc-126 (1:500), pRb cat#sc-102 (1:250) (Santa Cruz Biotechnology, Santa Cruz, CA), β -actin cat#A3853 (1:1,500) (Sigma Aldrich) and rabbit polyclonal antibody against RBL2/p130 cat#sc-317 (1:250).

Preparation of MBs and US Platform.

Targeson (Targeson) custom synthesis US contrast agent (perfluorocarbon MBs, encapsulated by a lipid monolayer and polyethylene glycol) stabilizer were reconstituted as previously described [53]. MBs were reconstituted in the presence or absence of 1 ml of 10^{12} plaque-forming units of Ads [53]. Unenclosed, surface-associated Ads were inactivated using incubation with FBS as previously described [53, 214]. For *in vivo* experiments US exposure was achieved with a Micro-Maxx SonoSite (SonoSite) ultrasound machine equipped with the transducer L25 set at 0.7 Mechanical Index, 1.8 MPa for 10 minutes as previously described [53, 214].

Animal Study

Animal studies were performed in accordance with National Institutes of Health recommendations and the approval of the institutional animal research committee. DU145, human prostate carcinoma cells were xenografted to 8- to 12-week-old female or male athymic BALB/c nude mice, homozygous mutant for the nu/nu allele, bred in our laboratory. The colony of mice was developed from breeding stock obtained from Charles Rivers Laboratories, Wilmington, MA. Mice were sedated in an IMPAQ6 anesthesia apparatus (VetEquip, Pleasanton, CA) that was saturated with 3–5% isoflurane and 10–15% oxygen with the aid of a precision vaporizer (VetEquip) to deliver the appropriate amount of anesthetic and to induce anesthesia. Mice received subcutaneous injections along each of their dorsal flanks (both sides per mouse), of 2×10^6 DU145 cells in 200 μ L of PBS using a 22-gauge needle. Tumors were measured post-injection in their longest dimension and at 90° to their longest dimension using vernier calipers. Once the tumors reached a volume of approximately 200mm³ the mice were divided into their various treatment groups. Tumor volumes were calculated using the formula tumor volume = (long arm x short arm²)/2 [265].

Sonoporation: Gray scale-B-mode US imaging was performed with a SonoSite scanner (SonoSite) equipped with the transducer L25 set at 0.7 Mechanical Index, 1.8 MPa for 10 minutes. US images were recorded as digital clips. Tumors on the right flank were sonoporated immediately after the MB encapsulated viral vector intravenous injections using a 27-gauge needle. Tumors on the contralateral flank (on the left flank) would serve as internal controls. Radiation of 8Gy was given to the appropriate groups followed by four weeks of MB guided delivery of Ad.p53, Ad.RB or Ad.p130.

Radiation: Radiation treatments were provided to groups of mice, generally 11 mice/pie-

cage. Groupings were limited by the number of available slots in the Braintree Scientific, Inc. (Braintree, MA) Model MPC pie cage. The LINAC was programmed to provide an 8Gy radiation. Radiation was given to the appropriate groups followed by four weeks of adenoviral treatments.

The DU145 tumor-bearing mice were directly injected in the tumor (IT) or through the dorsal tail vein (IV). Each control group got an IT injection of 100 μ L of PBS MBs or 100 μ L of un-encapsulated Ad.p53, Ad.RB or Ad.p130 viruses at a concentration of 10⁹ pfu/ μ L. Radiation of 8Gy alone constituted an additional control group. Experimental groups were injected IV with 100 μ L of MB encapsulated Ad.p53, Ad.RB or Ad.p130 at a concentration of 10⁹ pfu/ μ L. Tumor growth inhibition rate was calculated using the formula (1-(treated group/control group))*100%.

The animals were sacrificed by CO₂ asphyxiation. Tumors, heart, lungs and liver were harvested at the end of the treatment course. Tissues used for molecular biological analysis were snap frozen in liquid nitrogen and stored at -80°C. Frozen tissues were homogenized and total proteins were extracted. Western blot studies allowed determining if the enhanced gene expression was specific to microbubble encapsulation and restricted to the US treated tumors instead of other tissues. The combination of external beam radiation, ultrasound treatment and systemic delivery of MB protected genetic material by viruses was examined for expression of the transduced tumor suppressor genes.

***In Vivo* Bioluminescence Imaging**

We imaged animals with the IVIS Lumina II (Caliper Life Sciences) at 24hrs and one week after MB-assisted gene delivery, to quantify photons emitted by the control animals that

received Ad.LUC. For each imaging session mice were injected intraperitoneally with D-luciferin (150 mg kg⁻¹) under anesthesia using 1.5–2.5% isoflurane/oxygen mixture. Images were acquired 10 min after injection of D-luciferin as follows. The anesthetized mice were placed in a light-tight chamber, and images were generated over a 1-minute exposure using a cryogenically cooled charge-coupling device camera IVIS Lumina II (Caliper Life Sciences) to quantify photons spontaneously emitted by the animal. Images were pseudocolored using the Xenogen (Caliper Life Sciences, Hopkinton, MA, USA) software and overlaid on a black-and-white photograph of the animal generated with cabinet lighting. The visual output represents the number of photons emitted s⁻¹ cm⁻² as a pseudocolor image where the maximum is red and the minimum is purple. Image acquisition and BLI data analysis were done using Living Image software (Caliper Life Sciences).

Statistical Analyses

All statistical analyses were performed using IBM SPSS software. Comparisons were conducted using an ANOVA test with post hoc test of Dunnett's T3. P values of less than 0.05 were considered statistically significant.

A comparison of tumor volumes was done for week 19 after the treatment at the end of the study. Statistical analyses for comparisons of different types of treatments were done using one-way analysis of variance using a post hoc test of Dunnett's T3. P value <0.05 was considered significant.

RESULTS

Phase Contrast Microscopic Analysis: Irradiated DU145 Cells that were then Transduced with p53, RB, and p130 Genes

We observed that after 96 hours, radio-resistant DU145 cells, which were x-ray irradiated and then transduced with 50 MOIs of Ad.*p53*, Ad.*RB*, or Ad.*p130* had a higher number of dead cells than cells which did not receive the transgenes and that there was an increase in the number of apoptotic cells as radiation dose was escalated from 10 to 20Gy (Fig. 29a). Microscopic analysis revealed that following radiation induced DNA damage, cells adopted a large flattened shape with distorted cell membranes and multiple nuclei typical of senescent cells. We also observed that at 96 hours, the *RB* or *p53* gene transfer and radiation therapy resulted in a higher increase of cell death than p130 gene transfer (Fig. 29a). Non-irradiated and non-transduced control cells exhibited similar percentages of cell death when compared to control non-coding CMV-Adenoviruses transduced cells (data not shown).

Interestingly, cells x-ray irradiated and transduced with Ad.*p53*, Ad.*RB* or Ad.*p130* showed an increase in cell death, compared to the control x-irradiated group from 24-72 hours (Fig. 29b). Few dead DU145 cells were observed at 24-72 hours following x-ray irradiation when compared to the non-transduced control (Fig. 29b). Radiation combined with adenoviral transductions increased the number of dead cells regardless of the transduced genes (*p53*, *RB* & *p130*) in a time and dose dependent manner (Fig. 29a and b). Taken together, these data suggest that gene transfer of *RB* or *p53* resulted in an improvement in the cell death of the radio-resistant DU145 cells.

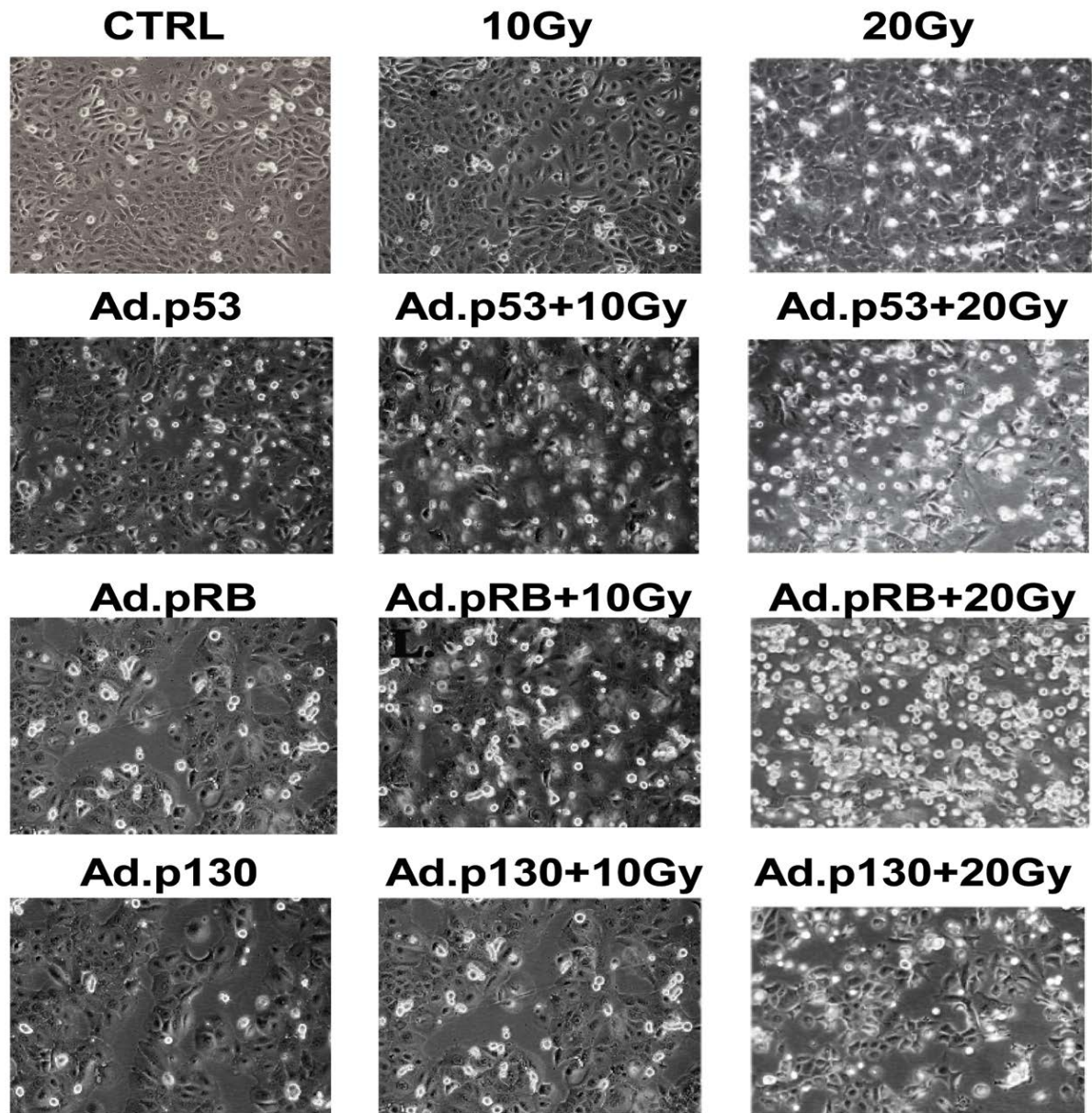


Figure 29a. Microscopy image analysis of DU145 cells transduced with Ads carrying tumor suppressor genes (p53, RB and p130) \pm radiation from 72hrs. Apoptotic cells appear as floating in the bright field microscopy image. Top row images are of control DU145 cells and the ones that received radiation of 10Gy or 20Gy only. The second row images are DU145 cells that received 50MOI adenoviral transduction of p53 alone and those combined with 10Gy and 20Gy radiation. The third row images are of DU145 cells that received 50MOI adenoviral transduction of pRB alone and those combined with 10Gy and 20Gy radiation. The fourth row images are of

DU145 cells that received 50MOI of adenoviral transduction of p130 alone and those combined with 10Gy and 20Gy radiation.

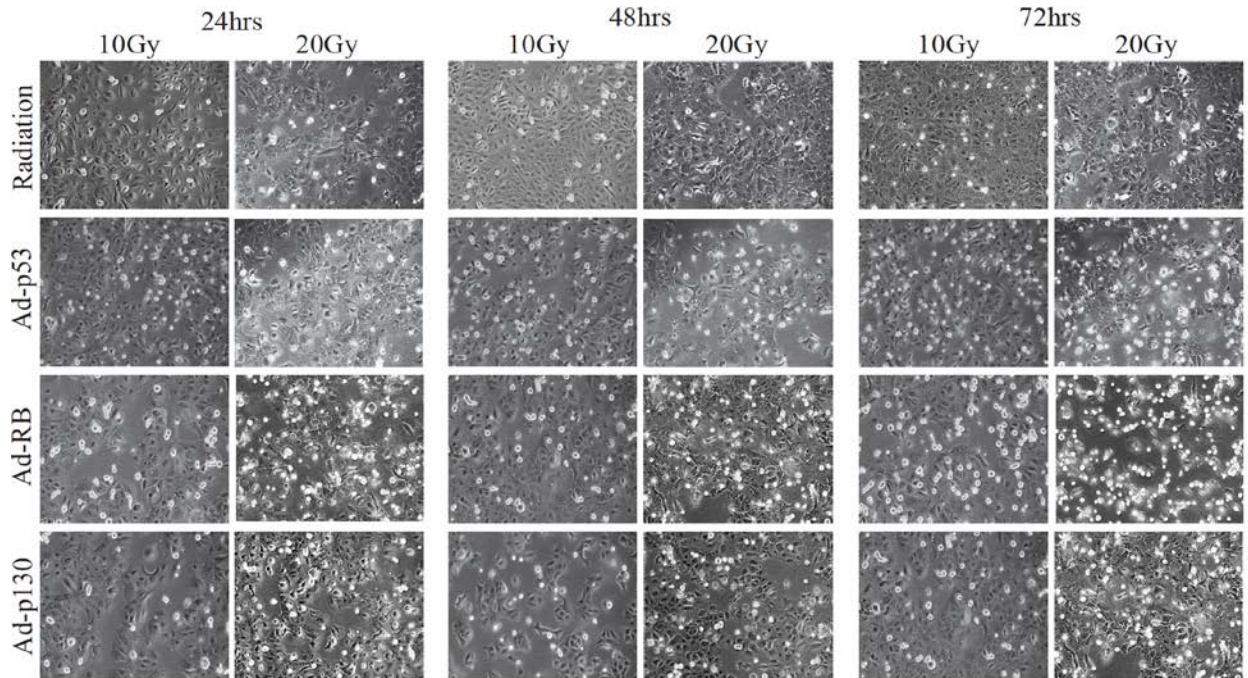


Figure 29b. Microscopy images of adenovirally transduced tumor suppressor genes (*p53*, *RB* and *p130*) \pm radiation from 24-72hrs. Top row images are of DU145 cells that received radiation of 10Gy and 20Gy only at 24, 48, and 72 hours, respectively. The second row images are DU145 cells that received 50MOI of Ad.p53 combined with 10Gy and 20Gy radiation at 24, 48, and 72 hours, respectively. The third row images of DU145 cells that received 50MOI of Ad.pRB combined with 10Gy and 20Gy radiation at 24, 48, and 72 hours, respectively. The bottom row images are of DU145 cells that received 50MOI of Ad.p130 combined with 10Gy and 20Gy radiation at 24, 48, and 72 hours, respectively.

Transgene Expression of p53, pRb, and p130 in Irradiated DU145 Cells

Western blot studies were done to confirm the adenoviral transduction of DU145 cells by adenoviruses carrying genes *p53*, *pRb* and *p130*. Normally, irradiation induced cell death results in the accumulation of proteins p53 and hypo-phosphorylated pRb leading to G1 arrest. We found that following x-ray irradiation there was no change in the expression of mutant p53 and truncated pRb in the control DU145 cells regardless of the irradiation dose (Fig. 30). Mutant p53 and truncated pRb are stabilized and non-functional in DU145 cells leading resistance to radiation-induced cell death [252, 254]. We also observed an accumulation of p130, which occurred in a time dependent manner following x-ray irradiation, regardless of the irradiation dose (Fig. 30). Cells transduced with adenoviral Ad.*p53*, Ad.*RB*, and Ad.*p130* showed increased expression of these functional recombinant proteins (Fig. 30). Higher expression levels of all of the adenovirally transferred recombinant proteins were observed as the x-ray dose was increased from 10Gy to 20Gy.

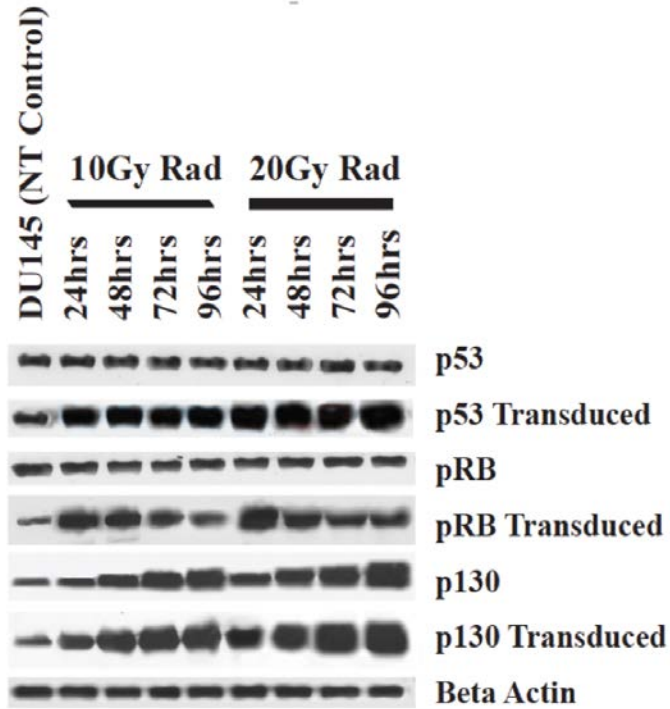


Figure 30. Western Blot analysis of the cell lysates collected at 24, 48, 72 & 96 hours post-adenoviral transduction. Treatments and time of collection after radiations are as labeled at the top, protein detected are labeled on the right. Anti-beta-actin was used as a loading control. 50 μ g of total lysates were run in SDS polyacrylamide gels.

Cell Cycle Analysis of DU145 Cells Following X-ray Irradiation and Gene Transduction

The replication status of DU145 cells following radiation therapy, adenoviral gene transfer of *p53*, *RB*, or *p130*, or combined radiation and adenoviral gene transfer was computed as the percentage of cells accumulated in the G1, S or G2 cell cycle phases by a propidium iodide staining. The data was plotted on a linear diagram to show points in time where there was accumulation or reduction of G1- and G2-phases at 24-96 hours of DU145 cells treated with the various adenoviruses and x-ray irradiation (Fig. 31a-f). Control DU145 cells showed a small (8-11%) fraction of cells in S-phase (Table 4). The cells treated with Ad.*p53*, Ad.*RB*, or Ad.*p130*

showed accumulation at the G1-phase with reduction in G2-phase of the cell cycle suggesting a block of the G1/S phase transition (Fig. 31a, c and e). Notably, x-ray irradiated DU145 cells showed a marked accumulation in the G2-phase with a reduction in the G1-phase of the cell cycle suggesting a block at the G2/M transition (Fig. 31a-f). The combined treatment of Ad.p53 or Ad.RB transduction and x-ray irradiation showed a reduction of the number of cells in the G2-phase with accumulation of cells in the G1-phase (Fig. 31a,b & c,d). However, combined treatment of Ad.p130 transduction and x-ray irradiation showed a G2/M block (Fig. 31e-f), suggesting that this cell cycle response was most likely due to the irradiation.

Table 4. The percentage of DU145 cells in G1, S and G2 cell cycle phase with its standard deviation that received treatments of adenovirus, radiation and combined (radiation + adenovirus) treatment as analyzed by flow cytometry at 24-96 hours.

| Groups | G1 phase (Mean \pm SD) | | | | S phase (Mean \pm SD) | | | | G2 phase (Mean \pm SD) | | | |
|-------------|-----------------------------|-------------------------|------------------------|------------------------|----------------------------|------------------------|------------------------|------------------------|-----------------------------|-------------------------|-------------------------|---------------------------------|
| | 24 hrs | 48 hrs | 72 hrs | 96 hrs | 24 hrs | 48 hrs | 72 hrs | 96 hrs | 24 hrs | 48 hrs | 72 hrs | 96 hrs |
| Control | 40 \pm 18.53 | 35.53 \pm 15.65 | 39.2 \pm 13.86 | 40.9 \pm 12.80 | 11.33 \pm 5.28 | 10 \pm 1.15 | 9 \pm 1.42 | 8.87 \pm 1.16 | 48.83 \pm 23.25 | 49.27 \pm 11.07 | 45.93 \pm 19.87 | 45.5 3 \pm 20.6 8 |
| 10Gy Rad | 70.87 \pm 2.63 | 62.3 \pm 1.51 | 51.67 \pm 4.29 | 40.53 \pm 0.76 | 15.63 \pm 1.45 | 14.03 \pm 2.20 | 19.83 \pm 2.55 | 24.17 \pm 1.05 | 13.93 \pm 1.67 | 23.9 \pm 2.52 | 29.4 \pm 0.96 | 34.9 7 \pm 1.7 |
| 20Gy Rad | 60.93 \pm 3.93 | 38.27 \pm 0.75 | 33.1 \pm 0.34 | 16.77 \pm 3.09 | 15.13 \pm 3.8 | 22.47 \pm 1.75 | 12.67 \pm 1.58 | 13.43 \pm 4.22 | 25.2 \pm 0.17 | 40.1 \pm 1.7 | 52.97 \pm 1.31 | 67.3 7 \pm 1.62 |
| Ad.p53 | 27.33 \pm 4.98 | 36.93 \pm 1.59 | 49.37 \pm 3.42 | 55.8 \pm 2.17 | 8.07 \pm 2.89 | 10.06 \pm 1.26 | 16.87 \pm 3.35 | 6.16 \pm 2.39 | 65.1 \pm 3.82 | 53.63 \pm 1.66 | 34.33 \pm 1.53 | 36.2 7 \pm 3.42 |

| | | | | | | | | | | | | |
|-----------------------------|--------------------|--------------------|--------------------|--------------------|--------------------|--------------------|--------------------|--------------------|--------------------|--------------------|--------------------|------------------------|
| Ad.p53 + 10Gy Rad | 27.2 ± 1.61 | 36 ± 1.08 | 48.83 ± 3.27 | 59.47 ± 2.35 | 6.07 ± 0.15 | 9.47 ± 1.94 | 14.1 ± 2.36 | 13.07 ± 2.15 | 67.13 ± 1.53 | 53.33 ± 3.19 | 32.63 ± 3.86 | 27.1 7 ± 1.46 |
| Ad.p53 + 20Gy Rad | 39.87 ± 2.10 | 56.1 ± 1.67 | 64.7 ± 0.72 | 74.27 ± 2.33 | 17.87 ± 2.19 | 9.7 ± 1.21 | 11.03 ± 1.60 | 10.77 ± 1.27 | 42.83 ± 3.5 | 34.83 ± 0.91 | 24.7 ± 1.97 | 15.2 7 ± 3.09 |
| Ad.pR B | 19.9 ± 3.74 | 30.87 ± 4.27 | 37.33 ± 2.2 | 44.1 ± 2.36 | 11.33 ± 3.76 | 8.3 ± 3.65 | 7.43 ± 0.59 | 12.6 ± 1.4 | 69.03 ± 1.80 | 60.97 ± 2.18 | 55.37 ± 1.96 | 42.9 7 ± 3.72 |
| Ad.pR B + 10Gy Rad | 23.23 ± 1.93 | 31.1 ± 2.08 | 38.77 ± 4.58 | 51.93 ± 4.68 | 8.13 ± 2.0 | 10.23 ± 0.87 | 6.97 ± 1.47 | 11.33 ± 2.35 | 68.9 ± 1.83 | 58.77 ± 1.69 | 54.4 ± 3.27 | 36.4 ± 2.0 |
| Ad.pR B + 20Gy Rad | 26.7 ± 2.08 | 33.6 ± 2.07 | 47.57 ± 2.42 | 68.13 ± 2.87 | 11.4 ± 5.38 | 10.53 ± 3.89 | 13.87 ± 0.64 | 6.93 ± 3.27 | 61.63 ± 2.83 | 54.9 ± 1.68 | 38.53 ± 2.61 | 24.9 3 ± 3.95 |
| Adp13 0 | 45.43 ± 3.30 | 54.2 ± 4.33 | 58.47 ± 3.05 | 67.2 ± 3.22 | 21.8 ± 2.26 | 19.47 ± 4.31 | 20.9 ± 3.96 | 17.47 ± 2.40 | 32.9 ± 3.99 | 26.23 ± 1.60 | 20.47 ± 0.67 | 15.3 ± 3.54 |
| Adp13 0 + 10Gy Rad | 59.73 ± 1.65 | 52.57 ± 3.13 | 43.87 ± 0.93 | 27.73 ± 7.70 | 20.47 ± 1.50 | 19.2 ± 1.35 | 13.23 ± 3.21 | 15.17 ± 7.41 | 19.27 ± 1.65 | 27.8 ± 2.41 | 42.23 ± 1.70 | 56.7 ± 1.15 |
| Adp13 0 + 20Gy Rad | 57.9 ± 1.35 | 52.47 ± 3.86 | 34.27 ± 2.96 | 18.73 ± 4.46 | 18.8 ± 0.82 | 14.53 ± 2.07 | 15.33 ± 1.72 | 10.07 ± 4.79 | 24.5 ± 0.79 | 33.33 ± 5.76 | 51.57 ± 1.53 | 70.5 ± 1.06 |

*Ad-adenovirus, *Rad- radiation, *SD- standard deviation

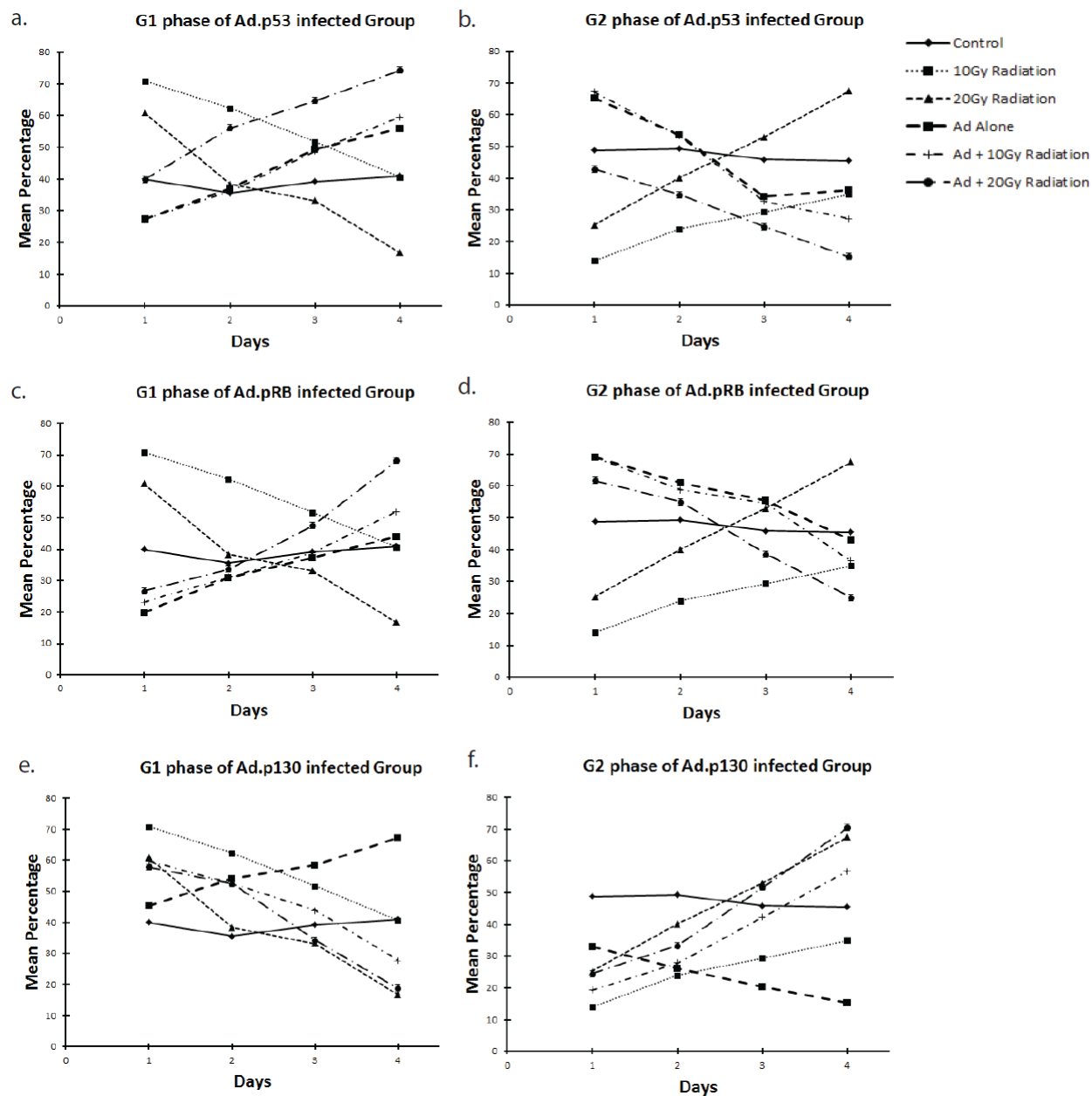


Figure 31. The accumulation/reduction of cells in G1- and G2-phase of cell cycle from a population of DU145 cells that received adenoviral *p53* (panels a and b), *RB* (panels c and d) or *p130* (panels e and f) with or without radiation treatments. The days after radiation are indicated on the ordinate. The percentage of cells in G1/G2 phase of cell cycle are indicated on the abscissa. A best-fit line was drawn on data points collected over four days.

External Beam Radiation Followed by Adenoviral p53, pRb, p130 Transduction Increased the Apoptotic Rate of DU145 Cells *In Vitro*

Apoptotic cell death of Ad.*p53*, Ad.*RB*, or Ad.*p130* transduced and irradiated DU145 cells was detected using a fluorescent-labeled Annexin-V antibody (Annexin-V-FITC) in combination with propidium iodide (PI) by flow cytometry 24-96 hours after irradiation. We observed that the apoptotic rate of DU145 cells transduced with control CMV non-coding adenovirus (Ad.CMV) was comparable to the untreated control DU145 cells regardless of time point (Fig. 32 & 33). Compared to the control, there was a significant ($p < 0.05$) increase in cell death for all treatments (Fig. 32 & Table 5). As radiation was increased from 10Gy (14.23%±0.87) to 20Gy (24.67%±2.28) there was a ~10% increase in cell death at 96 hours. A trend of increased cell death was also observed in all treated groups as time progressed (Fig. 33). The highest percentage of cell death was observed at 96hrs following radiation for all treated groups.

The percentage of cell death increased when adenoviral transduction of *p53*, *RB* or *p130* was combined with x-ray irradiation in comparison to the control or to adenoviral transduced groups regardless of the time point (Fig. 32 & 33). Compared to the 10 Gy irradiated cells there was a significant ($p < 0.01$) increase in cell death for p53 overexpressing cells (Fig. 32 & Table 5). Compared to the 10 and 20 Gy irradiated cells there was a significant ($p < 0.01$) increase in cell death for pRb overexpressing cells (Fig. 32 & Table 5). The highest percentage (41.17%±1.46) of cell death was observed at 96 hours for Ad.*RB* transduced DU145 cells in combination with x-ray irradiation (Fig. 32).

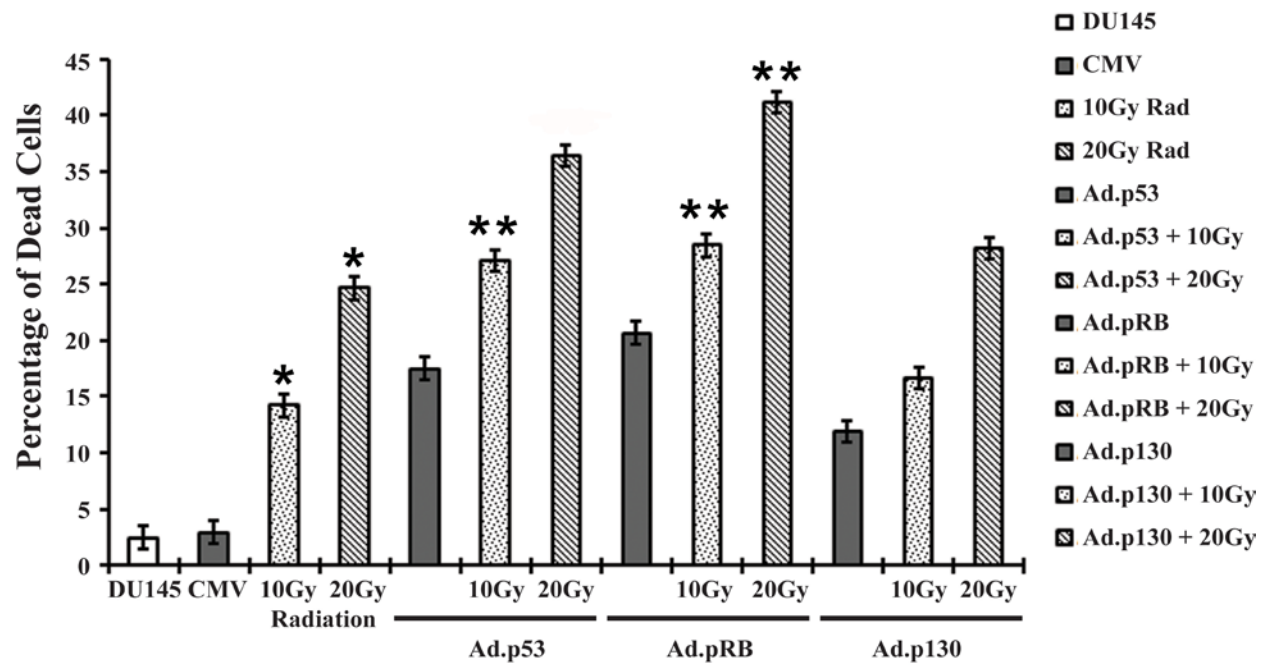


Figure 32. Bar graph representation of apoptosis assay with Annexin-V and Propidium Iodide staining of adenoviral infected tumor suppressor genes (p53, RB and p130) ± external beam radiation at 96hrs analyzed on Accuri C6 flow cytometer. The percentages of dead cells are indicated on the ordinate. The control and treatment groups are indicated on the abscissa. * indicates statistical significance between control and 10-20 Gy irradiated cells. ** indicates statistical significance between irradiated cells and cells that received combination of adenoviral gene transfer and external beam radiation.

Annexin V staining results from 24-72 hrs

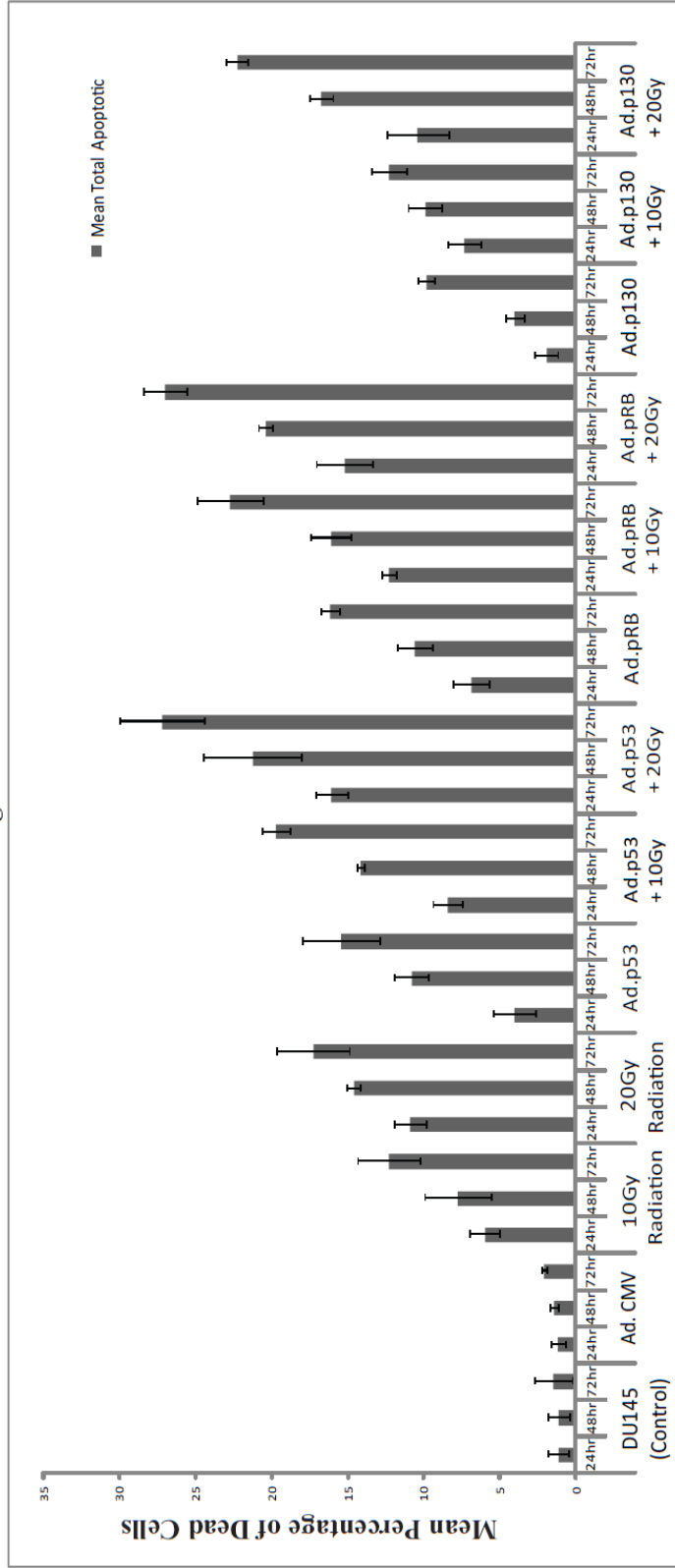


Figure 33. Graph representation of apoptosis assay by Annexin-V and Propidium Iodide staining of adenovirally transduced tumor suppressor genes (p53, pRB and p130) ± radiation from 24-72hrs analyzed on Accuri C6 flow cytometer. On the ordinate the percentages of dead cells are indicated. On the abscissa are indicated the different adenoviral vectors and combination therapeutic groups (Ads and x-ray radiation).

Table 5. Multiple comparison ANOVA (Analysis of Variance) significance table with a Dunnett's T3 test for Annexin-V assay experiment of DU145 cells following radiation and adenoviral gene transfer for 96hrs time point. The statistical analysis was run using IBM SPSS software.

| (I) groups | (J) groups | Mean Difference (I-J) | Std. Error | Sig. |
|------------|---------------|-----------------------|------------|------|
| DU145 | CMV | -.43 | .50 | 1.0 |
| | Rad 10gy | -11.73* | .60 | .00 |
| | Rad 20gy | -22.17* | 1.36 | .02 |
| | Adp53 | -15.00* | 1.02 | .02 |
| | Adp53+ 10gy | -24.60* | .96 | .00 |
| | Adp53+ 20gy | -33.90* | 1.92 | .02 |
| | AdpRB | -18.13* | 1.12 | .02 |
| | AdpRB+ 10gy | -25.93* | .54 | .00 |
| | AdpRB+ 20gy | -38.67* | .90 | .00 |
| | Adp130 | -9.43* | .94 | .04 |
| | Adp130+ 10gy | -14.13* | .98 | .02 |
| | Adp130+ 20gy | -25.67* | .87 | .00 |
| CMV | Rad 10gy | -11.30* | .63 | .00 |
| | Rad 20gy | -21.73* | 1.37 | .02 |
| | Ad.p53 | -14.57* | 1.04 | .02 |
| | Ad.p53+ 10gy | -24.17* | .98 | .00 |
| | Ad.p53+ 20gy | -33.47* | 1.93 | .02 |
| | Ad.pRB | -17.70* | 1.14 | .01 |
| | Ad.pRB+ 10gy | -25.50* | .58 | .00 |
| | Ad.pRB+ 20gy | -38.23* | .92 | .00 |
| | Ad.p130 | -9.00* | .96 | .04 |
| | Ad.p130+ 10gy | -13.70* | 1.0 | .02 |
| | Ad.p130+ 20gy | -25.23* | .90 | .00 |
| Rad 10Gy | Rad 20gy | -10.43 | 1.41 | .08 |
| | Ad.p53 | -3.27 | 1.09 | .49 |
| | Ad.p53+ 10gy | -12.87* | 1.03 | .01 |
| | Ad.p53+ 20gy | -22.17* | 1.96 | .04 |
| | Ad.pRB | -6.40 | 1.19 | .15 |
| | Ad.pRB+ 10gy | -14.20* | .67 | .00 |
| | Ad.pRB+ 20gy | -26.93* | .98 | .00 |
| | Ad.p130 | 2.30 | 1.02 | .74 |
| | Ad.p130+ 10gy | -2.40 | 1.05 | .73 |

| | | | | |
|-------------|---------------|---------|------|-----|
| | Ad.p130+ 20gy | -13.93* | .95 | .01 |
| Rad 20Gy | Ad.p53 | 7.17 | 1.63 | .19 |
| | Ad.p53+ 10gy | -2.43 | 1.60 | .96 |
| | Ad.p53+ 20gy | -11.73 | 2.31 | .13 |
| | Ad.pRB | 4.03 | 1.70 | .69 |
| | Ad.pRB+ 10gy | -3.77 | 1.39 | .60 |
| | Ad.pRB+ 20gy | -16.50* | 1.56 | .02 |
| | Ad.p130 | 12.73* | 1.59 | .03 |
| | Ad.p130+ 10gy | 8.03 | 1.61 | .14 |
| | Ad.p130+ 20gy | -3.50 | 1.55 | .74 |
| Ad.p53 | Ad.p53+ 10gy | -9.60* | 1.32 | .03 |
| | Ad.p53+ 20gy | -18.90* | 2.12 | .04 |
| | Ad.pRB | -3.13 | 1.44 | .77 |
| | Ad.pRB+ 10gy | -10.93* | 1.06 | .03 |
| | Ad.pRB+ 20gy | -23.67* | 1.28 | .00 |
| | Ad.p130 | 5.57 | 1.31 | .20 |
| | Ad.p130+ 10gy | .87 | 1.33 | 1.0 |
| | Ad.p130+ 20gy | -10.67* | 1.26 | .02 |
| Ad.p53+10Gy | Ad.p53+ 20gy | -9.30 | 2.10 | .23 |
| | Ad.pRB | 6.47 | 1.40 | .16 |
| | Ad.pRB+ 10gy | -1.33 | 1.00 | .98 |
| | Ad.pRB+ 20gy | -14.07* | 1.23 | .01 |
| | Ad.p130 | 15.17* | 1.26 | .01 |
| | Ad.p130+ 10gy | 10.47* | 1.28 | .02 |
| | Ad.p130+ 20gy | -1.07 | 1.21 | 1.0 |
| Ad.p53+20Gy | Ad.pRB | 15.77 | 2.18 | .06 |
| | Ad.pRB+ 10gy | 7.97 | 1.94 | .33 |
| | Ad.pRB+ 20gy | -4.77 | 2.07 | .72 |
| | Ad.p130 | 24.47* | 2.09 | .02 |
| | Ad.p130+ 10gy | 19.77* | 2.11 | .03 |
| | Ad.p130+ 20gy | 8.23 | 2.06 | .30 |
| Ad.pRB | Ad.pRB+ 10gy | -7.80 | 1.16 | .1 |
| | Ad.pRB+ 20gy | -20.53* | 1.37 | .00 |
| | Ad.p130 | 8.7 | 1.39 | .06 |
| | Ad.p130+ 10gy | 4.0 | 1.42 | .52 |
| | Ad.p130+ 20gy | -7.53 | 1.35 | .09 |
| Ad.pRB+10Gy | Ad.pRB+ 20gy | -12.73* | .95 | .01 |
| | Ad.p130 | 16.5* | .99 | .01 |
| | Ad.p130+ 10gy | 11.80* | 1.02 | .02 |
| | Ad.p130+ 20gy | .27 | .92 | 1.0 |
| Ad.pRB+20Gy | Ad.p130 | 29.23* | 1.22 | .00 |
| | Ad.p130+ 10gy | 24.53* | 1.25 | .00 |
| | Ad.p130+ 20gy | 13.0* | 1.17 | .01 |

| | | | | |
|--------------|---------------|---------|------|-----|
| Ad.p130 | Ad.p130+ 10gy | -4.70 | 1.28 | .29 |
| | Ad.p130+ 20gy | -16.23* | 1.20 | .00 |
| Ad.p130+10Gy | Ad.p130+ 20gy | -11.53* | 1.23 | .01 |

Microbubble Assisted Adenoviral p53, pRb, and p130 Gene Transfer in Combination with External Beam Radiation Enhanced Therapy of Radio-resistant DU145 Tumor Xenografts.

We have been focusing on developing a safe and effective means of gene delivery *in vivo* to realize the therapeutic potential of the synergistic effects of tumor suppressor gene expression and ionizing radiation to combat human malignancy, specifically prostate carcinoma. To follow up on our previous studies on the use of microbubble assisted adenoviral gene transfer in radio-resistant prostate cancer [53], we decided to compare the effects of microbubble assisted adenoviral *p53*, *RB*, and *p130* gene delivery combined with radiation therapy on xenografted DU145 tumors in nude mice.

We have employed here a novel systemic delivery approach to target adenovirus (Ad) release in a site-specific manner that consists of Ad incorporated in MBs combined with diagnostic US [53, 214]. Proof-of-principle for this strategy comes from studies using Ad to systemically deliver the GFP gene or a target gene (Mda-7/IL-24) in a tissue specific manner [53, 214].

For these current studies, we used DU145 human prostate carcinoma cells. The therapeutic arm included three different non-replicating adenoviral constructs to deliver *p53*, *RB*, and *p130* that have been previously shown to increase radiation therapy response or to reduce tumor growth in various tumor types [254, 258, 266, 267]. The control arms of the study included Adenovirus expressing the green fluorescent protein (GFP) and the firefly luciferase gene (LUC). To test the specificity of intravenous injection of Ads complexed MBs for gene delivery *in vivo* we used the reporter firefly luciferase gene (LUC). We showed exclusive

bioluminescence in the sonoporated tumor at 24hrs from MB-assisted gene delivery using whole animal bioluminescence imaging (BLI) (Fig. 34), which was not extended to other districts of the animal even after one week from LUC gene delivery.

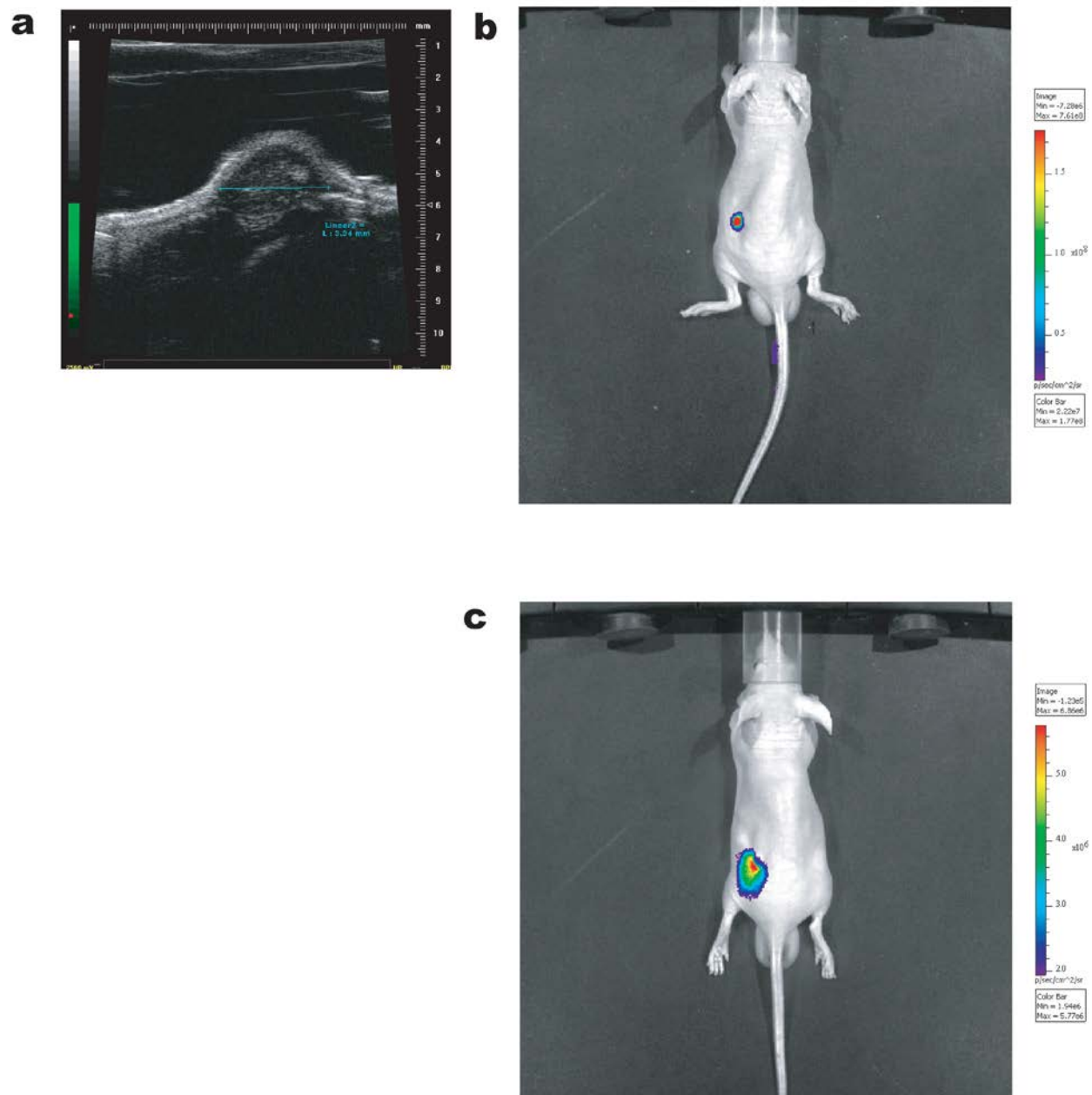


Figure 34. Detection of MB-assisted Firefly Luciferase gene transfer through whole animal imaging. **Panel a)** is the ultrasound image of a tumor xenograft. **Panel b)** is the image from a mouse sonoporated on the tumor xenografted in the left flank showing specific luciferase

luminescent signal at 24 hours from the treatment. **Panel c**) is the image from the same mouse as in panel b showing specific luminescent signal at 1 week from the treatment.

To test this new therapeutic approach for targeted tumor delivery of p53, pRb and p130, prostate tumor xenografts were established on both flanks of nude mice by injecting 4×10^6 DU145 cells in the subcutaneous region of each flank of the animals. DU145 tumor bearing nude mice (n=5 each group) were then injected in their tail veins with 100 μ L of US contrast agent that was reconstituted with PBS or Ad.GFP as controls. Additional DU145 tumor control nude mice (n=5 each group) were injected intratumorally (IT) with 100 μ L of unprotected Ad.p53, Ad.RB or Ad.p130. In the treatment arm tumor-bearing animals were injected in their tail vein with 100 μ L of US contrast agent (Targeson, San Diego, CA) that was reconstituted with Ad.p53, Ad.RB or Ad.p130. Tumors implanted on the right-side, were sonoporated as previously reported [53]. The treatment schedule is described in figure 4. In this study, gene transfer treatments were started twelve weeks after the injection of the cell lines, when tumors reached an approximate volume of 200-250 mm³. Mice were irradiated with 8Gy of x-ray irradiation from a clinical linear particle accelerator (LINAC) on week 12. Three days after radiation therapy, mice were injected once a week for four weeks (wks 13-16) and were again irradiated at week 16 (Fig. 35). Mice were then injected once a week for three additional weeks (wks 17-19) and were sacrificed one week after the end of the treatments because the control tumors reached an approximate volume of 1,000 mm³ (Fig. 35). Compared to untreated or to irradiated control, tumors transduced with MB-assisted gene transfer using adenoviruses overexpressing p53, pRb, and p130 in combination with radiation treatments showed marked reduction of tumor size which was statistically significant ($p < 0.05$) (Fig. 36). Tumors treated with ultrasound MB-

assisted gene transfer of *p53*, *RB*, and *p130* were smaller in size (Fig. 36) with an inhibition rate of 91.24%, 92.27%, and 48.31% respectively, when compared to the final tumor volume of control tumors (Table 6). Irradiated tumors were smaller in size than control tumors (Fig. 36) with an inhibition rate of 21.98% (Table 6). B-mode US scanned images showed in figure 38 demonstrate tumor reduction in real time (Fig. 38) as the US images were recorded during the course of the treatment. US scanned images for groups that were transduced with *p53* or *RB* showed a marked reduction in tumor growth, whereas tumors transduced with *p130* exhibited a plateaued growth (Fig. 38).

Compared to untreated or to irradiated control, intratumoral injections (IT) of Ad.*p53* or Ad.*RB* significantly reduced tumor size ($p < 0.05$) with an inhibition rate of 81.29% and 85.99%, respectively (Fig. 36 and Tables 6 and 7). Compared to radiation only groups, tumor treatment with Ad.*p53* ($p = 0.015$) and Ad.pRB ($p = 0.014$) significantly decreased tumor growth (Table 7). The effect was further significantly enhanced ($p < 0.05$) when gene transfer with Ad.*p53* or Ad.*RB* was combined with radiation showing a growth inhibition rate of 88.04% and 87.82% compared to radiation control, respectively (Table 6 and 7). We also observed that when IT treatment of Ad.*p53* or Ad.*RB* was combined with radiation there was reduction in tumor growth (Fig. 36) compared to gene transfer groups alone, although the difference was not statistically significant (Table 7). Interestingly, the IT injection with Ad.*p130* slowed the growth of the tumors with an inhibition rate of 52.70%. However, IT injection of Ad.*p130* combined with x-ray irradiation improved its efficacy by only about 4% (Table 6).

The intravenous injection (IV) of MB complexed with Ad.*p53* or Ad.*RB* did not result in inhibition of tumor growth when no ultrasound was applied (Fig. 37). Only tumors on the flank that received ultrasound (right flank) exhibited tumor growth reduction (Fig. 36 and 37). Tumors

on the sonoporated flank (right side) that were transduced with Ad.p53 or Ad.RB (but not irradiated) showed a growth inhibition rate of 91.24% and 92.27%, respectively. Tumors treated with ultrasound MB-assisted gene transfer of Ad.p53 showed better (but not significant) growth inhibition than IT Ad.p53 (p=0.363) or combined x-ray irradiation with IT Ad.p53 (p=0.65). This trend was also observed in tumors treated with ultrasound MB-assisted gene transfer of Ad.RB versus IT injections of Ad.RB (p=0.630) or combined x-ray irradiation with IT Ad.RB (p=0.283) (Table 7). Tumors treated with x-ray irradiation combined with microbubble assisted gene transfer of Ad.p130 resulted in 66.0% tumor reduction respect to the radiation control. Notably, the greatest tumor reduction was observed in tumors that were treated with x-ray irradiation combined with microbubble assisted gene transfer of Ad.p53 or Ad.RB with an inhibition rate of 94.44% and 95.95%, respectively (Table 6) (p<0.05).

Table 6. Mean percentage inhibition rate and standard deviation of final tumor volume at week 19 compared against the control non-treated group.

| Groups | Inhibition Rate (%) | SD |
|------------------------|---------------------|-------|
| Radiation (Control) | 21.98 | 2.92 |
| IT Ad.p53 | 81.29 | 5.71 |
| IT Ad. p53 + Rad | 88.05 | 2.76 |
| IT Ad.pRB | 85.99 | 3.13 |
| IT Ad.pRB + Rad | 87.82 | 0.79 |
| IT Ad.p130 | 52.70 | 4.86 |
| IT Ad.p130 + Rad | 56.12 | 10.19 |
| IV MB Ad.p53 US | 91.24 | 0.22 |
| IV MB Ad.p53 US + Rad | 94.44 | 1.26 |
| IV MB Ad.pRB US | 92.27 | 2.39 |
| IV MB Ad.pRB US + Rad | 95.95 | 1.18 |
| IV MB Ad.p130 US | 48.31 | 2.47 |
| IV MB Ad.p130 US + Rad | 66.02 | 7.27 |

*SD-standard deviation *Rad-Radiation *% -Percentage

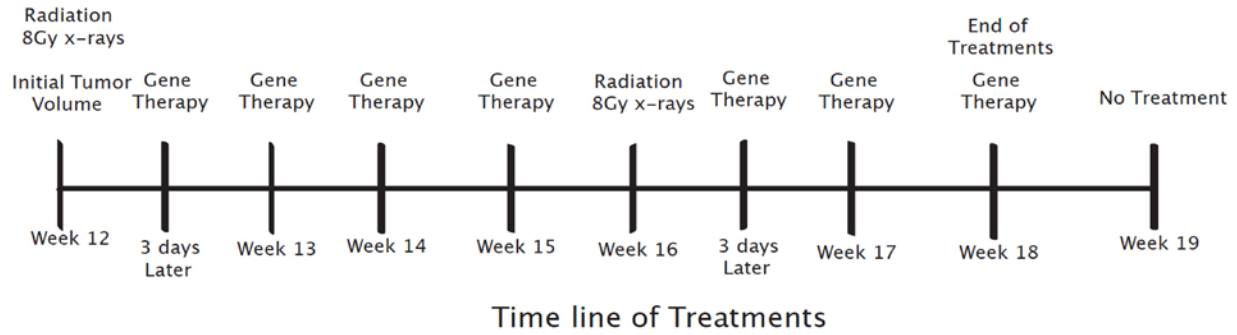


Figure 35. *In vivo* study timeline. Treatments are marked on the line from week 12 to week 19 (end of the study). Radiation followed by four gene transfer treatments is considered as a cycle. In the *in vivo* study there were two treatment cycles.

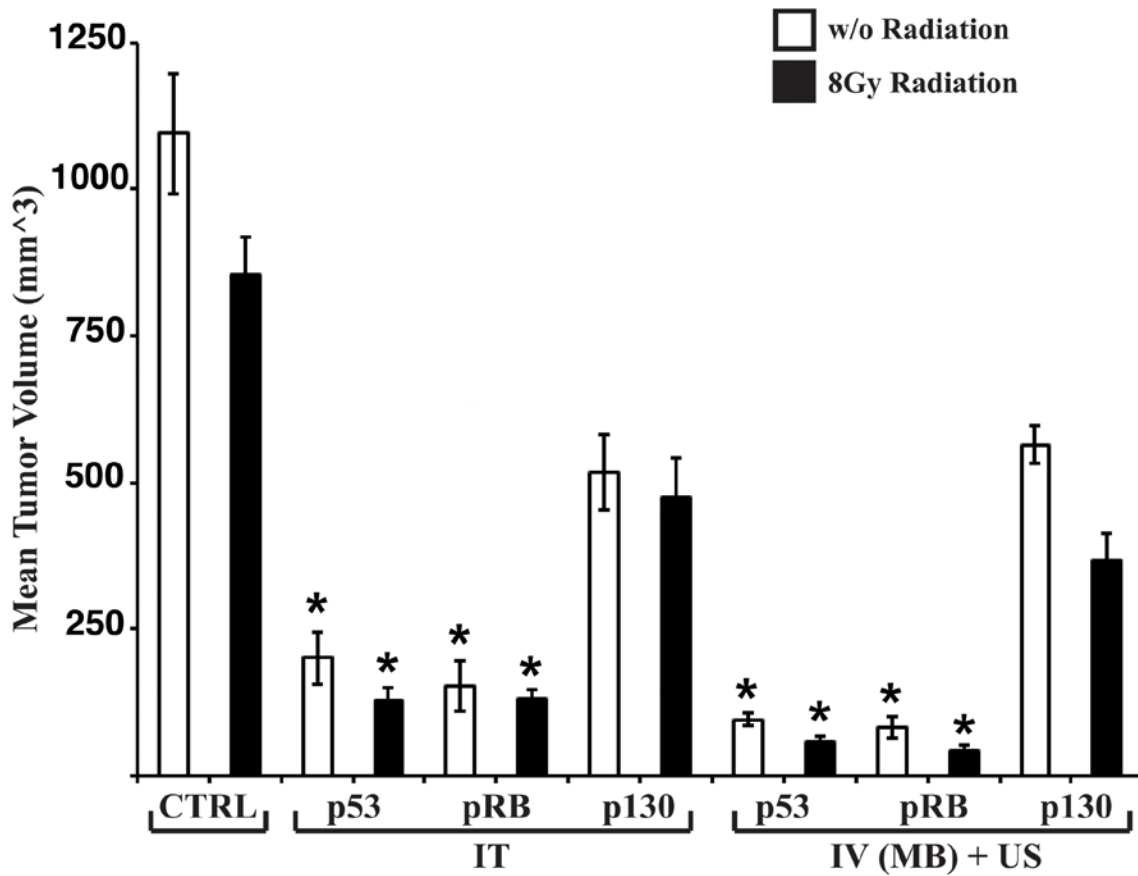


Figure 36. Bar graph of DU145 tumor xenografts volumes (\pm SD) at week 19 after direct intratumoral injection (IT) of Ad-GFP, Ad.p53, Ad.pRB, or Ad.p130 with and without radiation. Mean tumor volume for intravenous (IV) injections of MBs complexed with Ad.p53, Ad.RB or

Ad.p130 of sonoporated tumors (right flank) with or without external beam x-ray radiation was also plotted. The mean tumor volumes are indicated on the ordinate. The group is indicated on the abscissa. The IT and IV treatments were compared against the non-treated control and radiation control to determine the most effective treatment. * indicates statistical significance between control and treated cells.

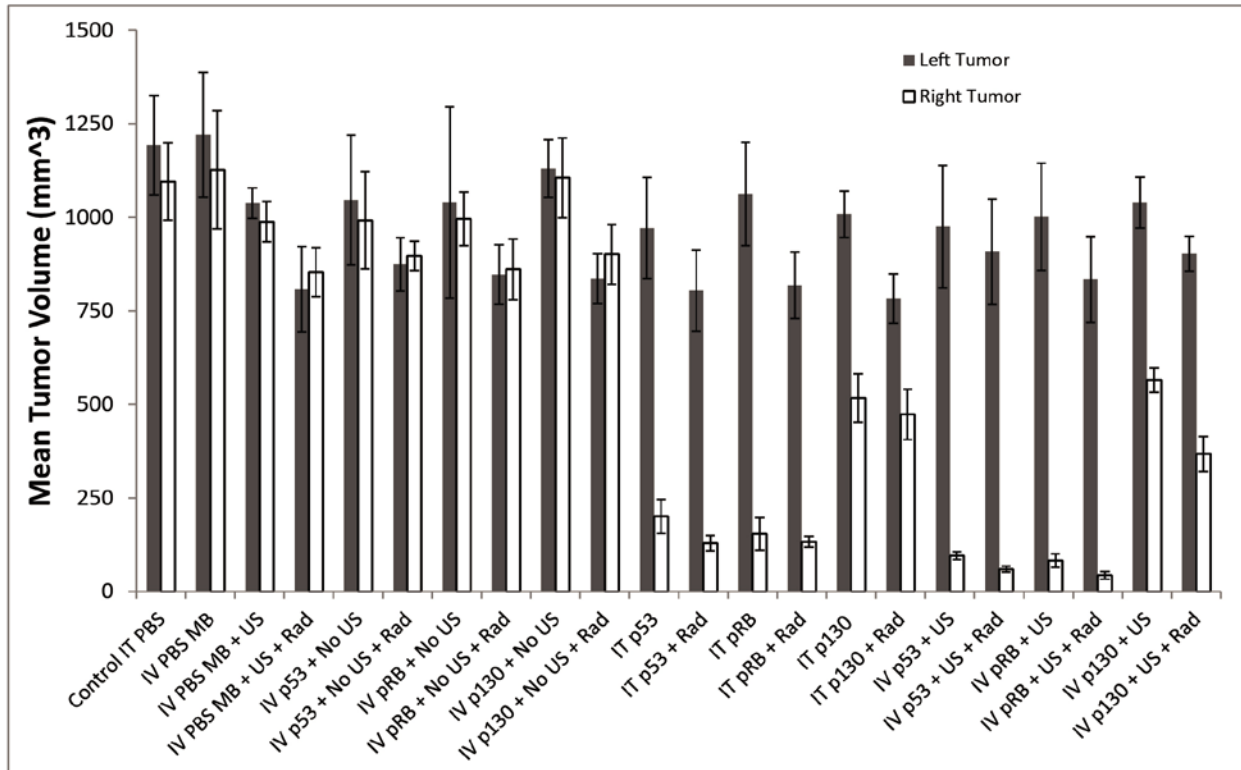


Figure 37. Bar graph representation of mean tumor volume for all groups (left and right flank mean tumor volume) with standard deviation error bars. The tumor on the left flanks served as internal controls to monitor any additional effect by the adenoviruses or MBs complexed with viruses on distant untreated tumors. Only tumors on the right flanks were treated with adenoviral vectors or UTMD of Ads/MBs regarding the sonoporated groups. On the ordinate the mean tumor volumes are indicated. On the abscissa are indicated the different treatment groups.

Table 7. Multiple comparisons ANOVA (Analysis of Variance) significance table with a post hoc Dunnett's T3 test for the *in vivo* experiment following radiation and adenoviral gene transfer on the treated right tumors at week 19. The statistical analysis was run using IBM SPSS software. Mean and standard deviation of final tumor volume obtained at week 19.

| (I) Group | (J) Group | Mean Difference (I-J) | Std. Error | Sig. |
|-------------|------------------------|-----------------------|------------|------|
| Control | Rad Control | 242.11 | 70.51 | .38 |
| | IT Ad.p53 | 894.55* | 64.95 | .02 |
| | IT Ad.p53 + Rad | 966.22* | 60.59 | .02 |
| | IT Ad.pRB | 941.38* | 64.50 | .01 |
| | IT Ad.pRB + Rad | 962.28* | 60.03 | .03 |
| | IT Ad.p130 | 578.16* | 70.36 | .04 |
| | IT Ad.p130 + Rad | 621.91* | 70.97 | .03 |
| | IV MB US Ad.p53 | 999.64* | 59.77 | .03 |
| | IV MB US Ad.p53 +Rad | 1035.58* | 59.64 | .02 |
| | IV MB US Ad.pRB | 1012.58* | 60.33 | .02 |
| | IV MB US Ad.pRB +Rad | 1052.10* | 59.72 | .02 |
| | IV MB US Ad.p130 | 530.80 | 62.32 | .07 |
| | IV MB US Ad.p130 +Rad | 727.83* | 65.38 | .03 |
| Rad Control | IT Ad.p53 | 652.44* | 46.05 | .01 |
| | IT Ad.p53 + Rad | 724.11* | 39.66 | .01 |
| | IT Ad.pRB | 699.28* | 45.41 | .00 |
| | IT Ad.pRB + Rad | 720.18* | 38.80 | .02 |
| | IT Ad.p130 | 336.05 | 53.40 | .06 |
| | IT Ad.p130 + Rad | 379.80* | 54.20 | .04 |
| | IV MB US Ad.p53 | 757.53* | 38.40 | .02 |
| | IV MB US Ad.p53 + Rad | 793.47* | 38.18 | .02 |
| | IV MB US Ad.pRB | 770.48* | 39.27 | .01 |
| | IV MB US Ad.pRB + Rad | 809.99* | 38.32 | .01 |
| | IV MB US Ad.p130 | 288.70 | 42.26 | .08 |
| | IV MB US Ad.p130 + Rad | 485.73* | 46.65 | .01 |
| IT Ad.p53 | IT Ad.p53 + Rad | 71.67 | 28.63 | .67 |
| | IT Ad.pRB | 46.84 | 36.18 | .99 |
| | IT Ad.pRB + Rad | 67.74 | 27.43 | .69 |
| | IT Ad.p130 | -316.39 | 45.81 | .06 |
| | IT Ad.p130 + Rad | -272.64 | 46.74 | .1 |
| | IV MB US Ad.p53 | 105.09 | 26.85 | .36 |

| | | | | |
|-----------------|------------------------|----------|-------|-----|
| | IV MB US Ad.p53 + Rad | 141.03 | 26.55 | .22 |
| | IV MB US Ad.pRB | 118.04 | 28.08 | .29 |
| | IV MB US Ad.pRB + Rad | 157.55 | 26.74 | .18 |
| | IV MB US Ad.p130 | -363.75* | 32.13 | .01 |
| | IV MB US Ad.p130 + Rad | -166.71 | 37.72 | .18 |
| IT Ad.p53 + Rad | IT Ad.pRB | -24.83 | 27.59 | 1.0 |
| | IT Ad.pRB + Rad | -3.93 | 14.30 | 1.0 |
| | IT Ad.p130 | -388.06 | 39.37 | .05 |
| | IT Ad.p130 + Rad | -344.31 | 40.46 | .07 |
| | IV MB US Ad.p53 | 33.42 | 13.16 | .66 |
| | IV MB US Ad.p53 + Rad | 69.36 | 12.52 | .16 |
| | IV MB US Ad.pRB | 46.37 | 15.52 | .49 |
| | IV MB US Ad.pRB + Rad | 85.88 | 12.93 | .09 |
| | IV MB US Ad.p130 | -435.41* | 22.01 | .00 |
| | IV MB US Ad.p130 + Rad | -238.38 | 29.58 | .06 |
| IT Ad.pRB | IT Ad.pRB + Rad | 20.90 | 26.34 | 1.0 |
| | IT Ad.p130 | -363.22* | 45.16 | .04 |
| | IT Ad.p130 + Rad | -319.48 | 46.11 | .06 |
| | IV MB US Ad.p53 | 58.26 | 25.74 | .75 |
| | IV MB US Ad.p53 + Rad | 94.20 | 25.42 | .40 |
| | IV MB US Ad.pRB | 71.20 | 27.02 | .63 |
| | IV MB US Ad.pRB + Rad | 110.72 | 25.63 | .31 |
| | IV MB US Ad.p130 | -410.58* | 31.21 | .01 |
| | IV MB US Ad.p130 + Rad | -213.55 | 36.94 | .08 |
| IT Ad.pRB + Rad | IT Ad.p130 | -384.13 | 38.51 | .06 |
| | IT Ad.p130 + Rad | -340.38 | 39.62 | .08 |
| | IV MB US Ad.p53 | 37.36 | 10.30 | .33 |
| | IV MB US Ad.p53 + Rad | 73.30 | 9.47 | .05 |
| | IV MB US Ad.pRB | 50.30 | 13.18 | .28 |
| | IV MB US Ad.pRB + Rad | 89.82* | 10.01 | .02 |
| | IV MB US Ad.p130 | -431.48* | 20.43 | .01 |
| | IV MB US Ad.p130 + Rad | -234.45 | 28.42 | .08 |
| IT Ad.p130 | IT Ad.p130 + Rad | 43.75 | 54.0 | 1.0 |
| | IV MB US Ad.p53 | 421.48 | 38.10 | .05 |
| | IV MB US Ad.p53 + Rad | 457.42* | 37.89 | .05 |
| | IV MB US Ad.pRB | 434.42* | 38.98 | .04 |
| | IV MB US Ad.pRB + Rad | 473.94* | 38.03 | .04 |
| | IV MB US Ad.p130 | -47.36 | 41.99 | 1.0 |
| | IV MB US Ad.p130 + Rad | 149.68 | 46.41 | .43 |

| | | | | |
|-----------------------|------------------------|----------|-------|-----|
| IT Ad.p130 + Rad | IV MB US Ad.p53 | 377.73 | 39.22 | .07 |
| | IV MB US Ad.p53 + Rad | 413.67 | 39.01 | .06 |
| | IV MB US Ad.pRB | 390.68 | 40.07 | .06 |
| | IV MB US Ad.pRB + Rad | 430.19 | 39.15 | .06 |
| | IV MB US Ad.p130 | -91.11 | 43.01 | .80 |
| | IV MB US Ad.p130 + Rad | 105.93 | 47.33 | .76 |
| IV MB US Ad.p53 | IV MB US Ad.p53 + Rad | 35.94 | 7.64 | .17 |
| | IV MB US Ad.pRB | 12.94 | 11.93 | 1.0 |
| | IV MB US Ad.pRB + Rad | 52.46 | 8.29 | .06 |
| | IV MB US Ad.p130 | -468.84* | 19.65 | .01 |
| | IV MB US Ad.p130 + Rad | -271.81 | 27.86 | .06 |
| IV MB US Ad.p53 + Rad | IV MB US Ad.pRB | -23.0 | 11.22 | .82 |
| | IV MB US Ad.pRB + Rad | 16.52 | 7.24 | .75 |
| | IV MB US Ad.p130 | -504.78* | 19.23 | .01 |
| | IV MB US Ad.p130 + Rad | -307.75 | 27.57 | .05 |
| IV MB US Ad.pRB | IV MB US Ad.pRB + Rad | 39.52 | 11.68 | .41 |
| | IV MB US Ad.p130 | -481.78* | 21.30 | .00 |
| | IV MB US Ad.p130 + Rad | -284.75* | 29.05 | .04 |
| IV MB US Ad.pRB + Rad | IV MB US Ad.p130 | -521.30* | 19.50 | .01 |
| | IV MB US Ad.p130 + Rad | -324.27* | 27.76 | .04 |
| IV MB US p130 | IV MB US Ad.p130 + Rad | 197.03 | 32.98 | .09 |

*IT – Intratumoral, *IV-Intravenous, *MB-Microbubble, *US-Ultrasound, *Ad-Adenovirus, *Rad-Radiation.

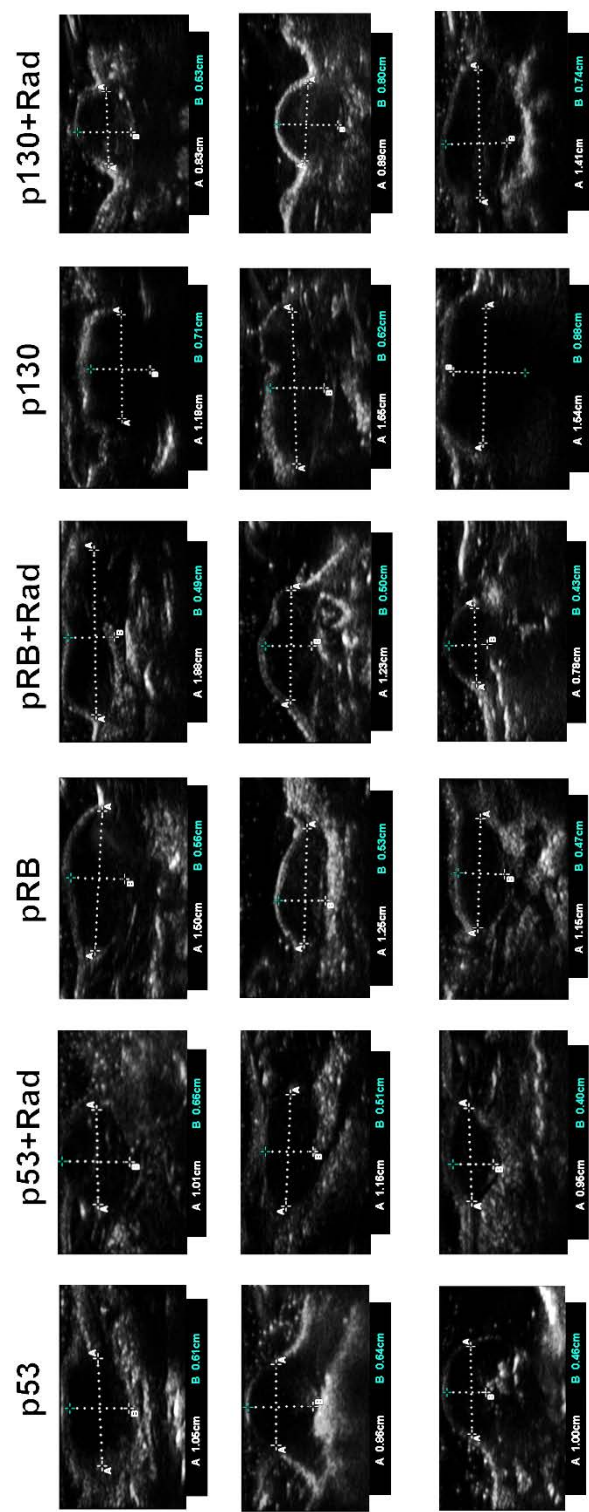


Figure 38. B-mode ultrasound (US) images of DU145 tumor xenografts treated with MBs/US-guided Ad.p53, Ad.pRB or Ad.p130 gene delivery and combination with radiation at different times during treatment schedule.

Microbubble-Assisted p53, pRB, and p130 Gene Transfer Results in Enhanced Protein Expression of Targeted Genes.

Protein expression of *p53*-, *RB*-, and *p130*-transduced genes in tumors that received US and x-ray irradiation was analyzed by western blots (Fig. 39). There was no change in expression of mutated p53 and pRb in all control tumors with either radiation or ultrasound (Fig. 39a). Only endogenous expression of p130 was increased when the tumors were irradiated (Fig. 39 a, d). Tumors that received direct intratumoral injection with Ad.*p53*, Ad.*RB*, or Ad.*p130* showed increased expression of the targeted tumor suppressor genes (Fig. 39a-d). Intravenous injection of complexed MBs showed high expression of transduced *p53*, *RB* and *p130* in tumors that were sonoporated (Fig. 39a-d).

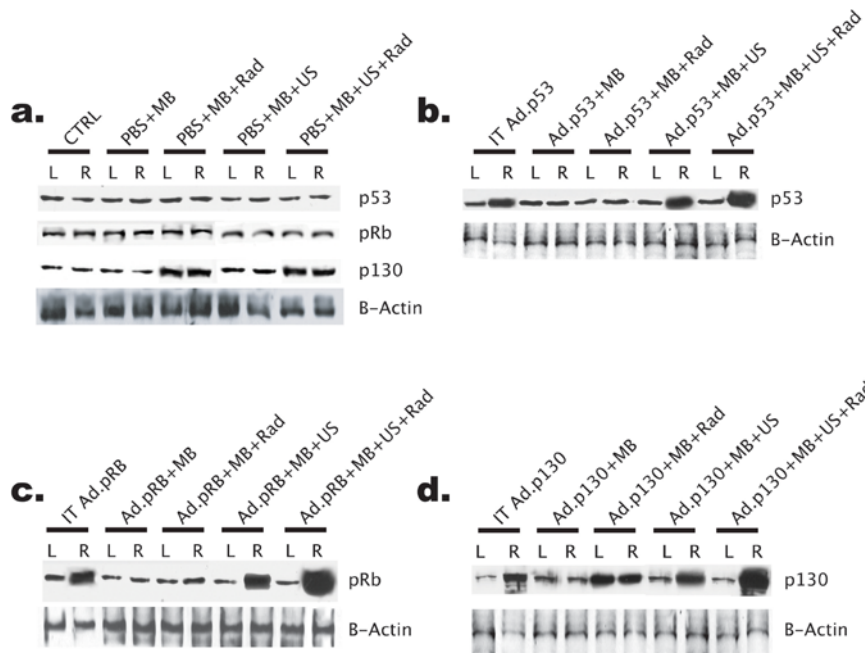


Figure 39. Western Blot analysis of the tumors collected at week 19 from *in vivo* study. L and R indicate tumors implanted in the left and right flank, respectively. (**Panel a**) Control (not treated) DU145 tumors and treated DU145 tumors, as labeled. PBS+MB = empty MBs; Rad = 8Gy radiation; US = Ultrasound. (**Panel b**) Tumors untreated and treated with Ad.*p53*

(Ad.p53+MBs), radiation and ultrasound, as labeled. (**Panel c**) Tumors untreated and treated with Ad.pRB (Ad.pRB+MBs), radiation and ultrasound, as labeled (**Panel d**). Tumors untreated and treated with Ad.p130 (Ad.p130+MBs), radiation and ultrasound, as labeled. Anti-beta-actin was used as a loading control. 50µg of total cell lysates were run on SDS polyacrylamide gels.

DISCUSSION

Primary prostate cancer (PC) can be tackled successfully in many cases with standard treatments, such as radical prostatectomy, radiation therapy, and hormone therapy, offering long-term cancer-specific survival for most patients. While surgery and radiation therapy may have similar outcomes for early-stage prostate cancer, radiation therapy is the primary option for locally advanced prostate cancer. However, over one third of patients who are treated with conventional curative therapy will progress to an androgen-independent (castration-resistant) prostate cancer. Development of androgen-independent, radio-resistant prostate cancer and metastatic progression are key concerns in the management of this disease [268, 269]. The strategies used to tackle these issues are the accurate stratification of patients whose early prostate cancer is likely to progress to hormone-refractory and metastatic disease, and of course improvement and broadening of the available therapeutic choices. Prostate cancer is regarded as relatively resistant to radiation [257]. Consistent with this notion, androgen-independent DU145 human prostate cancer cells manifest resistance to radiation-induced apoptotic death [254, 255].

Previous studies using UV- [254] and γ -radiation [270] have been shown to cause a G2/M cell cycle-phase block in DU145 cells at 24hrs. In our study, ionizing radiation of 10Gy and 20Gy also resulted in G2/M cell cycle-phase block with an increasing number of DU145 cells accumulated in the G2-phase of the cell cycle when assayed from 24 to 96hrs. Interestingly, we observed little apoptotic cell death in the DU145 cells at 24hrs for both 10Gy and 20Gy external beam radiation which could be explained by the fact that DU145 cells undergo DNA fragmentation as early as 4hrs after irradiation while end-stage DNA fragmentation does not peak until 24-36hrs [249]. Additionally, Bromfield et al. demonstrated with flow cytometry assays that greater than 70% of DU145 cells were non-proliferating following irradiation [251], which provided us with a rationale for investigating modalities to

increase the sensitivity of prostate cancer to radiation-induced DNA damage using gene transfer of key cell-cycle regulators.

The *p53*, *RB* and *p130* gene products are key factors that participate in cell-cycle arrest, apoptosis and cellular senescence. PCs manifest frequent mutations in tumor suppressor genes such as *p53* and *RB* [271], and we have demonstrated in the past an inverse association between histological grading in aggressive tumor types of prostate cancer [272] and p130 expression. Additionally, *p130* has been mapped to the human chromosome 16q12.2, an area in which deletions have been found in several human neoplasias including breast, ovarian, hepatic, and prostatic cancers [273].

Our model system, DU145 cells, a human prostate cancer cell line, has a mutant nonfunctional temperature sensitive *p53*, and expresses a truncated pRb protein [254]; however the functional status of *p130* is undetermined in DU145 prostate cancer cells. P53 and pRb overexpression have been shown to play a central role following radiation in PC cell lines [274] [256] while *RB* loss has been linked to radiation resistance in DU145 cells [256].

We decided to compare and contrast the ability of p53, RB and p130 to radio-sensitize prostate cancer cells *in vitro* and to investigate their efficacy in reducing tumor size following targeted gene transfer using a microbubble-assisted gene transfer method that we have perfected in our laboratory [53, 214, 218]. This strategy allows for systemic targeted delivery to prostate cancer xenografts of therapeutic adenovirus carrying therapeutic genes.

As expected, DU145 cells transduced with adenovirus carrying wt-p53 showed a shift from the G2/M to the G1-phase of the cell cycle regardless of the radiation dose, as previously demonstrated [255]. Apoptosis was observed for p53 groups treated with or without radiation. Overexpression of p53 in DU145 cells restored irradiation-induced senescence by forming the

characteristic heterochromatin structure called senescence-associated heterochromatic foci (SAHFs) [275]. SAHFs could account for the relatively low amount of apoptosis at 24 hrs. The downstream effectors such as Bax [251] or p21Waf1 that are attenuated/absent in DU145 [276] would hamper the cells from undergoing apoptosis. Additionally, the mutant p53 described in the DU145 cells has been shown to suppress the ability of wt-p53 to induce cell cycle arrest by exerting a dominant negative effect on the DNA binding activity of wt-53 and to reduce the trans-activation of target genes [277]. Even by lowering the temperature to 32°C from 37°C and activating the temperature sensitive nonfunctional p53 in DU145 cells, Bajgelman and Stauss were unable to trans-activate p21Waf1 [252]. However, we observed that adenoviral overexpression of wt-p53 restored the sensitivity of the DU145 cells to ionizing radiation indicating that gene transfer of wild-type copies of the p53 gene and its overexpression in the targeted cells could be a viable therapeutic option for radio-resistant PCs.

Proteins of the retinoblastoma family (pRb, p107 and p130) are known to exert control over the entry into S-phase of the cell cycle [278]. Gamma (γ) and ultraviolet (UV) radiation are known to be ineffective on pRb deficient cells. After DNA damage by γ -radiation, pRb is hypophosphorylated and induces growth arrest by blocking cell-cycle progression at the G1/S phase [279]. G1-phase blockage has been previously observed when cells were transduced with pRb in the presence or absence of radiation [254]. Some reports indicate that apoptosis of cells which are deficient in pRb protein is inhibited after restoring wt-pRb [280]. In our study, we observed that by restoring a wild-type RB in DU145 cells, which have a truncated pRb, we were able to facilitate apoptosis similarly to when we restored wt-p53. The highest apoptotic response was observed in pRb transduced DU145 cells which received 20Gy irradiation. Interestingly, our study showed increased expression of pRb protein when Adenoviral gene transfer treatment was

combined with radiation therapy. Similar results have been shown for pRb negative and positive esophageal squamous cell carcinoma (ESCC) treated with a combination of adenoviral gene delivery of RB94, a truncated more active RB gene product, and radiation therapy [267].

Hypophosphorylated p130 complexes with E2F transcription factors and has been associated with control over the G0/G1 phase of the cell cycle [278]. In our study we observed that overexpressed p130 in prostatic DU145 cells led to DNA accumulation at G0/G1 of the cell cycle. Interestingly, irradiated or combined irradiated and Ad.p130 gene transfer groups showed accumulation of cells in the G2 cell cycle phase suggesting a block at the G2/M transition. In several cell lines, the overexpression of p130 has been shown to result in binding to cyclins A and B promoter regions, regulating the expression of S- and G2-phase transitions, and dominating the p53-p21 DNA damage response pathway leading to senescence [281].

Our *in vitro* study confirmed an increase in expression of endogenous or transduced p130 after exposure to genotoxic stress such as radiation, as previously observed [275, 282]. Adenoviral overexpression of p130 increased the percentage of apoptotic cells after ionizing radiation, but to a lower extent than in groups transduced with *p53* or *RB*.

It has been shown in the prostatic cancer cell lines C4-2 and LNCap, that ionizing radiation exposure results in up-regulation of the transcription factor E2F4 which has been shown to complex with p130 and to co-localize in the nucleus regardless of androgen sensitivity, resulting in tumor growth suppression and G2 arrest [282]. The authors demonstrated that the formation of the E2F4/p130 complex is specifically regulated by IR in prostate cancer cells and suggested that the interaction between p130 and its natural partner CDK2 is also affected by IR, which may be a result of the increased levels of E2F4 associated with p130, leading to a decrease in p130 phosphorylation and decreased cell viability. The inhibition of E2F4 by siRNA in

prostate C4-2 cells results in apoptosis and increased sensitivity to radiation [282], thus suggesting a partial explanation of the lack of apoptosis and radiation resistance of the DU145 cells following overexpression of p130. Additionally, p130 induces accumulation of pro-apoptotic p73, a p53-related gene that alternatively splices and mediates radiation-induced apoptosis independent of p53 by interacting with c-Abl tyrosine kinase in glioblastoma cells indicating that p130 radiosensitization could be cell type specific [258].

Adenoviral gene transfer is limited by the ability of Adenovirus serotype 5 (Ad5) to transduce target cells and the inability to deliver it intravenously without causing liver inflammatory damage or elimination by the immune system [202]. Patients exposed to adenoviruses tend to develop neutralizing and anti-adenovirus antibodies [283, 284]. Another limitation of using Adenoviruses for gene transfer techniques in cancer is that the efficiency of these viruses to transfer genetic materials to cancer cells is dependent upon the availability of Coxsackie adenovirus receptor (CAR) on the surface of the targeted cells, which facilitates adenoviral entry. These difficulties in the use of Adenoviruses for cancer gene therapy have limited their use to direct injections to the tumoral mass, which resulted in partially transduced tumors [218, 285].

To circumvent the difficulties caused by the use of adenoviruses as vectors for gene transfer we used ultrasound contrast agents (microbubbles) to provide protection to the virus from the immune system as well as to increase target organ specificity, allowing intravenous injection and less aggressive viral administration [214]. Microbubbles (MBs) can be injected into peripheral veins, as these robust bubbles can re-circulate through the systemic circulation numerous times within the bloodstream [219]. Cavitation also improves the efficiency of viral infection by creating small shockwaves that increase cellular permeability [220]. Phase I to III

clinical trials have demonstrated that MBs are safe and well tolerated even at higher doses [286].

Previous studies of our lab demonstrated that MB complexes with Ad.GFP (Green Fluorescent Protein) were able to express GFP specifically localized to sonoporated tumors [53]. Our western blot studies on harvested tumors showed high levels of transgene expression at the tumor site by more efficient GFP gene transfer into the target cells [53].

In earlier studies, therapy resistant prostate cancer cell lines containing wt-p53, mutated p53 or p53 null were radio-sensitized by adenoviral mediated *p53* gene transfer [274, 287]. As expected, in our *in vitro* study the DU145 cells transduced with *p53* were radio-sensitized to ionizing radiation resulting in higher apoptotic rates than either irradiation group or adenoviral-*p53* transduced groups. Additionally, reduction of tumor volumes by ultrasound mediated microbubble destruction of wt-p53 or wt-pRb resulted in increased ablation of the tumors when compared to intra-tumoral injections. Ad.*p130* intra-tumoral injection in mice showed slower growth rate than the untreated control or irradiated groups. Interestingly, Ultrasound targeted microbubble destruction (UTMD) of Ad.*p130* MB complexes resulted in slower tumor growth, but no tumor reduction was observed (Fig. 36).

Clinical studies for combinational therapy of *p53* and *RB* gene transfer and ionizing radiation in lung [266], hepatocellular [288], and esophageal carcinomas [267] have been successful in eliciting partial and complete remission of tumors. Our study demonstrated that combination therapy of radiation and intratumoral injections of Ad.*p53*, Ad.*RB* or Ad.*p130* caused an enhanced effect in comparison to adenoviral intratumoral injections (IT) or radiation treatment alone. Currently, phase-I clinical studies of combination therapy with IT adenoviral *p53* gene delivery for prostate cancer are underway at M.D. Anderson Cancer Center, Texas and UCLA School of Medicine, California to test its efficacy [289]. Interestingly, we observed more

profound response in reducing tumor growth of treated tumors by combining the ultrasound-targeted destruction of Ad.p53 or Ad.RB MB/complexes with ionizing radiation. As demonstrated by western blot analysis, tumor volume reduction in these samples was associated with overexpression of the *p53* or *RB* genes (Fig. 39). UTMD of Ad.*p130* combined with radiation resulted instead in a relatively plateaued tumor growth curve, which was comparable to the initial volume of tumors at the beginning of the treatment schedule. Thus p130, in a comparative gene transfer study with other known cell cycle regulating proteins such as pRb and p53, caused a “tumorstatic” effect that was not significantly enhanced by radiation therapy. On the other hand, we showed that the highest decrease in tumor growth was observed when *p53* and *RB* genes were transferred by ultrasound-targeted destruction of Adenoviral-MB/complexes in combination with ionizing radiation.

An open question is: What effect would the pooled transfer of the cell cycle regulating genes p53, pRb and p130 with or without ionizing radiation have on tumor growth? It is possible that combined gene transfer of multiple cell cycle regulatory proteins could result in further tumor growth suppression. In fact, tumors are made of a heterogeneous population of cells that may contain a variety of genetic dysfunctions and/or changes. Thus exploring the effects of pooled transfer of therapeutic genes is needed in order to increase their antitumoral activity while possibly decreasing the number of injections needed to realize their radiosensitizing ability. Altogether, these findings highlight the translational therapeutic potential of this novel image-guided gene transfer technology in combination with external beam radiation for prostate cancer patients with therapy resistant disease.

ACKNOWLEDGEMENTS

We gratefully acknowledge the Marshall University Biochemistry and Microbiology Departments for their support. We are grateful to Francesco Salvatore, Professor of Human Biochemistry, University of Naples “Federico II”, for his collaboration. We are particularly grateful to Dr. Elaine W. Hardman for helpful discussion and critical review of the manuscript.

The present studies were supported by the NIH award number CA131395 from the National Cancer Institute (to PPC). The content of this manuscript is solely the responsibility of the authors and does not necessarily represent the official views of the National Cancer Institute or the National Institute of Health.

CHAPTER VI : CONCLUSION AND FUTURE DIRECTIONS

In Chapter 1, we reviewed current literature on prostate cancer (PC) and highlighted some of the therapeutic options in treating PC. We also reviewed some of the potentials and barriers to gene therapy with viral vectors. We chose to study metastatic PC because there are no successful treatment modalities available for the disease while treatment options for stage T1/T2 have decent 5 year survival rates.

In Chapter 2 we described the ultrasound targeted destruction of microbubbles as a gene delivery system. We reviewed current literature on the different types of available MBs that are currently used. We also described the behavior of the MBs when exposed to US and the biological changes that are associated with their interactions. Chapter 2 clearly shows that together MB and US become a reliable systemic drug delivery system.

In Chapter 3, we explored human DU145 and murine TRAMP-C2 PC cells as potential animal models for testing the UTMD drug delivery system. Infection studies were carried out to establish whether human non-replicative viruses (Ad.GFP and Ad.mda-7/IL-24) and replicative-competent virus (CTV.mda-7) could be used to determine a therapeutic response in cancer cells. We clearly observed that Ad.GFP and Ad.mda-7/IL-24 could infect and transfer their transgene in both PC cells, although only CTV.mda-7 could be replicated in DU145 cells. UTMD gene delivery system was also tested in an *in vitro* setting showing an increased enhancement of Ad.GFP transgene expression. This clearly showed that US with MBs caused pore formation on the plasma membrane thereby increasing the permeability of the membrane to allow increased Ad uptake. Thus, animal studies on xenografted DU145 PC studies in immune-compromised *nude* mice and syngeneic model of TRAMP-C2 PC injected in immune-competent mice become attractive to test the UTMD gene delivery system.

In Chapter 4, we described our studies of the UTMD gene delivery system for Ad.GFP, Ad.mda-7 and CTV.mda-7 in a xenografted DU145 PC model with tumors on both flanks of *nude* mice. Targeson MBs/Ads complexes were injected into the tail vein while only the tumor on the right flank was sonoporated. The study was designed to define an improved therapeutic approach for delivering Ad.mda-7, which will permit systemic delivery and targeted tumor release by US specifically and effectively in the primary tumor. This treatment resulted in a dramatic reduction in the size of not only the treated tumor on the right flank, but also of the non-treated tumor on the left flank due to mda-7 bystander effect [53]. US-guided focused release of entrapped materials from the MBs will increase the delivery specificity and therapeutic efficiency of Ad.mda-7 towards PC xenografts. Our findings in combination with the positive results of Phase-I Clinical trial with Ad.mda-7 [211] suggest that this cytokine has considerable potential as a gene therapy for cancer.

In Chapter 5, we described the combined therapy approach of using radiation and UTMD for the delivery of Ad.p53, Ad.RB and Ad.p130 in a xenografted DU145 PC model with tumors on both flanks of *nude* mice. Similar to the previous animal study, Targeson MBs/Ads complexes were injected into the tail vein while only the tumor on the right flank was sonoporated. We demonstrated that combined radiation and UTMD gene therapy enhanced the therapeutic benefit of tumor suppressor genes in radiation resistant PC. There was no bystander activity that was observed in this study as tumor suppressor genes such as p53, pRb and p130 are not secreted proteins. The increased expression of p53, Rb and p130 further proved that UTMD targets only the tumor that is sonoporated making it a specific gene delivery therapy system.

In addition to the experiments that were performed, we propose to further develop the UTMD system using immune-competent animals to facilitate its translation into a clinically

feasible technology for the effective delivery of therapeutic genes to treat human PC. Our data shows that murine TRAMP-C2 PC cells are efficiently infected by non-replicative Ad.GFP and Ad.mda-7/IL-24 using the MB/Adenoviral system cavitated by US, which results in the expression of the transduced genes. Additionally, mda-7/IL-24 acts as a pro-apoptotic gene resulting in the increased cell death of PC cells. Thus we believe that MBs will effectively shield the Ads from immune surveillance in immune-competent mice, and target the delivery of Ad.GFP & Ad.mda-7 specifically to PCs. These studies would further establish the efficiency and specificity of gene delivery in primary advanced prostate cancer by using an innovative system consisting of ultrasound contrast agents, viral vectors and ultrasound waves.

In conclusion, our present body of work supports the hypothesis that the UTMD systemic gene delivery system we have developed is a promising therapeutic approach for PC that deserves further investigation in immune competent organisms to warrant its future translation from bench to bedside.

REFERENCES

1. Damber, J.E. and G. Aus, *Prostate cancer*. Lancet, 2008. **371**(9625): p. 1710-21.
2. Society, A.C., *Prostate cancer facts. In: Cancer facts and figures 2009*. American Cancer Society, 2009. **Atlanta, GA**: p. 19-20.
3. Tao, Z.Q., et al., *Epidemiology of prostate cancer: current status*. Eur Rev Med Pharmacol Sci, 2015. **19**(5): p. 805-12.
4. Jemal, A., et al., *Global cancer statistics*. CA Cancer J Clin, 2011. **61**(2): p. 69-90.
5. Punnen, S. and M.R. Cooperberg, *The epidemiology of high-risk prostate cancer*. Curr Opin Urol, 2013. **23**(4): p. 331-6.
6. Uchida, T., et al., *Transrectal high-intensity focused ultrasound for the treatment of localized prostate cancer: eight-year experience*. Int J Urol, 2009. **16**(11): p. 881-6.
7. Zelefsky, M. and J. Eastman, *Cancer of the prostate*, in *Cancer: Principles and Practice of Oncology* V. DeVita, T.S. Lawrence, and S.A. Rosenberg, Editors. 2008, JB Lippincott: Philadelphia, PA. p. 1392-1452.
8. Shao, Y.H., et al., *Risk profiles and treatment patterns among men diagnosed as having prostate cancer and a prostate-specific antigen level below 4.0 ng/ml*. Arch Intern Med, 2010. **170**(14): p. 1256-61.
9. Cooperberg, M.R., J.M. Broering, and P.R. Carroll, *Time trends and local variation in primary treatment of localized prostate cancer*. J Clin Oncol, 2010. **28**(7): p. 1117-23.
10. Hull, G.W., et al., *Cancer control with radical prostatectomy alone in 1,000 consecutive patients*. J Urol, 2002. **167**(2 Pt 1): p. 528-34.
11. Kupelian, P.A., et al., *Hypofractionated intensity-modulated radiotherapy (70 Gy at 2.5 Gy per fraction) for localized prostate cancer: Cleveland Clinic experience*. Int J Radiat Oncol Biol Phys, 2007. **68**(5): p. 1424-30.
12. Zelefsky, M.J., et al., *Multi-institutional analysis of long-term outcome for stages T1-T2 prostate cancer treated with permanent seed implantation*. Int J Radiat Oncol Biol Phys, 2007. **67**(2): p. 327-33.
13. Toohar, R., et al., *Laparoscopic radical prostatectomy for localized prostate cancer: a systematic review of comparative studies*. J Urol, 2006. **175**(6): p. 2011-7.
14. Han, K.R., et al., *Treatment of organ confined prostate cancer with third generation cryosurgery: preliminary multicenter experience*. J Urol, 2003. **170**(4 Pt 1): p. 1126-30.
15. Sternberg, C.N., *Highlights of contemporary issues in the medical management of prostate cancer*. Crit Rev Oncol Hematol, 2002. **43**(2): p. 105-21.
16. Sternberg, C.N., *Hormone refractory metastatic prostate cancer*. Ann Oncol, 1992. **3**(5): p. 331-5.
17. Dyrstad, S.W., P. Shah, and K. Rao, *Chemotherapy for prostate cancer*. Curr Pharm Des, 2006. **12**(7): p. 819-37.
18. Sarkar, D., et al., *Eradication of therapy-resistant human prostate tumors using a cancer terminator virus*. Cancer Res, 2007. **67**(11): p. 5434-42.
19. Romero-Weaver, A.L., Howard, C., *Radiation in Cancer Therapy*, in *Cutting Edge Therapies for Cancer in the 21st Century*, P.P. Claudio, Vogiatzi, P., Editor. 2014, Bentham Science Publishers. p. 81-110.
20. Matsumoto, K., et al., *Detection of free radical reactions in an aqueous sample induced by low linear-energy-transfer irradiation*. Biol Pharm Bull, 2009. **32**(4): p. 542-7.

21. Willers, H. and K.D. Held, *Introduction to clinical radiation biology*. Hematol Oncol Clin North Am, 2006. **20**(1): p. 1-24.
22. Hogle, W.P., *The state of the art in radiation therapy*. Semin Oncol Nurs, 2006. **22**: p. 212-220.
23. Kassis, A.I., *Therapeutic radionuclides: biophysical and radiobiologic principles*. Semin Nucl Med, 2008. **38**(5): p. 358-66.
24. Gomez-Millan, J., et al., *Advances in the treatment of prostate cancer with radiotherapy*. Crit Rev Oncol Hematol, 2015.
25. Perez, B.A., Koontz, B.F. , *Radiotherapy before and after radical prostatectomy for high-risk and locally advanced prostate cancer*. Urologic Oncology: Seminars and Original Investigations, 2014.
26. Thompson, I.M., Jr., et al., *Adjuvant radiotherapy for pathologically advanced prostate cancer: a randomized clinical trial*. JAMA, 2006. **296**(19): p. 2329-35.
27. Nilsson, S., B.J. Norlen, and A. Widmark, *A systematic overview of radiation therapy effects in prostate cancer*. Acta Oncol, 2004. **43**(4): p. 316-81.
28. Sanfilippo, N.J. and B.T. Cooper, *Hypofractionated radiation therapy for prostate cancer: biologic and technical considerations*. Am J Clin Exp Urol, 2014. **2**(4): p. 286-93.
29. Pollack, A., et al., *Prostate cancer radiation dose response: results of the M. D. Anderson phase III randomized trial*. Int J Radiat Oncol Biol Phys, 2002. **53**(5): p. 1097-105.
30. Dearnaley, D.P., et al., *Escalated-dose versus control-dose conformal radiotherapy for prostate cancer: long-term results from the MRC RT01 randomised controlled trial*. Lancet Oncol, 2014. **15**(4): p. 464-73.
31. Zelefsky, M.J., et al., *Changing trends in national practice for external beam radiotherapy for clinically localized prostate cancer: 1999 Patterns of Care survey for prostate cancer*. Int J Radiat Oncol Biol Phys, 2004. **59**(4): p. 1053-61.
32. Nande, R., et al., *Microbubble-assisted p53, RB, and p130 gene transfer in combination with radiation therapy in prostate cancer*. Curr Gene Ther, 2013. **13**(3): p. 163-74.
33. Madersbacher, S., et al., *Effect of high-intensity focused ultrasound on human prostate cancer in vivo*. Cancer Res, 1995. **55**(15): p. 3346-51.
34. Alkhorayef, M., et al., *High-Intensity Focused Ultrasound (HIFU) in Localized Prostate Cancer Treatment*. Pol J Radiol, 2015. **80**: p. 131-41.
35. Cordeiro, E.R., et al., *High-intensity focused ultrasound (HIFU) for definitive treatment of prostate cancer*. BJU Int, 2012. **110**(9): p. 1228-42.
36. Pfeiffer, D., J. Berger, and A.J. Gross, *Single application of high-intensity focused ultrasound as a first-line therapy for clinically localized prostate cancer: 5-year outcomes*. BJU Int, 2012. **110**(11): p. 1702-7.
37. Webb, H., M.G. Lubner, and J.L. Hinshaw, *Thermal ablation*. Semin Roentgenol, 2011. **46**(2): p. 133-41.
38. Ferrer, F.A. and R. Rodriguez, *Prostate cancer gene therapy*. Hematol Oncol Clin North Am, 2001. **15**(3): p. 497-508.
39. Rodriguez, R., et al., *Prostate attenuated replication competent adenovirus (ARCA) CN706: a selective cytotoxic for prostate-specific antigen-positive prostate cancer cells*. Cancer Res, 1997. **57**(13): p. 2559-63.

40. Miyake, H., et al., *Novel therapeutic strategy for advanced prostate cancer using antisense oligodeoxynucleotides targeting anti-apoptotic genes upregulated after androgen withdrawal to delay androgen-independent progression and enhance chemosensitivity*. *Int J Urol*, 2001. **8**(7): p. 337-49.
41. Muruve, D.A., *The innate immune response to adenovirus vectors*. *Hum Gene Ther*, 2004. **15**(12): p. 1157-66.
42. Vorburger, S.A. and K.K. Hunt, *Adenoviral gene therapy*. *Oncologist*, 2002. **7**(1): p. 46-59.
43. Harrach, B., Benko, M., Both, G., et al., *Adenoviridae - Ninth Report of the International Committee on Taxonomy of Viruses.*, in *Virus Taxonomy*, A.M.Q. King, Adams, M.J., Carstens, E.B., Lefkowitz, E.J., Editor. 2011, Elsevier, Oxford. p. 125-141.
44. Hendrickx, R., et al., *Innate immunity to adenovirus*. *Hum Gene Ther*, 2014. **25**(4): p. 265-84.
45. Arnberg, N., *Adenovirus receptors: implications for targeting of viral vectors*. *Trends Pharmacol Sci*, 2012. **33**(8): p. 442-8.
46. Chiocca, E.A., *Oncolytic viruses*. *Nat Rev Cancer*, 2002. **2**(12): p. 938-50.
47. Fallaux, F.J., A.J. van der Eb, and R.C. Hoeben, *Who's afraid of replication-competent adenoviruses?* *Gene Ther*, 1999. **6**(5): p. 709-12.
48. Zhang, W.W., *Development and application of adenoviral vectors for gene therapy of cancer*. *Cancer Gene Ther*, 1999. **6**(2): p. 113-38.
49. Alemany, R., C. Balague, and D.T. Curiel, *Replicative adenoviruses for cancer therapy*. *Nat Biotechnol*, 2000. **18**(7): p. 723-7.
50. Edelstein, M., *Gene Therapy Clinical Trials Worldwide*, 2011.
51. Green, N.K. and L.W. Seymour, *Adenoviral vectors: systemic delivery and tumor targeting*. *Cancer Gene Ther*, 2002. **9**(12): p. 1036-42.
52. Barker, D.D. and A.J. Berk, *Adenovirus proteins from both E1B reading frames are required for transformation of rodent cells by viral infection and DNA transfection*. *Virology*, 1987. **156**(1): p. 107-21.
53. Greco, A., et al., *Eradication of therapy-resistant human prostate tumors using an ultrasound-guided site-specific cancer terminator virus delivery approach*. *Mol Ther*, 2010. **18**(2): p. 295-306.
54. Choi, J.W., et al., *Evolution of oncolytic adenovirus for cancer treatment*. *Adv Drug Deliv Rev*, 2012. **64**(8): p. 720-9.
55. Miller, A.C., Russell, S.J., *Heterogeneous delivery is a barrier to the translational advancement of oncolytic virotherapy for treating solid tumors*. *Virus Adaptation and Treatment*, 2014. **6**: p. 11-31.
56. Tedcastle, A., et al., *Virotherapy--cancer targeted pharmacology*. *Drug Discov Today*, 2012. **17**(5-6): p. 215-20.
57. Heise, C.C., et al., *Efficacy of a replication-competent adenovirus (ONYX-015) following intratumoral injection: intratumoral spread and distribution effects*. *Cancer Gene Ther*, 1999. **6**(6): p. 499-504.
58. Lyons, M., et al., *Adenovirus type 5 interactions with human blood cells may compromise systemic delivery*. *Mol Ther*, 2006. **14**(1): p. 118-28.
59. Padera, T.P., et al., *Pathology: cancer cells compress intratumour vessels*. *Nature*, 2004. **427**(6976): p. 695.

60. Wang, Y. and F. Yuan, *Delivery of viral vectors to tumor cells: extracellular transport, systemic distribution, and strategies for improvement*. Ann Biomed Eng, 2006. **34**(1): p. 114-27.
61. Cardenas-Navia, L.I., et al., *The pervasive presence of fluctuating oxygenation in tumors*. Cancer Res, 2008. **68**(14): p. 5812-9.
62. Maeda, H., H. Nakamura, and J. Fang, *The EPR effect for macromolecular drug delivery to solid tumors: Improvement of tumor uptake, lowering of systemic toxicity, and distinct tumor imaging in vivo*. Adv Drug Deliv Rev, 2013. **65**(1): p. 71-9.
63. Prabhakar, U., et al., *Challenges and key considerations of the enhanced permeability and retention effect for nanomedicine drug delivery in oncology*. Cancer Res, 2013. **73**(8): p. 2412-7.
64. Yang, Y., et al., *Immune responses to viral antigens versus transgene product in the elimination of recombinant adenovirus-infected hepatocytes in vivo*. Gene Ther, 1996. **3**(2): p. 137-44.
65. Worgall, S., et al., *Innate immune mechanisms dominate elimination of adenoviral vectors following in vivo administration*. Hum Gene Ther, 1997. **8**(1): p. 37-44.
66. Cichon, G., et al., *Complement activation by recombinant adenoviruses*. Gene Ther, 2001. **8**(23): p. 1794-800.
67. Roberts, D.M., et al., *Hexon-chimaeric adenovirus serotype 5 vectors circumvent pre-existing anti-vector immunity*. Nature, 2006. **441**(7090): p. 239-43.
68. Hernot, S. and A.L. Klibanov, *Microbubbles in ultrasound-triggered drug and gene delivery*. Adv Drug Deliv Rev, 2008. **60**(10): p. 1153-66.
69. Liu, Y., H. Miyoshi, and M. Nakamura, *Encapsulated ultrasound microbubbles: therapeutic application in drug/gene delivery*. J Control Release, 2006. **114**(1): p. 89-99.
70. Zagzebski, J., *Essentials of Ultrasound Physics*. 1996, Mosby, St. Louis.
71. Klibanov, A.L., *Ultrasound molecular imaging with targeted microbubble contrast agents*. J Nucl Cardiol, 2007. **14**(6): p. 876-84.
72. Faez, T., et al., *20 years of ultrasound contrast agent modeling*. IEEE Trans Ultrason Ferroelectr Freq Control, 2013. **60**(1): p. 7-20.
73. Gramiak, R. and P.M. Shah, *Echocardiography of the aortic root*. Invest Radiol, 1968. **3**(5): p. 356-66.
74. Calliada, F., et al., *Ultrasound contrast agents: basic principles*. Eur J Radiol, 1998. **27 Suppl 2**: p. S157-60.
75. Soliman, O.I., et al., *The use of contrast echocardiography for the detection of cardiac shunts*. Eur J Echocardiogr, 2007. **8**(3): p. S2-12.
76. Xu, H.X., *Contrast-enhanced ultrasound: The evolving applications*. World J Radiol, 2009. **1**(1): p. 15-24.
77. Feinstein, S.B., et al., *Two-dimensional contrast echocardiography. I. In vitro development and quantitative analysis of echo contrast agents*. J Am Coll Cardiol, 1984. **3**(1): p. 14-20.
78. Wiencek, J.G., et al., *Pitfalls in quantitative contrast echocardiography: the steps to quantitation of perfusion*. J Am Soc Echocardiogr, 1993. **6**(4): p. 395-416.
79. Azmin, M., et al., *How do microbubbles and ultrasound interact? Basic physical, dynamic and engineering principles*. Curr Pharm Des, 2012. **18**(15): p. 2118-34.
80. Sutton, J.T., et al., *Ultrasound-mediated drug delivery for cardiovascular disease*. Expert Opin Drug Deliv, 2013. **10**(5): p. 573-92.

81. Cavaliere, F., M. Zhou, and M. Ashokkumar, *The design of multifunctional microbubbles for ultrasound image-guided cancer therapy*. *Curr Top Med Chem*, 2010. **10**(12): p. 1198-210.
82. Alkan-Onyuksel, H., et al., *Development of inherently echogenic liposomes as an ultrasonic contrast agent*. *J Pharm Sci*, 1996. **85**(5): p. 486-90.
83. Huang, S.L., et al., *Physical correlates of the ultrasonic reflectivity of lipid dispersions suitable as diagnostic contrast agents*. *Ultrasound Med Biol*, 2002. **28**(3): p. 339-48.
84. Wickline, S.A. and G.M. Lanza, *Nanotechnology for molecular imaging and targeted therapy*. *Circulation*, 2003. **107**(8): p. 1092-5.
85. Wickline, S.A., et al., *Blood contrast enhancement with a novel, non-gaseous nanoparticle contrast agent*. *Acad Radiol*, 2002. **9 Suppl 2**: p. S290-3.
86. Klibanov, A.L., et al., *Detection of individual microbubbles of an ultrasound contrast agent: fundamental and pulse inversion imaging*. *Acad Radiol*, 2002. **9 Suppl 2**: p. S279-81.
87. Klibanov, A.L., et al., *Detection of individual microbubbles of ultrasound contrast agents: imaging of free-floating and targeted bubbles*. *Invest Radiol*, 2004. **39**(3): p. 187-95.
88. Bohmer, M.R., et al., *Ultrasound triggered image-guided drug delivery*. *Eur J Radiol*, 2009. **70**(2): p. 242-53.
89. Lindner, J.R., *Molecular imaging of cardiovascular disease with contrast-enhanced ultrasonography*. *Nat Rev Cardiol*, 2009. **6**(7): p. 475-81.
90. Gessner, R. and P.A. Dayton, *Advances in molecular imaging with ultrasound*. *Mol Imaging*, 2010. **9**(3): p. 117-27.
91. Skyba, D.M., et al., *Direct in vivo visualization of intravascular destruction of microbubbles by ultrasound and its local effects on tissue*. *Circulation*, 1998. **98**(4): p. 290-3.
92. Tachibana, K. and S. Tachibana, *Albumin microbubble echo-contrast material as an enhancer for ultrasound accelerated thrombolysis*. *Circulation*, 1995. **92**(5): p. 1148-50.
93. van Wamel, A., et al., *Vibrating microbubbles poking individual cells: drug transfer into cells via sonoporation*. *J Control Release*, 2006. **112**(2): p. 149-55.
94. Sheikov, N., et al., *Effect of focused ultrasound applied with an ultrasound contrast agent on the tight junctional integrity of the brain microvascular endothelium*. *Ultrasound Med Biol*, 2008. **34**(7): p. 1093-104.
95. Meijering, B.D., et al., *Ultrasound and microbubble-targeted delivery of macromolecules is regulated by induction of endocytosis and pore formation*. *Circ Res*, 2009. **104**(5): p. 679-87.
96. Juffermans, L.J., et al., *Ultrasound and microbubble-induced intra- and intercellular bioeffects in primary endothelial cells*. *Ultrasound Med Biol*, 2009. **35**(11): p. 1917-27.
97. Kooiman, K., et al., *Increasing the endothelial layer permeability through ultrasound-activated microbubbles*. *IEEE Trans Biomed Eng*, 2010. **57**(1): p. 29-32.
98. Morse, P.M., Ingard K. U., *Theoretical Acoustics*. 1968, Princeton, NJ: Princeton University Press.
99. Cavaliere, F., et al., *Methods of preparation of multifunctional microbubbles and their in vitro / in vivo assessment of stability, functional and structural properties*. *Curr Pharm Des*, 2012. **18**(15): p. 2135-51.

100. Postema, M., et al., *Ultrasound-induced gas release from contrast agent microbubbles*. IEEE Trans Ultrason Ferroelectr Freq Control, 2005. **52**(6): p. 1035-41.
101. Seward, J.B., et al., *Peripheral venous contrast echocardiography*. Am J Cardiol, 1977. **39**(2): p. 202-12.
102. Epstein, P.S., Plesset, M. S., *On the Stability of Gas Bubbles in Liquid-Gas Solutions*. Journal of Chemical Physics, 1950. **18**(11): p. 1505-1509.
103. Chen, W.S., T.J. Matula, and L.A. Crum, *The disappearance of ultrasound contrast bubbles: observations of bubble dissolution and cavitation nucleation*. Ultrasound Med Biol, 2002. **28**(6): p. 793-803.
104. Barry B. Goldberg, J.S.R., *Ultrasound Contrast Agents: Basic Principles and Clinical Applications* 2001, United Kindom: Martin Dunitz Ltd.
105. Blomley, M., M. Claudon, and D. Cosgrove, *WFUMB Safety Symposium on Ultrasound Contrast Agents: clinical applications and safety concerns*. Ultrasound Med Biol, 2007. **33**(2): p. 180-6.
106. Keller, M.W., S.B. Feinstein, and D.D. Watson, *Successful left ventricular opacification following peripheral venous injection of sonicated contrast agent: an experimental evaluation*. Am Heart J, 1987. **114**(3): p. 570-5.
107. Porter, T.R. and F. Xie, *Visually discernible myocardial echocardiographic contrast after intravenous injection of sonicated dextrose albumin microbubbles containing high molecular weight, less soluble gases*. J Am Coll Cardiol, 1995. **25**(2): p. 509-15.
108. Geiser, E.A., et al., *Evidence for a relation between inspired gas mixture and the left ventricular contrast achieved with Albunex in a canine model*. Clin Cardiol, 1996. **19**(4): p. 289-95.
109. Sirsi, S. and M. Borden, *Microbubble Compositions, Properties and Biomedical Applications*. Bubble Sci Eng Technol, 2009. **1**(1-2): p. 3-17.
110. Schutt, E.G., et al., *Injectable microbubbles as contrast agents for diagnostic ultrasound imaging: the key role of perfluorochemicals*. Angew Chem Int Ed Engl, 2003. **42**(28): p. 3218-35.
111. Alzaraa, A., et al., *Targeted microbubbles in the experimental and clinical setting*. Am J Surg, 2012. **204**(3): p. 355-66.
112. Nomikou, N. and A.P. McHale, *Exploiting ultrasound-mediated effects in delivering targeted, site-specific cancer therapy*. Cancer Lett, 2010. **296**(2): p. 133-43.
113. Van Liew, H.D. and M.E. Burkard, *Bubbles in circulating blood: stabilization and simulations of cyclic changes of size and content*. J Appl Physiol, 1995. **79**(4): p. 1379-85.
114. Moghimi, S.M., Hamad, I. , *Factors controlling pharmacokinetics of intravenously injected nanoparticulate systems*. Biotechnology: Pharmaceutical Aspects., 2009. **10**: p. 267-282.
115. Tartis, M.S., et al., *Dynamic microPET imaging of ultrasound contrast agents and lipid delivery*. J Control Release, 2008. **131**(3): p. 160-6.
116. de Jong, N., et al., *Absorption and scatter of encapsulated gas filled microspheres: theoretical considerations and some measurements*. Ultrasonics, 1992. **30**(2): p. 95-103.
117. Lindner, J.R., Wei, K. , *Contrast echocardiography*. Curr. Probl. Cardiol. , 2002. **27**: p. 454-519.
118. Postema, M. and G. Schmitz, *Ultrasonic bubbles in medicine: influence of the shell*. Ultrason Sonochem, 2007. **14**(4): p. 438-44.

119. Lauterborn, W., Kurz, T., *Physics of bubble oscillations*. Reports on Progress in Physics, 2010. **73**(10): p. 106501.
120. Church, C.C., Carstensen EL., "*Stable*" inertial cavitation. *Ultrasound Med Biol*, 2001. **27**(10): p. 1435-1437.
121. Holland, C.K., et al., *In vitro detection of cavitation induced by a diagnostic ultrasound system*. *IEEE Trans Ultrason Ferroelectr Freq Control*, 1992. **39**(1): p. 95-101.
122. McNamara W.B., D.Y.T., Suslick K.S., *Sonoluminescence temperatures during multi-bubble cavitation*. *Nature*, 1999. **401**: p. 772-775.
123. Suslick, K.S., *Sonochemistry*. *Science*, 1990. **247**(4949): p. 1439-45.
124. Riesz, P. and T. Kondo, *Free radical formation induced by ultrasound and its biological implications*. *Free Radic Biol Med*, 1992. **13**(3): p. 247-70.
125. Chomas, J.E., Dayton P.A., May, D., Allen, J., Klivanov, A., Ferrara, K., *Optical observation of contrast agent destruction*. *Applied Physics Letters*, 2000. **77**: p. 1056-1058.
126. Hill, C.R., ed. *Physical Principles of Medical Ultrasonics*. 2004, Wiley-Blackwell.
127. Elder, S., Nyborg W.L., *Acoustic Streaming Resulting from A Resonance Bubble*. *Journal of the Acoustical Society of America*, 1956. **28**(1): p. 155.
128. Marmottant, P., Biben, T., Hilgenfeldt, S., *Deformation and rupture of lipid vesicles in the strong shear flow generated by ultrasound-driven microbubbles*. *Proceedings of the Royal Society A*, 2008. **464**(2095): p. 1781-1800.
129. Datta, S., et al., *Correlation of cavitation with ultrasound enhancement of thrombolysis*. *Ultrasound Med Biol*, 2006. **32**(8): p. 1257-67.
130. Marmottant, P. and S. Hilgenfeldt, *Controlled vesicle deformation and lysis by single oscillating bubbles*. *Nature*, 2003. **423**(6936): p. 153-6.
131. Rooney, J.A., *Hemolysis near an ultrasonically pulsating gas bubble*. *Science*, 1970. **169**(3948): p. 869-71.
132. Tran, T.A., Roger, S., Le, J.Y., Guennec, J.Y., Tranquart, F., Bouakaz, A., *Effect of ultrasound activated microbubbles on the cell electrophysiological properties*. *Ultrasound Med Biol*, 2006. **33**: p. 158-163.
133. Ward, M., J. Wu, and J.F. Chiu, *Ultrasound-induced cell lysis and sonoporation enhanced by contrast agents*. *J Acoust Soc Am*, 1999. **105**(5): p. 2951-7.
134. Bloch, S.H., Wan, M., Dayton P.A., Ferrara, K.W., *Optical observation of lipid- and polymer-shelled ultrasound microbubble contrast agents*. *Applied Physics Letters*, 2004. **84**: p. 631-633.
135. Chomas, J.E., et al., *Mechanisms of contrast agent destruction*. *IEEE Trans Ultrason Ferroelectr Freq Control*, 2001. **48**(1): p. 232-48.
136. Lawrie, A., et al., *Microbubble-enhanced ultrasound for vascular gene delivery*. *Gene Ther*, 2000. **7**(23): p. 2023-7.
137. de Jong, N., Cornet, R. and Lancee, C. , *Higher harmonics of vibrating gas-filled microspheres. Part one: Simulations*. *Ultrasonics*, 1994. **32**(6): p. 447-453.
138. de Jong, N. and L. Hoff, *Ultrasound scattering properties of AlbuNex microspheres*. *Ultrasonics*, 1993. **31**(3): p. 175-81.
139. Unger, E.C., et al., *Therapeutic applications of lipid-coated microbubbles*. *Adv Drug Deliv Rev*, 2004. **56**(9): p. 1291-314.

140. Cavaliere, F., Finelli, I., Tortora, M., Mozetic, P., Chiessi, E., Polizio, F., Brismar, T., Paradossi, G., *Microbubbles as (NO) delivery device*. Chem. Matter, 2008. **20**: p. 3254-3258.
141. Postema, M.A.B., *Medical Bubbles*. 2004, Veenendaal: Universal Press.
142. Howard, C.M., *The role of ultrasound contrast agents in gene therapy*. Applied Radiology, 2004. **33**: p. 126.
143. Smith, N.B., et al., *Ultrasound-mediated transdermal transport of insulin in vitro through human skin using novel transducer designs*. Ultrasound Med Biol, 2003. **29**(2): p. 311-7.
144. Ferrara, K.W., M.A. Borden, and H. Zhang, *Lipid-shelled vehicles: engineering for ultrasound molecular imaging and drug delivery*. Acc Chem Res, 2009. **42**(7): p. 881-92.
145. ter Haar, G., *Safety and bio-effects of ultrasound contrast agents*. Med Biol Eng Comput, 2009. **47**(8): p. 893-900.
146. Dalecki, D., *WFUMB Safety Symposium on Echo-Contrast Agents: bioeffects of ultrasound contrast agents in vivo*. Ultrasound Med Biol, 2007. **33**(2): p. 205-13.
147. Price, R.J., et al., *Delivery of colloidal particles and red blood cells to tissue through microvessel ruptures created by targeted microbubble destruction with ultrasound*. Circulation, 1998. **98**(13): p. 1264-7.
148. Choi, J.J., et al., *Noninvasive, transcranial and localized opening of the blood-brain barrier using focused ultrasound in mice*. Ultrasound Med Biol, 2007. **33**(1): p. 95-104.
149. Wible, J.H., Jr., et al., *Microbubbles induce renal hemorrhage when exposed to diagnostic ultrasound in anesthetized rats*. Ultrasound Med Biol, 2002. **28**(11-12): p. 1535-46.
150. Li, T., et al., *Mechanisms of prostate permeability triggered by microbubble-mediated acoustic cavitation*. Cell Biochem Biophys, 2012. **64**(2): p. 147-53.
151. van Wamel, A., et al., *Ultrasound microbubble induced endothelial cell permeability*. J Control Release, 2006. **116**(2): p. e100-2.
152. Mehier-Humbert, S., et al., *Plasma membrane poration induced by ultrasound exposure: implication for drug delivery*. J Control Release, 2005. **104**(1): p. 213-22.
153. Fan, L., Liu, Y., Ying, H., Xue, Y., Zhang, Z., Wang, P., Liu, L., Zhang, H., *Increasing of blood-tumor barrier permeability through paracellular pathway by low-frequency ultrasound irradiation in vitro*. J Mol Neurosci., 2011. **43**(3): p. 541-548.
154. Hsieh, D.Y., Plesset, M.S., *Theory of rectified diffusion of mass into gas bubbles*. J. Acoust. Soc. Am., 1961. **33**: p. 206-211.
155. Marmottant, P., Biben, T., Hilgenfeldt, S., *Deformation and rupture of lipid vesicles in the strong shear flow generated by ultrasound-driven microbubbles*. Proc. R. Soc. A - Mathl Phys. Engng Sci., 2008. **464**: p. 1781-1800.
156. Allen, J.S., D.J. May, and K.W. Ferrara, *Dynamics of therapeutic ultrasound contrast agents*. Ultrasound Med Biol, 2002. **28**(6): p. 805-16.
157. Collis, J., et al., *Cavitation microstreaming and stress fields created by microbubbles*. Ultrasonics, 2010. **50**(2): p. 273-9.
158. Leighton, T., *The Acoustic Bubble*. 1994, San Diego: Academic Press.
159. Vykhodtseva, N., N. McDannold, and K. Hynynen, *Progress and problems in the application of focused ultrasound for blood-brain barrier disruption*. Ultrasonics, 2008. **48**(4): p. 279-96.
160. Hamill, O.P., *Twenty odd years of stretch-sensitive channels*. Pflugers Arch, 2006. **453**(3): p. 333-51.

161. Mihran, R.T., F.S. Barnes, and H. Wachtel, *Temporally-specific modification of myelinated axon excitability in vitro following a single ultrasound pulse*. *Ultrasound Med Biol*, 1990. **16**(3): p. 297-309.
162. Mihran, R.T., F.S. Barnes, and H. Wachtel, *Transient modification of nerve excitability in vitro by single ultrasound pulses*. *Biomed Sci Instrum*, 1990. **26**: p. 235-46.
163. Yang, F.Y., et al., *Reversible blood-brain barrier disruption by repeated transcranial focused ultrasound allows enhanced extravasation*. *J Control Release*, 2011. **150**(1): p. 111-6.
164. Schnitzer, J.E., *Vascular Endothelium: Physiology, Pathology and Therapeutic Opportunities*. , ed. G.V.R. Born, Schwartz, C.J. 1997, Stuttgart: Schattauer.
165. Deli, M.A., *Potential use of tight junction modulators to reversibly open membranous barriers and improve drug delivery*. *Biochim Biophys Acta*, 2009. **1788**(4): p. 892-910.
166. Jalali, S., Huang, Y., Dumont, D.J., Hynynen, K., *Focused ultrasound-mediated BBB disruption is associated with an increase in activation of AKT: experimental study in rats*. *BMC Neurology*, 2010. **10**: p. 114.
167. Ghitescu, L., et al., *Specific binding sites for albumin restricted to plasmalemmal vesicles of continuous capillary endothelium: receptor-mediated transcytosis*. *J Cell Biol*, 1986. **102**(4): p. 1304-11.
168. Chen, H., et al., *Blood vessel rupture by cavitation*. *Urol Res*, 2010. **38**(4): p. 321-6.
169. Niles, W.D. and A.B. Malik, *Endocytosis and exocytosis events regulate vesicle traffic in endothelial cells*. *J Membr Biol*, 1999. **167**(1): p. 85-101.
170. Schnitzer, J.E., et al., *Filipin-sensitive caveolae-mediated transport in endothelium: reduced transcytosis, scavenger endocytosis, and capillary permeability of select macromolecules*. *J Cell Biol*, 1994. **127**(5): p. 1217-32.
171. McIntosh, D.P., et al., *Targeting endothelium and its dynamic caveolae for tissue-specific transcytosis in vivo: a pathway to overcome cell barriers to drug and gene delivery*. *Proc Natl Acad Sci U S A*, 2002. **99**(4): p. 1996-2001.
172. Taniyama, Y., et al., *Local delivery of plasmid DNA into rat carotid artery using ultrasound*. *Circulation*, 2002. **105**(10): p. 1233-9.
173. Fan, Z., et al., *Spatiotemporally controlled single cell sonoporation*. *Proc Natl Acad Sci U S A*, 2012. **109**(41): p. 16486-91.
174. Deng, C.X., et al., *Ultrasound-induced cell membrane porosity*. *Ultrasound Med Biol*, 2004. **30**(4): p. 519-26.
175. Zhou, Y., J. Cui, and C.X. Deng, *Dynamics of sonoporation correlated with acoustic cavitation activities*. *Biophys J*, 2008. **94**(7): p. L51-3.
176. Ta, C.N., et al., *Integrated processing of contrast pulse sequencing ultrasound imaging for enhanced active contrast of hollow gas filled silica nanoshells and microshells*. *J Vac Sci Technol B Nanotechnol Microelectron*, 2012. **30**(2): p. 2C104.
177. Li, W.W., *Tumor angiogenesis: molecular pathology, therapeutic targeting, and imaging*. *Acad Radiol*, 2000. **7**(10): p. 800-11.
178. Wheatley, M.A. and J. Lewandowski, *Nano-sized ultrasound contrast agent: salting-out method*. *Mol Imaging*, 2010. **9**(2): p. 96-107.
179. Pasqualini, R., W. Arap, and D.M. McDonald, *Probing the structural and molecular diversity of tumor vasculature*. *Trends Mol Med*, 2002. **8**(12): p. 563-71.
180. Zhao, Y.Z., et al., *Phospholipids-based microbubbles sonoporation pore size and reseal of cell membrane cultured in vitro*. *J Drug Target*, 2008. **16**(1): p. 18-25.

181. Dayton, P., et al., *Acoustic radiation force in vivo: a mechanism to assist targeting of microbubbles*. *Ultrasound Med Biol*, 1999. **25**(8): p. 1195-201.
182. Rapoport, N.Y., et al., *Controlled and targeted tumor chemotherapy by ultrasound-activated nanoemulsions/microbubbles*. *J Control Release*, 2009. **138**(3): p. 268-76.
183. Wickline, S.A. and G.M. Lanza, *Molecular imaging, targeted therapeutics, and nanoscience*. *J Cell Biochem Suppl*, 2002. **39**: p. 90-7.
184. Unger, E.C., et al., *Therapeutic applications of microbubbles*. *Eur J Radiol*, 2002. **42**(2): p. 160-8.
185. Tsutsui, J.M., F. Xie, and R.T. Porter, *The use of microbubbles to target drug delivery*. *Cardiovasc Ultrasound*, 2004. **2**: p. 23.
186. Shohet, R.V., et al., *Echocardiographic destruction of albumin microbubbles directs gene delivery to the myocardium*. *Circulation*, 2000. **101**(22): p. 2554-6.
187. Chen, S., et al., *Optimization of ultrasound parameters for cardiac gene delivery of adenoviral or plasmid deoxyribonucleic acid by ultrasound-targeted microbubble destruction*. *J Am Coll Cardiol*, 2003. **42**(2): p. 301-8.
188. Mukherjee, D., et al., *Ten-fold augmentation of endothelial uptake of vascular endothelial growth factor with ultrasound after systemic administration*. *J Am Coll Cardiol*, 2000. **35**(6): p. 1678-86.
189. Ganly, I., V. Mautner, and A. Balmain, *Productive replication of human adenoviruses in mouse epidermal cells*. *J Virol*, 2000. **74**(6): p. 2895-9.
190. Hallden, G., et al., *Novel immunocompetent murine tumor models for the assessment of replication-competent oncolytic adenovirus efficacy*. *Mol Ther*, 2003. **8**(3): p. 412-24.
191. Caudell, E.G., et al., *The protein product of the tumor suppressor gene, melanoma differentiation-associated gene 7, exhibits immunostimulatory activity and is designated IL-24*. *J Immunol*, 2002. **168**(12): p. 6041-6.
192. Ramesh, R., et al., *Melanoma differentiation-associated gene 7/interleukin (IL)-24 is a novel ligand that regulates angiogenesis via the IL-22 receptor*. *Cancer Res*, 2003. **63**(16): p. 5105-13.
193. Yacoub, A., et al., *mda-7 (IL-24) Inhibits growth and enhances radiosensitivity of glioma cells in vitro via JNK signaling*. *Cancer Biol Ther*, 2003. **2**(4): p. 347-53.
194. Su, Z., et al., *Unique aspects of mda-7/IL-24 antitumor bystander activity: establishing a role for secretion of MDA-7/IL-24 protein by normal cells*. *Oncogene*, 2005. **24**(51): p. 7552-66.
195. Fisher, P.B., *Is mda-7/IL-24 a "magic bullet" for cancer?* *Cancer Res*, 2005. **65**(22): p. 10128-38.
196. Fisher, P.B., et al., *mda-7/IL-24, a novel cancer selective apoptosis inducing cytokine gene: from the laboratory into the clinic*. *Cancer Biol Ther*, 2003. **2**(4 Suppl 1): p. S23-37.
197. Sarkar, D., et al., *Melanoma differentiation associated gene-7 (mda-7)/IL-24: a 'magic bullet' for cancer therapy?* *Expert Opin Biol Ther*, 2007. **7**(5): p. 577-86.
198. Pestka, S., et al., *Interleukin-10 and related cytokines and receptors*. *Annu Rev Immunol*, 2004. **22**: p. 929-79.
199. Huang, E.Y., et al., *Genomic structure, chromosomal localization and expression profile of a novel melanoma differentiation associated (mda-7) gene with cancer specific growth suppressing and apoptosis inducing properties*. *Oncogene*, 2001. **20**(48): p. 7051-63.

200. Zhu, J., X. Huang, and Y. Yang, *Innate immune response to adenoviral vectors is mediated by both Toll-like receptor-dependent and -independent pathways*. J Virol, 2007. **81**(7): p. 3170-80.
201. Zhu, J., et al., *Innate immunity against vaccinia virus is mediated by TLR2 and requires TLR-independent production of IFN-beta*. Blood, 2007. **109**(2): p. 619-25.
202. Dash, R., et al., *Developing an effective gene therapy for prostate cancer: New technologies with potential to translate from the laboratory into the clinic*. Discov Med, 2011. **11**(56): p. 46-56.
203. Cunningham, C.C., et al., *Clinical and local biological effects of an intratumoral injection of mda-7 (IL24; INGN 241) in patients with advanced carcinoma: a phase I study*. Mol Ther, 2005. **11**(1): p. 149-59.
204. Sarkar, D., et al., *A cancer terminator virus eradicates both primary and distant human melanomas*. Cancer Gene Ther, 2008. **15**(5): p. 293-302.
205. Sarkar, D., et al., *Dual cancer-specific targeting strategy cures primary and distant breast carcinomas in nude mice*. Proc Natl Acad Sci U S A, 2005. **102**(39): p. 14034-9.
206. Su, Z.Z., et al., *The cancer growth suppressor gene mda-7 selectively induces apoptosis in human breast cancer cells and inhibits tumor growth in nude mice*. Proc Natl Acad Sci U S A, 1998. **95**(24): p. 14400-5.
207. Moon, C., et al., *Current status of experimental therapeutics for prostate cancer*. Cancer Lett, 2008. **266**(2): p. 116-34.
208. Shi, X.B., P.H. Gumerlock, and R.W. deVere White, *Molecular biology of prostate cancer*. World J Urol, 1996. **14**(5): p. 318-28.
209. Lebedeva, I.V., et al., *Bcl-2 and Bcl-x(L) differentially protect human prostate cancer cells from induction of apoptosis by melanoma differentiation associated gene-7, mda-7/IL-24*. Oncogene, 2003. **22**(54): p. 8758-73.
210. Lebedeva, I.V., et al., *Melanoma differentiation associated gene-7, mda-7/interleukin-24, induces apoptosis in prostate cancer cells by promoting mitochondrial dysfunction and inducing reactive oxygen species*. Cancer Res, 2003. **63**(23): p. 8138-44.
211. Lebedeva, I.V., et al., *mda-7/IL-24, novel anticancer cytokine: focus on bystander antitumor, radiosensitization and antiangiogenic properties and overview of the phase I clinical experience (Review)*. Int J Oncol, 2007. **31**(5): p. 985-1007.
212. Lebedeva, I.V., et al., *mda-7/IL-24: exploiting cancer's Achilles' heel*. Mol Ther, 2005. **11**(1): p. 4-18.
213. Sarkar, D., et al., *Acquired and innate resistance to the cancer-specific apoptosis-inducing cytokine, mda-7/IL-24: not insurmountable therapeutic problems*. Cancer Biol Ther, 2008. **7**(1): p. 109-12.
214. Howard, C.M., et al., *Ultrasound guided site specific gene delivery system using adenoviral vectors and commercial ultrasound contrast agents*. J Cell Physiol, 2006. **209**(2): p. 413-21.
215. Jiang, H., et al., *Recombinant adenovirus vectors activate the alternative complement pathway, leading to the binding of human complement protein C3 independent of anti-ad antibodies*. Mol Ther, 2004. **10**(6): p. 1140-2.
216. Ng, K.Y. and Y. Liu, *Therapeutic ultrasound: its application in drug delivery*. Med Res Rev, 2002. **22**(2): p. 204-23.
217. Larina, I.V., B.M. Evers, and R.O. Esenaliev, *Optimal drug and gene delivery in cancer cells by ultrasound-induced cavitation*. Anticancer Res, 2005. **25**(1A): p. 149-56.

218. Howard, C.M., *The role of ultrasound contrast agents in gene therapy*. Applied Radiology, 2004. **33**, suppl(10): p. 126-35.
219. Goldberg, B.B., J.B. Liu, and F. Forsberg, *Ultrasound contrast agents: a review*. Ultrasound Med Biol, 1994. **20**(4): p. 319-33.
220. Pitt, W.G., G.A. Hussein, and B.J. Staples, *Ultrasonic drug delivery--a general review*. Expert Opin Drug Deliv, 2004. **1**(1): p. 37-56.
221. Puisieux, I., et al., *Canarypox virus-mediated interleukin 12 gene transfer into murine mammary adenocarcinoma induces tumor suppression and long-term antitumoral immunity*. Hum Gene Ther, 1998. **9**(17): p. 2481-92.
222. Dayton, P.A. and J.J. Rychak, *Molecular ultrasound imaging using microbubble contrast agents*. Front Biosci, 2007. **12**: p. 5124-42.
223. Eager, R., L. Harle, and J. Nemunaitis, *Ad-MDA-7; INGN 241: a review of preclinical and clinical experience*. Expert Opin Biol Ther, 2008. **8**(10): p. 1633-43.
224. Fisher, P.B., et al., *Melanoma differentiation associated gene-7/interleukin-24 (mda-7/IL-24): novel gene therapeutic for metastatic melanoma*. Toxicol Appl Pharmacol, 2007. **224**(3): p. 300-7.
225. Inoue, S., et al., *mda-7 In combination with bevacizumab treatment produces a synergistic and complete inhibitory effect on lung tumor xenograft*. Mol Ther, 2007. **15**(2): p. 287-94.
226. Ramesh, R., et al., *Local and systemic inhibition of lung tumor growth after nanoparticle-mediated mda-7/IL-24 gene delivery*. DNA Cell Biol, 2004. **23**(12): p. 850-7.
227. Tahara, I., et al., *Systemic cancer gene therapy using adeno-associated virus type 1 vector expressing MDA-7/IL24*. Mol Ther, 2007. **15**(10): p. 1805-11.
228. Tong, A.W., et al., *Intratumoral injection of INGN 241, a nonreplicating adenovector expressing the melanoma-differentiation associated gene-7 (mda-7/IL24): biologic outcome in advanced cancer patients*. Mol Ther, 2005. **11**(1): p. 160-72.
229. Yacoub, A., et al., *MDA-7 (interleukin-24) inhibits the proliferation of renal carcinoma cells and interacts with free radicals to promote cell death and loss of reproductive capacity*. Mol Cancer Ther, 2003. **2**(7): p. 623-32.
230. Zerbini, L.F., et al., *A novel pathway involving melanoma differentiation associated gene-7/interleukin-24 mediates nonsteroidal anti-inflammatory drug-induced apoptosis and growth arrest of cancer cells*. Cancer Res, 2006. **66**(24): p. 11922-31.
231. Nishikawa, T., et al., *Adenovirus-mediated mda-7 (IL24) gene therapy suppresses angiogenesis and sensitizes NSCLC xenograft tumors to radiation*. Mol Ther, 2004. **9**(6): p. 818-28.
232. Gupta, P., et al., *mda-7/IL-24: multifunctional cancer-specific apoptosis-inducing cytokine*. Pharmacol Ther, 2006. **111**(3): p. 596-628.
233. Sauane, M., et al., *Autocrine regulation of mda-7/IL-24 mediates cancer-specific apoptosis*. Proc Natl Acad Sci U S A, 2008. **105**(28): p. 9763-8.
234. Beerli, R., et al., *New efficient catheter-based system for myocardial gene delivery*. Circulation, 2002. **106**(14): p. 1756-9.
235. Jiang, H., et al., *Subtraction hybridization identifies a novel melanoma differentiation associated gene, mda-7, modulated during human melanoma differentiation, growth and progression*. Oncogene, 1995. **11**(12): p. 2477-86.
236. Jiang, H., et al., *The melanoma differentiation associated gene mda-7 suppresses cancer cell growth*. Proc Natl Acad Sci U S A, 1996. **93**(17): p. 9160-5.

237. Sarkar, D., Z.Z. Su, and P.B. Fisher, *Unique conditionally replication competent bipartite adenoviruses-cancer terminator viruses (CTV): efficacious reagents for cancer gene therapy*. Cell Cycle, 2006. **5**(14): p. 1531-6.
238. Freytag, S.O., et al., *Phase I study of replication-competent adenovirus-mediated double-suicide gene therapy in combination with conventional-dose three-dimensional conformal radiation therapy for the treatment of newly diagnosed, intermediate- to high-risk prostate cancer*. Cancer Res, 2003. **63**(21): p. 7497-506.
239. Small, E.J., et al., *A phase I trial of intravenous CG7870, a replication-selective, prostate-specific antigen-targeted oncolytic adenovirus, for the treatment of hormone-refractory, metastatic prostate cancer*. Mol Ther, 2006. **14**(1): p. 107-17.
240. Heise, C., et al., *ONYX-015, an E1B gene-attenuated adenovirus, causes tumor-specific cytolysis and antitumoral efficacy that can be augmented by standard chemotherapeutic agents*. Nat Med, 1997. **3**(6): p. 639-45.
241. Sarkar, D., et al., *Targeted virus replication plus immunotherapy eradicates primary and distant pancreatic tumors in nude mice*. Cancer Res, 2005. **65**(19): p. 9056-63.
242. Su, Z.Z., et al., *Targeting gene expression selectively in cancer cells by using the progression-elevated gene-3 promoter*. Proc Natl Acad Sci U S A, 2005. **102**(4): p. 1059-64.
243. Su, Z.Z., Y. Shi, and P.B. Fisher, *Subtraction hybridization identifies a transformation progression-associated gene PEG-3 with sequence homology to a growth arrest and DNA damage-inducible gene*. Proc Natl Acad Sci U S A, 1997. **94**(17): p. 9125-30.
244. Gao, P., et al., *Secretable chaperone Grp170 enhances therapeutic activity of a novel tumor suppressor, mda-7/IL-24*. Cancer Res, 2008. **68**(10): p. 3890-8.
245. Yacoub, A., et al., *MDA-7/IL-24 plus radiation enhance survival in animals with intracranial primary human GBM tumors*. Cancer Biol Ther, 2008. **7**(6): p. 917-33.
246. Tsai, C.H., J.H. Lin, and C.P. Ju, *Gamma-radiation-induced changes in structure and properties of tetracalcium phosphate and its derived calcium phosphate cement*. J Biomed Mater Res B Appl Biomater, 2007. **80**(1): p. 244-52.
247. Kastan, M.B., C.E. Canman, and C.J. Leonard, *p53, cell cycle control and apoptosis: implications for cancer*. Cancer Metastasis Rev, 1995. **14**(1): p. 3-15.
248. Udayakumar, T., et al., *The E2F1/Rb and p53/MDM2 pathways in DNA repair and apoptosis: understanding the crosstalk to develop novel strategies for prostate cancer radiotherapy*. Seminars in radiation oncology, 2010. **20**(4): p. 258-66.
249. Algan, O., et al., *Radiation inactivation of human prostate cancer cells: the role of apoptosis*. Radiat Res, 1996. **146**(3): p. 267-75.
250. Pawlik, T.M. and K. Keyomarsi, *Role of cell cycle in mediating sensitivity to radiotherapy*. Int J Radiat Oncol Biol Phys, 2004. **59**(4): p. 928-42.
251. Bromfield, G.P., et al., *Cell death in irradiated prostate epithelial cells: role of apoptotic and clonogenic cell kill*. Prostate Cancer Prostatic Dis, 2003. **6**(1): p. 73-85.
252. Bajgelman, M.C. and B.E. Strauss, *The DU145 human prostate carcinoma cell line harbors a temperature-sensitive allele of p53*. Prostate, 2006. **66**(13): p. 1455-62.
253. Kuerbitz, S.J., et al., *Wild-type p53 is a cell cycle checkpoint determinant following irradiation*. Proc Natl Acad Sci U S A, 1992. **89**(16): p. 7491-5.
254. Bowen, C., S. Spiegel, and E.P. Gelmann, *Radiation-induced apoptosis mediated by retinoblastoma protein*. Cancer Res, 1998. **58**(15): p. 3275-81.

255. Sasaki, R., et al., *Additional gene therapy with Ad5CMV-p53 enhanced the efficacy of radiotherapy in human prostate cancer cells*. *Int J Radiat Oncol Biol Phys*, 2001. **51**(5): p. 1336-45.
256. Bowen, C., M. Birrer, and E.P. Gelmann, *Retinoblastoma protein-mediated apoptosis after gamma-irradiation*. *J Biol Chem*, 2002. **277**(47): p. 44969-79.
257. Crook, J.M., et al., *Prostate motion during standard radiotherapy as assessed by fiducial markers*. *Radiother Oncol*, 1995. **37**(1): p. 35-42.
258. Pucci, B., et al., *pRb2/p130 promotes radiation-induced cell death in the glioblastoma cell line HJC12 by p73 upregulation and Bcl-2 downregulation*. *Oncogene*, 2002. **21**(38): p. 5897-905.
259. Stevens, C.W., M. Zeng, and G.J. Cerniglia, *Ionizing radiation greatly improves gene transfer efficiency in mammalian cells*. *Hum Gene Ther*, 1996. **7**(14): p. 1727-34.
260. Nande, R., et al., *Targeting a newly established spontaneous feline fibrosarcoma cell line by gene transfer*. *PLoS One*, 2012. **7**(5): p. e37743.
261. Aimola, P., et al., *Cadmium induces p53-dependent apoptosis in human prostate epithelial cells*. *PLoS One*, 2012. **7**(3): p. e33647.
262. Mukerjee, R., et al., *Transcriptional regulation of HIV-1 gene expression by p53*. *Cell Cycle*, 2010. **9**(22): p. 4569-78.
263. Claudio, P.P., et al., *Cdk9 phosphorylates p53 on serine 392 independently of CKII*. *Journal of cellular physiology*, 2006. **208**(3): p. 602-12.
264. Gossman, M.S., et al., *A novel phantom model for mouse tumor dose assessment under MV beams*. *Health Phys*, 2011. **101**(6): p. 746-53.
265. Lowe, S.W., et al., *p53 status and the efficacy of cancer therapy in vivo*. *Science*, 1994. **266**(5186): p. 807-10.
266. Swisher, S.G., et al., *Induction of p53-regulated genes and tumor regression in lung cancer patients after intratumoral delivery of adenoviral p53 (INGN 201) and radiation therapy*. *Clin Cancer Res*, 2003. **9**(1): p. 93-101.
267. Zhang, H., et al., *Retinoblastoma 94 enhances radiation treatment of esophageal squamous cell carcinoma in vitro and in vivo*. *J Radiat Res*, 2012. **53**(1): p. 117-24.
268. Vogiatzi, P., et al., *Targeted therapy for advanced prostate cancer: Looking through new lenses*. *Drug news & perspectives*, 2009. **22**(10): p. 593-601.
269. Vogiatzi, P. and P.P. Claudio, *Efficacy of abiraterone acetate in post-docetaxel castration-resistant prostate cancer*. *Expert review of anticancer therapy*, 2010. **10**(7): p. 1027-30.
270. Teyssier, F., et al., *[Cell cycle regulation after exposure to ionizing radiation]*. *Bull Cancer*, 1999. **86**(4): p. 345-57.
271. Lee, J.T., et al., *Targeting prostate cancer based on signal transduction and cell cycle pathways*. *Cell cycle*, 2008. **7**(12): p. 1745-62.
272. Claudio, P.P., et al., *Expression of cell-cycle-regulated proteins pRb2/p130, p107, p27(kip1), p53, mdm-2, and Ki-67 (MIB-1) in prostatic gland adenocarcinoma*. *Clinical cancer research : an official journal of the American Association for Cancer Research*, 2002. **8**(6): p. 1808-15.
273. Claudio, P.P., T. Tonini, and A. Giordano, *The retinoblastoma family: twins or distant cousins?* *Genome biology*, 2002. **3**(9): p. reviews3012.
274. Cowen, D., et al., *Prostate cancer radiosensitization in vivo with adenovirus-mediated p53 gene therapy*. *Clin Cancer Res*, 2000. **6**(11): p. 4402-8.

275. Lehmann, B.D., et al., *Distinct roles for p107 and p130 in Rb-independent cellular senescence*. Cell Cycle, 2008. **7**(9): p. 1262-8.
276. Bott, S.R., et al., *p21WAF1/CIP1 gene is inactivated in metastatic prostatic cancer cell lines by promoter methylation*. Prostate Cancer Prostatic Dis, 2005. **8**(4): p. 321-6.
277. Willis, A., et al., *Mutant p53 exerts a dominant negative effect by preventing wild-type p53 from binding to the promoter of its target genes*. Oncogene, 2004. **23**(13): p. 2330-8.
278. Helmbold, H., W. Deppert, and W. Bohn, *Regulation of cellular senescence by Rb2/p130*. Oncogene, 2006. **25**(38): p. 5257-62.
279. Harrington, E.A., et al., *pRB plays an essential role in cell cycle arrest induced by DNA damage*. Proc Natl Acad Sci U S A, 1998. **95**(20): p. 11945-50.
280. Haas-Kogan, D.A., et al., *Inhibition of apoptosis by the retinoblastoma gene product*. EMBO J, 1995. **14**(3): p. 461-72.
281. Helmbold, H., et al., *Rb2/p130 is the dominating pocket protein in the p53-p21 DNA damage response pathway leading to senescence*. Oncogene, 2009. **28**(39): p. 3456-67.
282. DuPree, E.L., S. Mazumder, and A. Almasan, *Genotoxic stress induces expression of E2F4, leading to its association with p130 in prostate carcinoma cells*. Cancer Res, 2004. **64**(13): p. 4390-3.
283. Dummer, R., et al., *Biological activity and safety of adenoviral vector-expressed wild-type p53 after intratumoral injection in melanoma and breast cancer patients with p53-overexpressing tumors*. Cancer Gene Ther, 2000. **7**(7): p. 1069-76.
284. Yen, N., et al., *Cellular and humoral immune responses to adenovirus and p53 protein antigens in patients following intratumoral injection of an adenovirus vector expressing wild-type p53 (Ad-p53)*. Cancer Gene Ther, 2000. **7**(4): p. 530-6.
285. Rochlitz, C.F., *Gene therapy of cancer*. Swiss medical weekly, 2001. **131**(1-2): p. 4-9.
286. Bhatia, V.K. and R. Senior, *Contrast echocardiography: evidence for clinical use*. J Am Soc Echocardiogr, 2008. **21**(5): p. 409-16.
287. Colletier, P.J., et al., *Adenoviral-mediated p53 transgene expression sensitizes both wild-type and null p53 prostate cancer cells in vitro to radiation*. Int J Radiat Oncol Biol Phys, 2000. **48**(5): p. 1507-12.
288. Yang, Z.X., et al., *Clinical study of recombinant adenovirus-p53 combined with fractionated stereotactic radiotherapy for hepatocellular carcinoma*. J Cancer Res Clin Oncol, 2010. **136**(4): p. 625-30.
289. Lupold, S.E. and R. Rodriguez, *Adenoviral gene therapy, radiation, and prostate cancer*. Rev Urol, 2005. **7**(4): p. 193-202.

APPENDIX

Letters from Office of Research Integrity IRB Approval



Joan C. Edwards School of Medicine
Animal Resource Facility

Dear Sir/Madam:

The following application and protocol to use laboratory animals at Marshall University was reviewed and received final approval by the Institutional Animal Care and Use Committee (IACUC) on February 24, 2009

Title of application: "Efficacy of ultrasound contrast agents for targeted gene delivery in nude mice"

IACUC Project No.: 397

Name of Principal Investigator: Pier Paolo Claudio, Ph.D.

As a condition of approval, the Institutional Animal Care and Use Committee required the following modifications to the above-referenced application:

None

A handwritten signature in black ink, appearing to read 'Monica Valentovic'.

Monica A. Valentovic, Ph.D.
Chairperson, IACUC



Joan C. Edwards School of Medicine
Animal Resource Facility

Dear Sir/Madam:

The following application and protocol to use laboratory animals at Marshall University was reviewed and received final approval by the Institutional Animal Care and Use Committee (IACUC) on May 18, 2010

Title of application: "Efficacy of the use of Adenoviruses, Radiation and Ultrasound on tumor xenografts in nude mice"

IACUC Project No.: 456

Name of Principal Investigator: Pier Paolo Claudio

Co-Investigator:

As a condition of approval, the Institutional Animal Care and Use Committee required the following modifications to the above-referenced application:

None

Monica A. Valentovic, Ph.D.
Chairperson, IACUC

Curriculum Vitae

Rounak Nande

3800 Kendale Road, Annandale, VA 22003.

|(703)946-4534|nande@marshall.edu

Education **Marshall University, Huntington, WV 25755**
Ph.D. in Biomedical Sciences, May 2015
M.Sc. in Biomedical Sciences with Thesis, May 2013
Virginia Tech, Blacksburg, VA
B.Sc. in Biology, Psychology Minor, May 2007

Research Experience **Marshall University,**
Biomedical Sciences, Huntington, WV
Dr. Pier Paolo Claudio's Lab August 2008- May 2014

- Ultrasound Guided Microbubble Delivery of Adenoviruses
- Cell Culture, Cell line storage, Viability Assays
- Flow Cytometry
- Virus Expansion and Purification
- Radiation of Cell cultures and Mice
- Maintaining mice colonies, animal surgeries
- Polymerase chain reaction (PCR)
- Western Blots
- Chromosome Identification and Staining
- Protocols, grants writings
- Analyzed and recorded research data using various software programs

Johns Hopkins University,
Baltimore, MD
Department of Neurosurgery. June-August,2005,2006
Hunterian Brain Tumor Research Laboratory

- Performed microsurgical techniques including intracranial implantations
- Carried out release kinetic studies measuring drug concentrations in solvent systems using high pressure liquid chromatography
- Prepared specimens for histological staining and evaluation
- Analyzed and recorded research data using various software programs
- Prepared data for presentations at national conferences

Awards **Best Overall Poster Presentation.** ARCC conference. October 2012 & October 2014.
2nd Best Overall Poster Presentation. ARCC conference. October 2013.
NASA West Virginia Space Grant Consortium fund Graduate Fellowship 2013-14

NASA West Virginia Space Grant Consortium fund Graduate Fellowship
2014-15

Graduate Student Organization Scholarship, Outstanding Performance,
Marshall University School of Medicine, Biomedical Sciences, 2014

Travel Award from Marshall University for Experimental Biology (2013)

Publications Markus Bookland, B.S., **Rounak Nande**, Betty Tyler, B.A., Thomas Schluep, Ph.D., Jon Weingart, M.D., and Henry Brem, M.D. “*In vitro* and *in vivo* toxicity testing for the prolonged local delivery of a Cycloset[®]-camptothecin polymer.” **American Association of Neurological Surgeons**, San Francisco, CA, April 22-27, **2006**.

Greco A, Di Benedetto A, Howard CM, Kelly S, **Nande R**, Dementieva Y, Miranda M, Brunetti A, Salvatore M, Claudio L, Sarkar D, Dent P, Curiel DT, Fisher PB, Claudio PP. “Eradication of therapy-resistant human prostate tumors using an ultrasound-guided site-specific cancer terminator virus delivery approach.” **Molecular Therapy**, **2010** Feb; v18 (2): 295-306.

Nande R, Di Benedetto A, Aimola P, De Carlo F, Carper M, Claudio CD, Denvir J, Valluri J, Duncan GC, Claudio PP. “Targeting a newly established spontaneous feline fibrosarcoma cell line by gene transfer.” **PLoS One**. 2012; 7(5):e37743. Epub **2012** May 30.

Nande R, Greco A, Gossman MS, Lopez JP, Claudio L, Salvatore M, Brunetti A, Denvir J, Howard CM, Claudio PP. “Microbubble-assisted p53, RB, and p130 gene transfer in combination with radiation therapy in prostate cancer” **Current Gene Therapy**, **2013** Jun 1;13(3):163-74.

Nande R and Claudio P. “Ultrasound Contrast Agents in Cancer Therapy” **chapter in book** titled "Cutting edge therapies for cancer in the 21st century", **Bentham Science Publishers Ltd**, **2014** July 10: 425-512.

Mathis SE, Alberico A, **Nande R**, Neto W, Lawrence L, McCallister D, Denvir J, Kimmey G, Mogul M, Oakley G, Denning K, Dougherty T, Valluri J and Claudio PP. “Chemo-predictive assay for targeting cancer stem-like cells in patients affected by brain tumors” **PLoS One**, **2014 Aug** **21**;9(8):e105710.

Nande R and Claudio PP. “Ultrasound-mediated oncolytic virus delivery and uptake for increased therapeutic efficacy: state of the art” **Oncolytic Virotherapy**. **2015** (Submitted for approval)

Nande R, Nyugen K, Boskovic O, Claudio PP. “Ultrasound Targeted Microbubble Delivery in human and mice prostate cancer cells.” **2015** (Submitted for approval)

Oral Presentations Joan C. Edwards School of Medicine, 24th Annual Research Day, May 2012.
Joan C. Edwards School of Medicine, 25th Annual Research Day, May 2013.
Joan C. Edwards School of Medicine, 26th Annual Research Day, May 2014.
Joan C. Edwards School of Medicine, 27th Annual Research Day, May 2015.

Poster Presentations **American Society of Gene and Cell Therapy (ASGCT)** Conference, 13th Annual Meeting, Washington D.C., May 2010.
Joan C. Edwards School of Medicine, 22nd Annual Research Day, Huntington, March 2010.
STaR Symposium, 87th annual meeting of the West Virginia Academy of Science and the 4th biennial, WV State University, April, 2012.
Center for Clinical and Translational Science (CCTS) Spring Conference, Kentucky, 2012
Appalachian Regional Cell Conference (1st ARCC), Charleston Area Medical Center in Charleston, WV. October 2012.
Experimental Biology (EB) Conference 2013, Boston Convention and Exhibition Center, Boston MA. April 2013.
Appalachian Regional Cell Conference (2nd ARCC), Charleston Area Medical Center in Charleston, WV. October 2013.
Appalachian Regional Cell Conference (3rd ARCC), Marshall University, Huntington, WV. October 2014.

Clinical Experiences **Riverside Medical Associates**,
Riverside, MD
Intern
July, 2004

- Prepared cash and account receivable reports for physicians
- Processed and billed patient accounts
- Coordinated activities between patients, nurses, physicians and practice coordinators
- Organized patient records as well as updated medical databases
- Directed patients to appropriate resources for the effective treatment of personal needs
- Assisted with various laboratory experiments and preparatory work

Teaching Experiences **Marshall University**
Huntington, WV
Biomedical Teaching Practicum

- Angiogenesis Lecture in BMS 600 (Graduate Course)
- Cell Cycle Lecture in BMS 600 (Graduate Course)

Marshall University, Tutoring Services

Huntington, WV

- Tutoring in Biology, Chemistry, Physics, Mathematics (Algebra, Geometry, Pre-calculus, Calculus, Trigonometry.)

Fairfax County Public Schools,

Fairfax, VA

- Substitute Teacher for Elementary, Middle and High Schools.
-

Mentorship Experiences

- **Two 4th year Medical Students** from Marshall University
 - **Capstone Student**
 - **WV INBRE Undergraduate and High School Teacher**
 - Marshall University **Undergraduate student** now Virginia Tech **Veterinarian Student**
 - **Medical Student** now a **Radiologist** at **Cancer Centers of America**
 - **PhD student** from Virginia Commonwealth University
-

Work Experience

Virginia Tech, Chemistry Dept.

Blacksburg, VA

Lab Technician

January-May, 2006 - 2007

- Maintained and organized the lab on a daily basis
 - Prepped for labs and lecture material
 - Demonstrated reactions for students
-

Extra-curricular Activities

The Society of Indian American, Virginia Tech.

CCVT, Cricket Club, Intra-mural sport, Virginia Tech.

Basketball, Intramural Sport, Virginia Tech.

Basketball, Intramural Sport, Marshall University, 2010-14

Soccer, Intramural Sport, Marshall University, 2012-14.

Cricket Coach at Wicket Club, Sterling Virginia, 2012-14.

Volunteer at Corpus Christi Pre-School, Annandale, Virginia, 2010-14.

Volunteer Cook for Graduate Student Organization (GSO) Fund raising, Marshall University

Volunteer to Draw the Marshall University Biomedical Sciences T-shirt

Volunteer for Interview and Dinner sessions of potential PhD students
